Rice monitoring using radar remote sensing

Thi Hoa Phan

▶ To cite this version:

Thi Hoa Phan. Rice monitoring using radar remote sensing. Hydrology. Université Paul Sabatier - Toulouse III, 2018. English. NNT : 2018TOU30328 . tel-02450835

HAL Id: tel-02450835
https://theses.hal.science/tel-02450835

Submitted on 23 Jan 2020

THÈSE

En vue de l'obtention du

DOCTORAT DE L'UNIVERSITÉ DE TOULOUSE

Délivré par l'Université Toulouse 3 - Paul Sabatier

Présentée et soutenue par

HOA PHAN

Le 3 décembre 2018

Suivi des surfaces rizicoles par télédétection radar

Ecole doctorale : **SDU2E - Sciences de l'Univers, de l'Environnement et de l'Espace**

Spécialité : **Surfaces et interfaces continentales, Hydrologie**

Unité de recherche :
CESBIO - Centre d'Etudes Spatiales de la Biosphère

Thèse dirigée par
Mehrez ZRIBI et Thuy LE TOAN

Jury

Agnes BEGUE	Directrice de Recherche, CIRAD, Montpellier	Rapporteur
Francesco MATTIA	Senior Research Scientist CNR-Bari, Italie	Rapporteur
Nicolas BAGHDADI	Directeur de Recherche, IRSTEA, Montpellier	Examinateur
Laurent POLIDORI	Directeur de Recherche CNRS, Toulouse	Examinateur
Jerome HELBERT	Ingénieur de Recherche, TPZ, Toulouse	Examinateur
Mehrez ZRIBI	Directeur de Recherche CNRS, Toulouse	Directeur de thèse
Thuy LE TOAN	Ingénieur de Recherche CNRS, Toulouse	Co-directrice de thèse

Table of Contents

Acknowledgements

It is a genuine pleasure to express my deep sense of thanks and gratitude to Thuy Le Toan, my supervisor extraordinaire, who made these 3 years of thesis at CESBIO happen in the most enjoyable and motivational way. Without her help, inspiration, expertise, and encouragement, I would not be where I am today and this thesis would never have happened. Thank you very much for giving me so many wonderful opportunities!

I am extremely thankful to Mehrez Zribi for agreeing to be my administrative thesis director, for his great support and timely suggestions, with kindness and lots of encouragement throughout my thesis. I would like to thank Agnès Bégué, Francesco Mattia, Laurent Polidori, Nicola Baghdadi, and Jérôme Helbert for agreeing to be reviewers and examiners of this thesis, and especially for their relevant proofreading, valuable comments and enthusiasm for the manuscript and for the defense.

This thesis has been funded by Telespazio France and ANRT. I am very grateful to a number of people from Telespazio, particularly Jérôme Helbert, Christelle Barbey, and Guevara Sandrine who helped me coordinate my thesis in the best possible manner.

I would like to thank the many people with whom I had great international collaborations during my thesis. A special thanks goes to colleagues from AGS (Applied GeoSolutions, USA), particularly Williams Salas and Nathan Torbick for their great support and guidance me to carry out the DNDC modeling within the limited time; colleagues from IRRI (International Rice Research Institute, Philippines): Tri Deri Setiyono, Alice Laborte, Emma Quicho for helping me complete the work with the ORYZA2000 model. A sincere thanks goes to Arai Hironori, who has provided me with in-situ data for those models simulations.

I would also like to thank many friends and colleagues at CESBIO where it has been my pleasure and honor to work for the last 5 years. My sincere thanks to Juliette, Charlotte, Béatriz, Emilie and many other colleagues for the nice time we shared with each other. A special thanks goes to the BIOMASS team for their continuous support and encouragement. In particular Alexandre, Ludovic, Stéphane, Thierry, I appreciate all their contributions of time and ideas to make my PhD experience productive and stimulating.

I wish to thank many other people for all the emotional support, camaraderie, entertainment, and caring they provided. A special appreciation is due to Caroline and

Abstract

Rice is the primary staple food of more than half of world's population and plays an especially important role in global economy, food security, water use and climate change. The objective of this thesis was to develop methods for rice monitoring based on Sentinel-1 data and to effectively use the mapping products in various applications concerning food security and global environment.

Specifically, the study aims at providing tools for observation of the rice cultivation systems, by generating products such as map of rice planted area, map of rice start-of-season and phenological stages, and map of rice crop intensity, together with rice crop parameters such as category of rice varieties (long or short cycle), and plant height. The information to be provided is necessary for the estimation of crop production, and for the management of rice ecosystems at the regional scale. We also investigated on how the products derived from EO Sentinel-1 data can be integrated in process-based models for rice production estimation and methane emission estimation.

The test region is one of the world's major rice regions: the Mekong River Delta, in Vietnam. This region presents a diversity in rice cultivation practices, in cropping density, from single to triple crop a year, and in crop calendar.

The first step was to understand the temporal variation of the backscatter Sentinel-1 backscatter of rice fields, at VH and VV polarizations. For this purpose, in-situ data have been collected on 60 fields during 2 years, for the 5 rice seasons. It was found that backscatter time series of rice fields show very specific temporal behavior, with respect to other land use land cover types. The temporal and polarization variations of the rice backscatter have been interpreted with respect to physical interaction mechanisms to relate the backscatter dynamics to the key phenological stages, when the plants change its morphology and biomass. Because the same trend of temporal curves was observed over 5 rice seasons, it was possible to derive a mean curve to be used in the methodology developed for detecting rice phenology, and deriving information such as the date of sowing, the rice varieties of long and short duration cycle, or plant height, at each SAR acquisition date.

The methods have been developed and applied to the Mekong delta. Products validation provides a good agreement with the reference data sets: 98% in rice/non-rice accuracy, the sowing dates RMSE of about 4 days, plant height RMSE of 7.8 cm, the

long/short variety map has 91.7% accuracy and for phenology, only one season has been processed with good detection rate of 59/60.

Finally, the use of the rice monitoring products as inputs in two process-based models was assessed. The models are ORYZA2000 for rice production estimation and DNDC for methane emission and water demand estimation. Sentinel-1 data retrieved information (sowing date, phenology, long/short variety, plant height) were used as model inputs, giving good agreement with the results making use of ground survey only. Based on the two process models with inputs from Sentinel-1 data, it was possible to have an integrated result on rice yield, water use, and methane emissions. The preliminary results show a good potential for the optimization of water management in rice fields in order to reduce water use and GHG emission, without reducing the yield.

To achieve the objective which is the effective use of Sentinel-1 data for rice monitoring for food security and global environment, more works need to be done concerning the consolidation of the rice monitoring method development and the integration of Sentinel-1 derived information in models aiming at estimating and predicting rice production, methane emission and water use.

Résumé

Le riz est la principale denrée de plus de la moitié de la population mondiale et joue un rôle particulièrement important dans l'économie mondiale, la sécurité alimentaire, la consommation d'eau, et le changement climatique. L'objectif de cette thèse consistait à développer des méthodes pour le suivi du riz basées sur des données Sentinel-1 ainsi qu'a utiliser les produits de cartographie obtenus dans diverses applications portant sur la sécurité alimentaire et l'environnement mondial.

Plus spécifiquement, l'étude a pour but de fournir des outils pour observer la culture du riz, en produisant la cartographie des surfaces cultivées, celle des stades phénologiques de la plante comprenant le début de la saison, celle des deux principales catégories de variétés de riz à cycle court et cycle long, la hauteur de la plante, et la carte annuelle du nombre de récoltes de riz par an. Ces informations sont nécessaires à l'estimation de la production du riz, et à la gestion des cultures à l'échelle régionale. Nous étudions aussi l'intégration des produits ainsi développés dans un modèle de processus destinés à estimer le rendement du riz, et un modèle permettant la dérivation de l'émission du méthane et le volume d'eau nécessaire à la culture.

La région test est l'une des régions rizicoles majeures à l'échelle mondiale, qui est le Delta du Mékong, au Vietnam. Cette région est caractérisée par une grande diversité de pratiques agricoles, du nombre de cultures du riz par an, et dans les calendriers des récoltes.

La première phase du travail est la compréhension de la variation temporelle des valeurs de rétrodiffusion radar de Sentinel-1, en polarisation VH et VV. Pour cela, des données de terrain ont été collectées sur 60 champs, sur 5 saisons de riz pendant 2 ans. Les variations temporelles des mesures radar ont été interprétées en fonction de la croissance des plantes le long des stades phénologiques. Les mêmes courbes caractéristiques observées lors des 5 saisons ont suggéré l'utilisation d'une courbe 'type' dans le développement des méthodes pour fournir les produits requis.

Les résultats obtenus sur le Delta du Mékong ont été validés à l'aide des données terrain de référence, et sont très satisfaisants : 98% de précision pour la carte riz/non riz, une RMSE de 4 jours pour la date de semis, une RMSE de 0.78 cm pour la hauteur de plante, 91,7% de précision pour la distinction entre deux types de riz (cycle court et cycle long), et 98% de précision sur l'estimation du stade phénologique.

Enfin, nous avons évalué l'utilisation de ces produits issus de données Sentinel-1 dans le modèle ORYZA2000 destiné à estimer le rendement du riz, et dans le modèle DNDC destiné à estimer le volume d'eau nécessaire à la culture, ainsi que l'émission de méthane par les rizières. Les résultats, préliminaires, montrent le bon potentiel de l'approche pour fournir le rendement, le bilan d'eau, et les taux d'émission de méthane sur les champs de riz considérés. Cette approche permettrait de faire des analyses de sensibilité, par exemple pour optimiser la gestion d'irrigation afin de réduire la consommation d'eau et l'émission de méthane, tout en préservant le rendement du riz.

Ces travaux, qui démontrent le potentiel des données Sentinel-1 pour le suivi du riz à large échelle, seront à compléter afin de réaliser des applications effectives opérationnelles. Il s'agira de renforcer les méthodes et de les tester sur différents systèmes rizicoles, et de poursuive l'étude sur l'intégration de ces produits de télédétection dans les modèles permettant d'évaluer la productivité, les besoins en eau et les émissions des gaz à effet de serre des rizières.

List of Tables

List of Figures

<div align="right">

Chapter 1

Introduction

</div>

Contents

1.1.   Importance of rice

Rice is the primary staple food of more than half of world's population and plays an especially important role in global economy, food security, water use and climate change. In 2016, 754.6 million tons of world rice production were estimated over 166 million ha of world rice production area (FAO, 2017), making it the second most-produced cereal after maize (825 million tons of maize), the second after wheat in cultivated areas (215 million ha of wheat) (Prospects and Situation, 2018). Worldwide, more than 3.5/7.6 billion people depend on rice for more than 20% of their daily calorie intake. Moreover, rice cultivation is the principal activity and source of income for more than 144 million farm households in the world, a majority of those in low-income and developing countries (IRRI, 2010). Figure 1 shows that rice is the main crop for most countries in Asia where over 90% of the world's rice crop is produced and consumed.

The main crops in every country in the world
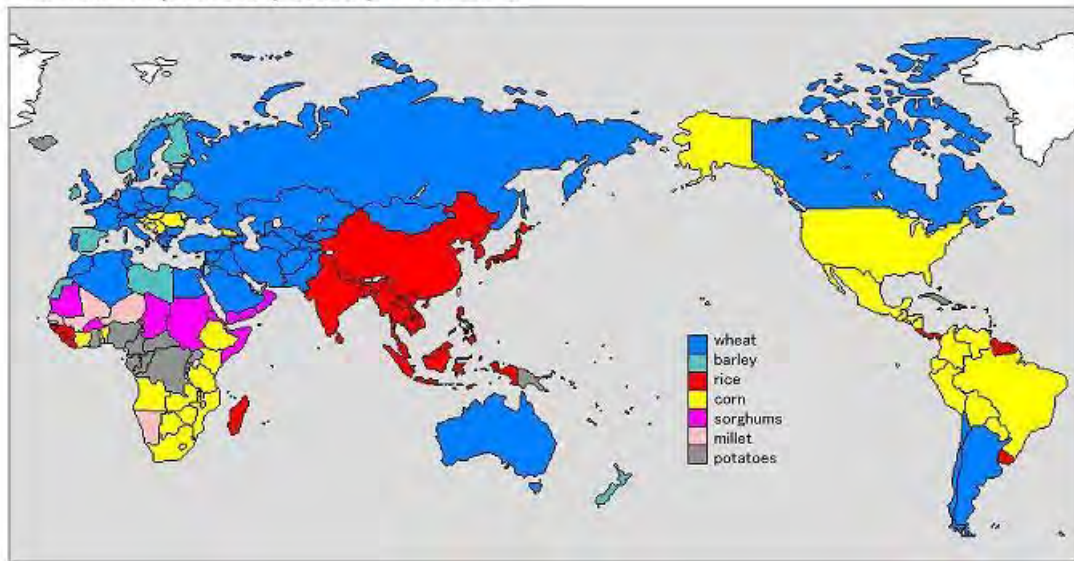
Figure 1. Main crop with the maximum harvested area in every country in the world (Source: FAOSTAT, 2004).

At the global scale, rice consumption was found to increase steadily as shown in Figure 2, because increases in population have kept overall demand on the rise, despite the tendency for per capita rice consumption to decline. Figure 2 also shows that the rice production exceeded consumption up to 2014-2015, and since then, production and consumption are of the same order. It is noted that the inter-annual variation of the production can be significant.
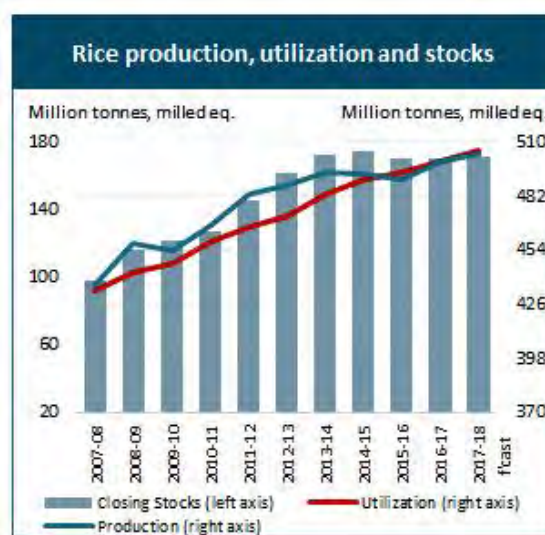
Figure 2. 2007-2018 variation of world rice production, rice utilization, and stocks (in Million tons) (source: FAO, 2018).

Eventually, with the extremely rapid growth of population, rice production will face a challenge of attaining rice self-sufficiency and food security. By 2035, world human population is expected to reach around 9 billion, whereas recent estimates indicate that to meet the projected demand, global rice production will have to increase by 78% from its 2010 levels, as illustrated in Figure 3.
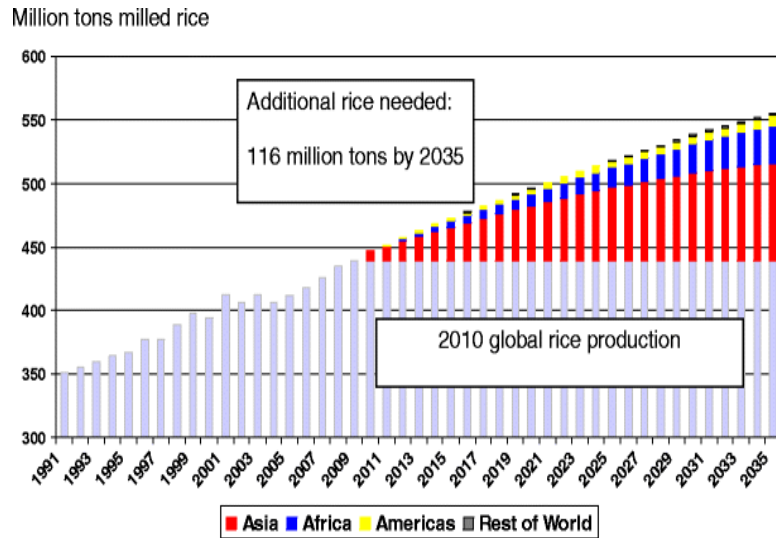
Figure 3. Projection of the additional rice needed by 2035, as compared to the 2010 level (Seck *et al.*, 2012).

Milled rice: rice with the husk and the bran layers removed to produce white rice for consumption. For most varieties, around 70% of milled rice is produced from rough rice.

On the other hand, rice agriculture is strongly linked to environmental issues from water management to climate change. Firstly, rice is a very sensitive cereal crop which is seriously affected by the adverse impacts of climate change. In the last decade, rice has become increasingly threatened by the effects of drought. Drought stress greatly influences the growth duration, but also leads to damages during reproductive stages of the rice crop, especially during flowering. Moreover, in the humid regions of Southeast Asia, there are many hectares that are technically appropriate for rice production but are left uncultivated or are grown with very low yields because of salt intrusion which affect the soils. Low water levels in Viet Nam's Mekong River Delta, the country's rice bowl, have resulted in an inward flow of salt water, increasing the salinity in the river water and endangering rice paddies (Redfern et al., 2015). In addition, the increase in the number of floods and some of the most devastating cyclones are also directly affected to rice production. Reversely, rice fields are a major generator of methane and nitrous oxide, responsible for 25% of the total budget of global methane emissions from agriculture (Saunois *et al.*, 2016).

3

In summary, it is evident that rice agriculture is globally significant in terms of food security, water resources, and climate change.

In this context, comprehensive, reliable and timely information on rice crop are highly needed for national food security, in terms of risk occurrence and annual production projections, with potential impact on political stability. With respect to global environment, accurate information is needed on the spatial distribution of rice fields, on water resource management and greenhouse gas emissions, to assess the role of rice agriculture in the global carbon and water cycle.

1.2. State of the art in the use of remote sensing for rice monitoring

The use of remote sensing imagery for rice mapping and monitoring has been demonstrated in several studies using different sensors of various spectral characteristics and spatial resolutions. Both optical and microwave remote sensing systems offer practical means for rice mapping and monitoring in different parts of the world.

Optical satellite sensors provide multi-temporal and multi-spectral reflectance data over croplands that can be used for deriving time-series of vegetation indices (VIs) in the spectral range 0.4 to 2.5 μm. The reflectance spectrum of a rice crop canopy is the result of a complex relationship between its biophysical and biochemical attributes. The most commonly applied optical sensors include Landsat, SPOT-VGT, MODIS, etc. to explore the ability of optical remote sensing instruments to identify rice areas (Xiao et al., 2005, Nguyen et al., 2012, Son et al.,2013, Clauss et al., 2018, Singha et al., 2017). However, cloud cover exceeding 70% of the time in most rice growing region in the tropics tropical regions limits the use of high resolution optical data (of the order of 10-30 m). On the other hand, coarse spatial resolution data (i.e., in the range 500 m to 1 km) with higher temporal resolution are less adapted to rice cropland monitoring at local scale where fields are not uniform and whose size is of the order of 1 ha or smaller (Bellon et al., 2017).

Microwave remote sensing techniques have the advantage of their all-weather capability, and Synthetic Aperture Radars (SAR) can provide high resolution data. Studies on rice fields monitoring using SAR systems have been carried out since late 80s. These studies have been conducted to assess the potential of SAR systems operating at different frequency bands for rice cropland monitoring, including L-band (Wang et al., 2005), C-band (Le Toan et al., 1997, Bouvet et al., 2009, Lam-Dao et al., 2009, Bouvet et al.,2011, Nguyen et al., 2015, Nguyen et al., 2016), and X-band (Lopez-Sanchez et al., 2011, Fan et al., 2011,

4

Inoue and Sakaiya 2014a). In a comprehensive study conducted using ground based experimental data by Inoue at al. (2002), the relations of radar backscatter at various frequencies (Ka-, Ku-, X-, C-, L-) polarization and incidence angles with rice biophysical parameters have been analysed.

However, those demonstration studies have not yet resulted in effective applications. One of the major obstacles is the lack of systematic, high resolution and cost effective SAR data. According to the studies, monitoring of rice from remote sensing requires cost effective SAR data at high resolution (10-30 m) and temporal resolution of the order of 10 days. With the launch of Copernicus Sentinel-1 satellite in 2014 (Sentinel 1A) and 2016 (Sentinel 1B), the required data, which are systematically and globally acquired every 12 (or 6) days, widely accessible at no cost, are now available.

Mapping the rice areas extent using SAR data has been widely demonstrated. In many studies, rice fields were identified by their low backscatter at the start of season where the fields are flooded (Shao et al., 2001, Nelson et al., 2014, Nguyen et al.,2016, Torbick et al., 2017). This is no longer adapted to rice fields with new planting practices of direct sowing on wet soil. Le Toan et al., (1997) found that the identification of rice fields cannot be conducted properly by employing standard classification methods based on the similarity in the image intensity of rice fields. Temporal change measurement methods were developed for the mapping of rice fields based on the temporal variation of the SAR signal in order to cope with inter-field differences (Le Toan et al., 1997, Chen et al., 2007, Liew et al., 1998, Ribbes et al., 1999, Bouvet et al., 2011) using ERS-2, RADARSAT-1, and ENVISAT/ASAR. The polarization behavior of rice fields resulting from the vertical structure of rice plants during the vegetative stage has been exploited in the use of polarization ratio (e.g. HH and VV of ENVISAT/ASAR) (Wang et al., 2005, Bouvet et al., 2009, Lam Dao et al., 2009, Lopez-Sanchez et al., 2010). Other use of both temporal and polarization variation of rice fields has been demonstrated, for example using a Wishart distribution-based multi-temporal classifier of ENVISAT-ASAR APS or a combined entropy decomposition and support vector machine (EDSVM) method using RADARSAT-1 data (Tan et al., 2011) (as described in the review of Kuenzer et al., 2013 and Mosleh et al., 2015).

A number of research efforts have been directed towards the detection of **rice growth stage**. The works have been realized with multi-temporal C-band SAR using ERS, RADARSAT-1 or ASAR (Inoue et al., 2014, Chakraborty et al., 1997, Inoue et al., 2002). To detect the start of the season (SoS), which corresponds to the sowing or transplanting

date, has been estimated in several studies, either as a mere step in the rice mapping process (Inoue et al., 2014a) or as a self-standing product (Liew *et al.*, 1998). Other studies use the polarimetric SAR data to detect phenology stages, these studies rely on the fact that the rice plant changes its structure at each phonological stage. This leads to the change in 'polarimetric signature' of rice fields. The studies were conducted by Lopez-Sanchez et al., (2012) in X- and C-band, and by Inoue et al., (2014) using the X- and C-band data from COSMO-Skymed and RADARSAT-2, respectively. Later on, the methods suggested by Vicente-Guijalba *et al.*, (2014), De Bernardis *et al.*, (2015), Nr et al., (2017), and Kucuk et al., (2016) improved the growth stage estimation algorithms using advanced methods such as Kalman filters, particle filters, and Support Vector Machines.

For **rice production estimation**, in most studies, yield data obtained by post harvest ground survey are combined with rice planted area detected by remote sensing to provide rice production (Shao et al., 2001, Ferencz et al., 2004). Other approaches are based on empirical relationships between backscatter temporal data and the final yield to extend the yield estimates over larger area (Prasad et al., 2006, Bolton et al., 2013, Koide et al., 2013, Maki et al., 2017). Despite the encouraging results (94% prediction accuracy), these approaches are difficult to generalize, and they have no prediction capability. Agro-meteorological yield prediction models are important tools to understand the impacts of weather, soil, plant characteristics, and cultural practices on the final yield. Regarding rice yield models, the most important model is ORYZA2000 (Bouman et al., 2001) and later on, different versions are proposed in literature (Li *et al.*, 2017). The models consider the factors impacting the growth rate which are solar radiation, temperature, and cultivar characteristics governing the phenological and morphological development of the plants. Until recently, the use of remote sensing in the model has been addressed through the Leaf Area Index, derived mainly from MODIS data (Doraiswamy et al., 2005). The SAR data have been used for localization of rice pixels, and in a recent paper (Setiyono *et al.*, 2018), for deriving the Start of Season as an input to the ORYZA model.

For **methane emission estimation** from rice fields, during the past two decades, many empirical and physical models have been developed to predict GHG emissions from rice fields. In a number of empirical models, the regression relationships between CH_4 emission rate and rice biomass or yield were used to estimate CH_4 production (Sinha et al., 1995, Kern et al., 1997, Anastasi et al., 1992, Zhang et al., 2011). Although these empirical approaches were easy to use, the accuracy and precision of estimated results could not be ensured, and the variation in emissions at regional scale also could not be explained

reasonably. The major models that are able to simulate CH_4 production include MEM (Cao et al., 1995a), MERES (Matthews et al., 2000), InfoCrop (Aggarwal et al., 2004), and DNDC (Li et al., 1992a). Among the candidate models, DNDC has been tested for the rice paddies in China and other Asian countries (Fumoto et al., 2008, 2010; Kai et al., 2010; Zhang et al., 2011; Katayanagi et al., 2017). As a process-based biogeochemical model, DNDC is able to track carbon (C) and nitrogen (N) cycles in agro-ecosystems driven by both the environmental factors and management practices. Model simulations have been conducted at experimental fields and compared with in situ measurements of methane emissions (Salas et al., 2010; Torbick, Salas, et al., 2017). Extension to emissions at regional scale has been done by assigning the same emissions to rice fields identified at the region using remote sensing.

For rice production estimation and prediction, and for methane emissions estimations, research still needs to be conducted on the effective use of remote sensing data as inputs or validation data in rice yield prediction and methane emission models.

1.3.   Research objectives and thesis structure

The objective of this PhD thesis is to exploit the time series of Sentinel-1 SAR data for rice mapping and monitoring. This thesis also aims to further apply the results of rice mapping and monitoring using SAR data, as inputs for models of rice production and methane emission estimations. The core of this work is to develop and test methods based on the knowledge of the temporal development of the rice plants and rice fields under different conditions, and on the understanding of the related temporal variation of the radar backscatter. The purpose here is not to derive the best possible rice map at each site through intensive calibration or large-scale fieldwork, but to introduce a simple approach that is robust, repeatable and suitable for rapid rice mapping over large extents with cost-effective field work. The overarching goal is to demonstrate that SAR-based operational mapping of rice crops across a diverse range of environments is possible based on the increasing availability of multi-temporal SAR data. The thesis is a timely contribution to remote-sensing applications for food security, since it presents a method to derive sufficiently accurate rice area maps under different conditions that are typical of the diversity of rice environments in Asia. The thesis is structured in 8 chapters, including introduction and conclusion.

The importance of rice in food security, methane emission and water consumption were presented in this chapter in order to determine the information requirements for rice monitoring with respect to rice productions and methane emissions. The state of the art concerning the rice mapping and monitoring using remote sensing and applications is also presented in this chapter.

Next, **chapter 2** gives an overview of the rice in the world including socio economical aspect, rice ecosystems and its growing cycle, rice productivity and methane emissions from rice cultivation.

Then, **chapter 3** describes our study area and the data sets used through this thesis. The first part presents the general characteristics of the study site and experimental studies. In the second part, the remote sensing data set characteristics and data available for this research as well as data pre-processing chain are presented.

Chapter 4 consists in SAR data analysis as a function of ground data, and then physical interpretation of the temporal and polarization behavior of the radar backscatter response on rice canopy. This chapter is concluded by derivation of indicators for rice mapping and monitoring. Based on the analysis and interpretation results, **chapter 5** describes the methodologies developed for the mapping of rice area, rice varieties, rice cropping intensity and rice parameters retrieval (sowing date, phenological stage and plant height).

Products derivation is presented in **chapter 6** together with products validation and accuracy assessment. At last, the applications of the rice monitoring products are described in the **chapter 7**. For that, two process-based models are used in this thesis for rice yield estimation and methane emission using the mapping products developed in this research as direct input parameters. To conclude the chapter, some discussion and conclusion-way forward are presented in order to improve the performances of the models.

Finally, **Chapter 8** concludes this thesis by summarizing and discussing the main finding in this thesis and dedicates the perspectives for future researches in relation to this thesis.

<div align="right">

Chapitre 1

Introduction

</div>

Contents

1.1.   L'importance du riz

Le riz est la principale denrée de plus de la moitié de la population mondiale et joue un rôle particulièrement important dans l'économie mondiale, la sécurité alimentaire, la consommation d'eau, et le changement climatique. En 2016, la production mondiale de riz a été estimée à 754,6 millions de tonnes sur 166 millions d'hectares de surface cultivée (Up, 2017), ce qui en fait la deuxième céréale la plus produite après le maïs (825 millions de tonnes), et la deuxième en termes de surface cultivée après le blé (215 millions d'hectares) (Prospects and Situation, 2018). Plus de 3,5 sur 7,6 milliards d'individus à travers le monde dépendent du riz pour plus de 20% de leur apport calorique journalier. De plus, la culture du riz est l'activité principale et la première source de revenus pour plus de 144 millions de foyers dans le monde, la plupart dans des pays en développement et à faibles revenus (IRRI, 2010). La Figure 1 montre que le riz est la culture principale pour la plupart des pays d'Asie, où plus de 90% de la production de riz est réalisée et consommée.
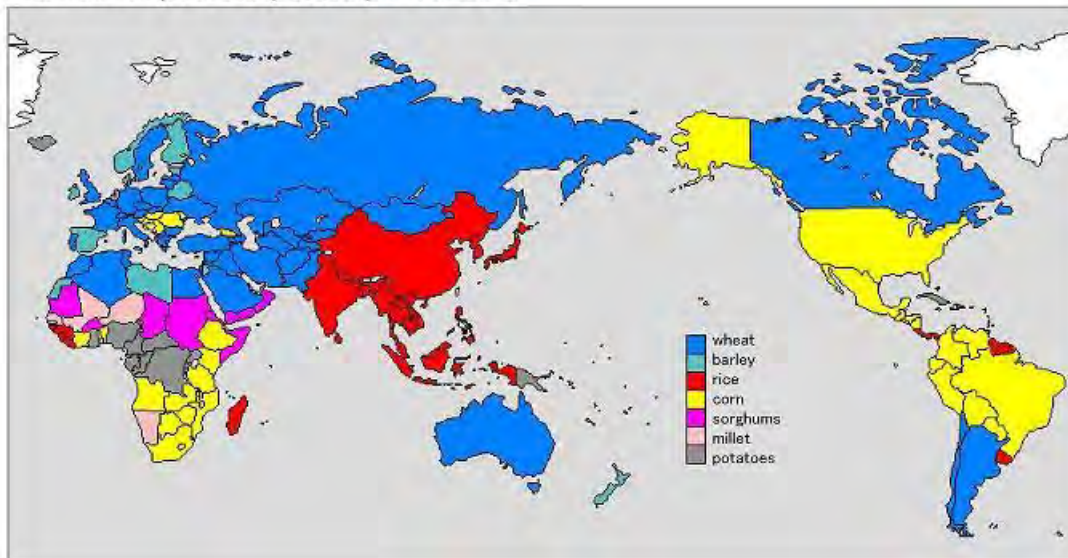
Figure 1. Culture avec la plus grande surface cultivée par pays (Source : FAOSTAT, 2004).

Comme le montre la figure 2, il a été observé au niveau mondial que la consommation de riz est en augmentation constante, ce qui est dû au fait que la croissance de la population a provoqué une hausse de la demande globale, malgré la tendance décroissante de la consommation de riz par personne. La figure 2 montre également que la production de riz était plus importante que la consommation jusqu'à 2014-2015, et que les deux quantités sont depuis du même ordre de grandeur. Il est également observé que la variation interannuelle de production peut être considérable.
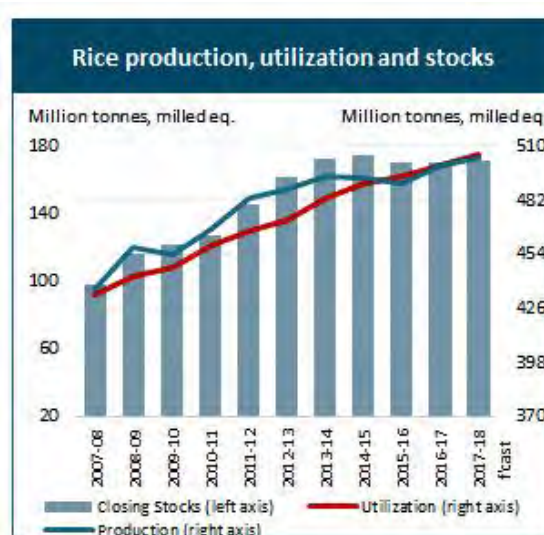
Figure 2. Evolution de la production de riz, de l'utilisation du riz produit, et des réserves de riz (en millions de tonnes) de 2007 à 2018 (Source : FAO, 2018).

À terme, étant donné la croissance importante de la population mondiale, la production de riz risque de ne plus être suffisante pour assurer les besoins alimentaires mondiaux. D'ici 2035, il est attendu que la population mondiale atteigne environ 9 milliards d'individus, et des estimations récentes indiquent que la production mondiale de riz devra augmenter de 78% par rapport à son niveau de 2010 pour satisfaire la demande prévue, comme indiqué sur la figure 3.
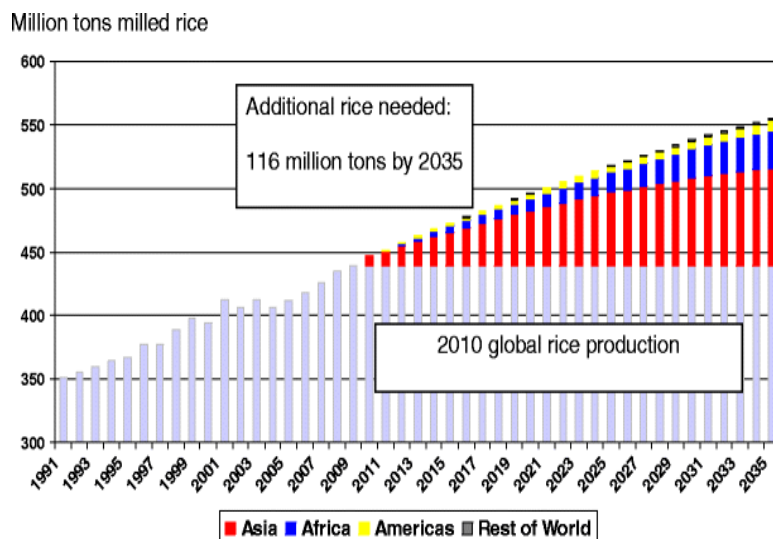
Figure 3. Prévision de la quantité de riz additionnelle nécessaire jusqu'en 2035, par rapport au niveau de 2010 (Seck *et al.*, 2016).

Milled rice : riz dont l'enveloppe et le son ont été retirés pour produire du riz blanc propre à la consommation. Pour la plupart des variétés, environ 70% de milled rice sont produits à partir du riz brut.

L'agriculture du riz est également fortement liée à des défis environnementaux de la gestion de l'eau au changement climatique. Tout d'abord, le riz est la culture céréalière la plus sensible aux effets néfastes du changement climatique. Dans la dernière décennie, le riz s'est vu de plus en plus menacé par les effets de sécheresse. Le stress hydrique provoqué par la sécheresse non seulement influence grandement la durée de croissance du riz, mais provoque également des dommages pendant le stade reproductif de la culture de riz, particulièrement pendant la floraison. De plus, dans les régions humides du Sud-Est de l'Asie, il existe de nombreux hectares de terrain en théorie appropriés à la production de riz, mais non cultivés ou alors avec des rendements très faibles à cause de la salinité des sols. Les basses altitudes de la région du Delta du Mekong vietnamien, le 'bol de riz' du pays, ont eu pour conséquence un afflux d'eau salée vers l'intérieur des terres, augmentant ainsi la salinité de l'eau de rivière et mettant en péril les rizières (Redfern et al., 2015). En outre, l'augmentation du nombre d'inondations et de typhons particulièrement violents affecte

directement la production de riz. Ensuite, les champs de riz sont des sources majeures de méthane et d'oxyde nitreux, responsables de 25% du bilan d'émission de méthane de l'agriculture mondiale (Saunois et al., 2016).

En résumé, il est évident que la culture du riz est mondialement très significative en termes de sécurité alimentaire, ressources en eau, et changement climatique.

Dans ce contexte, des informations complètes, sûres, et fréquentes sur les cultures de riz et leur évolution sont grandement nécessaires pour la sécurité alimentaire nationale, en termes de survenance de risque et de prévisions annuelles de production, qui éventuellement pour la stabilité politique du pays. Par rapport à l'environnement mondial, des informations précises sur la distribution spatiale des champs de riz, sur la gestion des ressources en eau, et sur les émissions de gaz à effet de serre, sont nécessaires pour estimer le rôle de la culture du riz dans le cycle mondial d'eau et de carbone.

1.2. Etat de l'art de l'utilisation de la télédétection pour le suivi du riz

L'utilité de l'imagerie satellite dans le suivi et la cartographie de riz a été démontrée dans plusieurs études à l'aide de différents capteurs de caractéristiques spectrales et résolutions spatiales variées. Les systèmes de télédétection aussi bien dans le domaine de l'optique que dans celui des micro-ondes offrent des moyens pratiques pour la cartographie et le suivi temporel des cultures de riz dans des zones variées du globe.

Les capteurs optiques procurent des données de réflectance multi-temporelles et multi-spectrales sur les cultures, qui peuvent être utilisées pour produire des séries temporelles d'indices de végétation dans le domaine spectral compris entre 0,4 et 2,5 µm. Le spectre de réflectance d'un couvert de riz est la résultante d'une relation complexe entre ses attributs biophysiques et biochimiques. Les capteurs les plus utilisés pour estimer la capacité des instruments de télédétection optique à détecter le riz comprennent Landsat, SPOT-VGT, MODIS, etc. (Xiao et al., 2005, Nguyen et al., 2012, Son et al.,2013, Clauss et al., 2018, Singha et al., 2017). Cependant, la couverture nuageuse est présente plus de 70% du temps dans la plupart des zones de culture de riz des régions tropicales (Nelson et al., 2014), et limite l'utilisation de données optiques à haute résolution spatiale (i.e. de l'ordre de 10-30m). Par ailleurs, les données de résolution spatiale plus grossière (i.e. de l'ordre de 500-1000m) mais de résolution temporelle plus élevée sont moins adaptées au suivi de cultures de riz à l'échelle locale pour laquelle les champs ne sont pas uniformes et ont habituellement une taille de l'ordre de 1 hectare ou moins (Bellon et al., 2017).

Les technologies de télédétection micro-onde ont l'avantage de fonctionner quelles que soient les conditions météorologiques, et les Radars à Synthèse d'Ouverture (RSO, ou Synthetic Aperture Radars – SARs) peuvent fournir des données à haute résolution spatiale. Des études sur le suivi des champs de riz utilisant ces systèmes RSO ont été réalisées depuis la fin des années 80. Ces études ont été menées dans le but d'estimer le potentiel des systèmes RSO opérant à différentes bandes de fréquence dans le suivi des cultures de riz, dont la bande L (Wang et al., 2009), la bande C (Le Toan et al., 1997, Bouvet et al., 2009, Lam-Dao et al., 2009, Bouvet et al., 2011, Fan et al., 2011, Nguyen et al., 2015, Nguyen et al., 2016), et la bande X (Lopez-Sanchez et al., 2011, Fan et al., 2011, Inoue and Sakaiya 2014a). Dans une étude exhaustive menée par Inoue et al. (2002) utilisant des données expérimentales de terrain, les relations entre les paramètres biophysiques du riz et la rétrodiffusion radar à différentes fréquences (Ka-, Ku-, X-, C-, L-), polarisations et angles d'incidence, ont été analysées.

Cependant, ces études de démonstration n'ont pas encore mené à des applications concrètes. L'un des principaux obstacles à cet objectif est le manque de données RSO acquises de manière systématique, à haute résolution spatiale, et bon marché. Selon les différentes études réalisées, le suivi des cultures de riz par télédétection requiert des données possédant une résolution spatiale de l'ordre de 10 à 30m, et une résolution temporelle de l'ordre de 10 jours. Avec le lancement des satellites Copernicus Sentinel-1 en 2014 (Sentinel-1A) et 2016 (Sentinel-1B), ces données nécessaires, acquises systématiquement et sur l'ensemble du globe tous les 12 (ou 6) jours, accessibles gratuitement par tous, sont aujourd'hui une réalité.

La **cartographie de l'étendue des zones de riz** via l'utilisation de données SAR a été largement démontrée. Dans de nombreuses études, des champs de riz ont été identifiés par leur faible rétrodiffusion en début de saison quand les champs sont inondés (Shao et al., 2001, Nelson et al., 2014, Nguyen et al.,2016; Torbick et al., 2017). Cette méthode n'est plus adaptée aux champs de riz utilisant de nouvelles pratiques de plantation consistant à semer directement sur du sol mouillé. Le Toan et al. (1997) a observé que l'identification de champs de riz ne peut pas être réalisée correctement en utilisant les méthodes de classification classiques basées sur une supposée similarité de la rétrodiffusion des champs de riz. Des méthodes basées sur la mesure du changement temporel ont été développées pour la cartographie des rizières ; elles utilisent la variation temporelle (plutôt que la valeur absolue à une date donnée) du signal SAR afin de s'affranchir de l'effet des différences de rétrodiffusion d'un champ à l'autre, à partir d'images issues de ERS-2, RADARSAT-1, et

ENVISAT/ASAR (Le Toan et al., 1997, Chen et al., 2006, Liew et al., 1998, Ribbes et al., 1999, Bouvet et al., 2011). Les caractéristiques de polarization des champs de riz, dues aux structures verticale des plants de riz pendant le stade végétatif, ont été exploitées via l'utilisation de rapports de polarization (par exemple HH et VV avec ENVISAT/ASAR) (Wang et al., 2005, Bouvet et al., 2009, Lam Dao et al., 2009, Lopez-Sanchez et al., 2010). D'autres exemples d'utilisation de variation temporelle et polarimétrique des champs de riz ont été proposés, utilisant par exemple un classificateur multi-temporel basé sur la distribution de Wishart appliqué à des données ENVISAT-ASAR APS, ou une utilisation combinée de décomposition d'entropie et de machine à vecteurs de support (EDSVM) à partir de données RADARSAT-1 (Tan et al., 2011) (comme décrit dans les revues de Kuenzer et al., 2013 et Mosleh et al., 2015).

Des efforts de recherche ont été dirigés vers la détection des **stades de croissance du riz**. Ces travaux ont utilisé des données RSO multi-temporelles en bande C des instruments ERS, RADARSAT-1 ou ASAR (Inoue et al., 2014, Chakraborty et al., 1997, Inoue et al., 2002, Boschetti et al., 2009). La détection du début de saison (DdS), qui correspond à la date de semis ou de repiquage, a été présentée dans plusieurs études, soit comme une simple étape du processus de cartographie des rizières (Inoue, Sakaiya and Wang, 2014a), soit comme un produit à part entière (Liew *et al.*, 1998). D'autres études utilisent le RSO polarimétrique pour détecter les stades phénologiques. Ces études reposent sur le fait que la structure de la plante de riz change à chaque stade phénologique, ce qui cause des changements dans la "signature polarimétrique" des champs de riz. Ces études ont été conduites par Lopez-Sanchez et al., (2012) et par Inoue et al., (2014) en bande X et bande C à partir de COSMO-Skymed et RADARSAT-2 respectivement. Par la suite, les méthodes proposées par Vicente-Guijalba et al., (2014), De Bernardis *et al.*, (2015), Nr et al., (2017), and Kucuk et al., (2016) ont amélioré les algorithmes d'estimation des stades phénologiques à l'aide de méthodes avancées telles que les filtres de Kalman, les filtres à particule, et les machines à vecteurs de support.

En ce qui concerne **l'estimation de la production de riz**, dans la plupart des cas, des données de rendement obtenues lors d'enquêtes de terrain après la récolte sont combinées avec les surfaces plantées en riz détectées par la télédétection pour fournir la production de riz (Shao et al., 2001, Ferencz et al., 2004). D'autres approches sont basées sur des relations empiriques entre des données temporelles de rétrodiffusion et le rendement final pour étendre l'estimation de rendement sur de grandes régions (Prasad et al., 2006, Bolton et al., 2013, Koide et al., 2013, Maki et al., 2017). Malgré des résultats encourageants (94% de

précision dans la prédiction), ces approches sont difficilement généralisables et n'ont pas de capacités prédictives. Les modèles agro-météorologiques de prédiction de rendement sont des outils importants pour comprendre l'impact du climat, du sol, des caractéristiques des plantes, et des pratiques culturales sur le rendement final. Parmi ces modèles de rendement de riz, le plus important est ORYZA2000 (Bouman et al., 2001), différentes versions ayant été proposées ensuite dans la littérature (Li *et al.*, 2017). Le modèle considère les facteurs qui impactent le taux de croissance, comme le rayons solaire, la température, et les caractéristiques du cultivar qui pilotent le développement phénologique et morphologique des plantes. Jusqu'à récemment, l'utilisation de la télédétection dans le modèle a été effectué au travers de la surface foliaire (Leaf Area Index), dérivé principalement de données MODIS (Doraiswamy et al., 2005). Les données SAR ont été utilisées pour la localisation des pixels de riz, et dans un article récent (Setiyono *et al.*, 2018), pour estimer la date de Début de Saison utilisée comme entrée du modèle ORYZA.

Concernant **l'estimation des émissions de méthane** des rizières, dans les deux dernières décennies, de nombreux modèles empiriques et physiques ont été développés pour prédire les émissions de gaz à effet de serre par les rizières. Dans certains modèles empiriques, les relations de régression entre le taux d'émission de CH_4 et la biomasse, ou le rendement du riz, ont été utilisés pour estimer la production de CH_4 (Sinha et al., 1995; Kern et al., 1997; Anastasi et al., 1992). Bien que ces relations empiriques soient faciles à utiliser, l'exactitude et la précision des estimations ne peuvent être assurés, et la variation des émissions à l'échelle régionale n'a pas pu être expliquée de manière raisonnable. Les principaux modèles capables de simuler la production de CH4 incluent MEM (Cao et al., 1995a), MERES (Matthews et al., 2000), InfoCrop (Aggarwal et al., 2004), et DNDC (Li et al., 1992a). Parmi les modèles candidats, DNDC a été testé sur les rizières en Chine et dans d'autres pays d'Asie (Fumoto et al., 2008, 2010; Kai et al., 2010; Zhang et al., 2011; Katayanagi et al., 2017). En tant que modèle bio-géochimique basé sur des processus, DNDC est capable de simuler les cycles du carbone (C) et de l'azote (N) dans les agro-écosèmes déterminés par les facteurs environnementaux et les pratiques de gestion. Des simulations ont été conduites sur des champs expérimentaux et les résultats ont été comparés à des mesures *in situ* d'émissions de méthane (Salas et al., 2010; Torbick, Salas, et al., 2017). L'extension à des émissions à l'échelle régionale a été faite en assignat les mêmes taux d'émissions aux champs de riz identifiés dans la région à partir de la télédétection.

L'estimation et la prédiction de la production de riz et l'estimation des émissions de méthane nécessitent de continuer la recherche sur l'utilisation effective des données de télédétection

comme entrées ou données de validation dans les modèles de prédiction de rendement de riz et d'émissions de méthane.

1.3.   Objectifs de recherche et structure du manuscrit

Ce travail de thèse a pour objectif l'utilisation de séries temporelles RSO de Sentinel-1 pour la cartographie et le suivi de rizières. De plus, cette thèse vise à évaluer l'apport des résultats de cartographie et de suivi de la culture du riz à partir des données RSO comme données d'entrée pour la calibration de modèles de rendement et d'émission de méthane. Les travaux menés ont principalement consisté à développer et tester des méthodes d'identification des rizières et de suivi du développement du riz dans différents contextes ainsi qu'à la compréhension de la variabilité temporelle de la rétrodiffusion radar en lien avec ces questions. Plutôt qu'une approche de calibration ardue ou de collecte de données sur des terrains très étendus, qui permettraient de générer des cartes complètement exhaustives de rizières mais à un coût très élevé, ces travaux visent la recherche d'alternatives simples, robustes, reproductibles et applicables sur de larges étendues à moindre coût et moyennant des relevés de terrain limités. L'objectif sous-jacent consiste donc à évaluer l'apport de données RSO pour des applications opérationnelles de cartographie des rizières pour une large diversité de contextes, apport que l'on suppose déjà très pertinent étant donnée notamment la disponibilité croissante de données RSO multi-temporelles. La thèse présentée dans ce manuscrit constitue une contribution très attendue en télédétection appliquée au maintien de la sécurité alimentaire. Elle présente en effet une méthode robuste et précise pour la cartographie des rizières dans différents contextes de production représentatifs de la diversité des systèmes de production rizicoles d'Asie.

Le manuscrit est organisé en huit chapitres, qui incluent une introduction et une conclusion générale. L'importance et les enjeux relatifs à la culture du riz en termes de sécurité alimentaire, d'émissions de méthane et d'utilisation des ressources en eau ont été présentés dans ce chapitre, afin d'identifier les attentes relatives à l'observation des surfaces de production du riz et de leurs émissions de méthane. Il présente aussi un état de l'art concernant les méthodes de télédétection permettant la cartographie et le suivi des rizières ainsi que leurs applications.

Ensuite le **chapitre 2** établit une vue d'ensemble des connaissances et questions relatives à la culture du riz dans le monde. Il couvre notamment ses aspects socio-économiques, agronomiques et environnementaux, avec une attention particulière portée à

la question des émissions de méthane, et rappelle les différents stades du cycle de croissance du riz.

Le **chapitre 3** présente alors le site d'étude qui a été sélectionné et le jeu de données qui a été utilisé au cours de cette thèse. Dans une première sous-partie, les caractéristiques générales du site d'étude et de l'approche expérimentale sont données. Dans une seconde sous-partie, le jeu de données de télédétection disponible et utilisé dans la suite des travaux est décrit ainsi que la chaine de pré-traitement qui a été implémentée.

Le **chapitre 4** rapporte tout d'abord une analyse de données RSO comme proxy de l'état de la surface puis une interprétation physique de la variabilité temporelle ainsi que de polarisation du signal rétrodiffusé par les rizières. Dans une dernière partie, ce chapitre présente une méthode pour le calcul de différents paramètres destinés à la cartographie et le suivi des parcelles en riz. Sur la base de ces résultats, le **chapitre 5** décrit les méthodes développées permettant la cartographie des surfaces en riz, des variétés de riz, de la densité du couvert, ainsi que l'extraction de certains paramètres (dates de semis, stades phénologiques, hauteur du couvert).

L'obtention de ces produits est présentée par le **chapitre 6** ainsi que leur validation et l'estimation de leur précision. Puis le **chapitre 7** décrit les différentes applications à partir des produits de suivi du riz. Deux modèles agronomiques de croissance du riz ont notamment été utilisés au cours de la thèse pour estimer les rendements en riz et les émissions de méthane. Dans ce but, les produits cartographiques générés par télédétection ont été utilisés directement comme paramètres d'entrée de ces modèles. Ce chapitre s'achève par une discussion et conclusion concernant les futurs développements qui permettront d'améliorer les performances de modélisation.

Enfin, le **chapitre 8** de conclusion générale résume et discute les principaux résultats de la thèse et propose des perspectives de recherche qui mériteront d'être poursuivies.

<div align="right">

Chapter 2

Rice in the world

</div>

Contents

This chapter gives an overview of the rice in the world including rice cultural practices, rice ecosystems and its growing cycle, rice productivity and methane emissions from rice cultivation. The information of rice growing system in the world is important to determine the needs and requirements for rice mapping and monitoring using Earth observation data.

2.1. Introduction

As described in the first chapter, rice is the world's most important food crop. It is harvested from over 166 million ha in more than 100 countries (Laborte *et al.*, 2017). Rice is grown in diverse cropping systems and various environmental conditions. These can go from single crop systems with both rainfed and irrigated in temperate and tropical climates, to multiple crop systems (2 or 3 crops annually) in tropical irrigated areas where rice is intensely cultivated.

Statistics exist and can be used to derive information on the rice area and production by region and country globally (e.g., FAOSTAT, USDA). However, for some countries, the

information on rice production distribution is only available at the national level, and if the data is available at a finer scale, the statistics are mostly given by year. Hence, deriving rice area and production information within the year is a more complicated issue. Yet, this information is very valuable for several reasons. Firstly, when linked to a crop calendar it can contribute to the analysis of the variations in rice production, both spatially and temporally. This can add insight to food security, for example by coupling this data with information on climatic events and available rice stocks, in order to estimate the variations of the rice supply and stimulate the continuous availability of rice during the year. Additionally, the information of the rice cultivation areas and its calendar is important to estimate the potential biotic and abiotic stresses than can happen during the growing of rice, as well as the impact of climate change and new technologies on rice yield and production. The reasons cited above highlight the value of good rice production and area estimations, coupled to a precise and comprehensive rice crop calendar.

Global rice crop calendar exists (Sacks et al., 2010, FAO, 2006, Portmann et al., 2010), such as MIRCA 2000, which is monthly, gridded, and covers both irrigated and rainfed rice, but they are not adequate for rice areas that are cultivated several times during the year. Indeed, some regions with two seasons of rice annually have data for only one in those calendars. Additionally, they allow a maximum of only two seasons, when some of the most important rice growing regions of the world (e.g. Bangladesh, South-Vietnam, some parts of China and India) have three distinct cropping seasons.

2.2. Cultural practices

Although rice can be found all over the world, rice needs high solar radiation levels, relatively favorable temperatures and water and is therefore grown mainly in the tropics and subtropics (temperature criterion), and in humid and sub-humid areas. According to the International Rice Research Institute (IRRI), the three main growth environments defined by the hydrological practices as followed:

(1) Irrigated rice implies complete water control by irrigation and drainage systems. Traditionally, a water layer of about 2 to 20 cm is maintained for most of the season to avoid the use of chemical weed killers. This type of rice cultivation is the dominant system, although it is only a little more than half of the cultivated area, it contributes 75% of world production in rice. Depending on when and how much water is available, irrigation may be

applied as a supplement in the rainy season and/or during the dry season. With adequate irrigation water, two or even three crops of rice can be produced in a year.

In addition, farmers are willing to apply more purchased inputs like fertilizers typically resulting in higher yields. These and other factors help make the irrigated rice ecosystem the most productive.

Table 1. Three main growth environments

Rice Ecosystem	Total production area (%)	Total rice production (%)
Irrigated lowland	55-60	≈75
Rainfed lowland	≈30	≈20
Rainfed upland	≈10	<5

(2) Rainfed lowland rice: Rainfed lowland rice areas lack water supply and/or water control for irrigation. As a result, they are more subject to flooding and drought than irrigated production areas. Salinity can be a problem in coastal areas where sea water submerges the rice production area but irrigation water is unavailable for salt removal. Different varieties and management systems are used compared to the irrigated ecosystem to help manage some of these risks. Drought and/or floods often limit yield levels in this cultural system. With 31% of cultivated areas, rainfed lowland growing rice represents 21% of world production, mostly in Thailand (72.2% of the rice area), Nepal (60.6%), Myanmar (52.8%) and Bangladesh (43.1%).

(3) Upland rice is produced without irrigation. It can be found in a range of environments from low-lying valley bottoms to steep sloping lands with high runoff. This type of culture, in which the fields are not flooded, represents only a very small proportion of world production (around 4%), for an area of 9%.

(4) Deep water or floating rice, where the water is supplied by river floods or by the tides that touch the mouths of the great deltas. Yields, dependent on the weather, remain low. With 8% of cultivated areas, this type of rice provides only 3% of world production, and is gradually being replaced by irrigated rice when hydraulic developments are realized.

In summary, the majority of rice in the world is irrigated rice (52% in area) and lowland rainfed rice (31%). In both cases, the rice fields are covered with a layer of water

during most of their growth cycle in traditional cultural practices. However, more recently, alternate wetting and drying (AWD), a new management practice in irrigated lowland rice that saves water and reduces greenhouse gas (GHG) emissions while maintaining yields has been recommended by IRRI. The AWD water regime starts two weeks after transplanting/ seeding. The rice field is left to dry, then the field is re-flooded once a certain water level (e.g. 15 cm below the soil surface) is reached. This cycle is done repeatedly except during flowering stage of crop growth.
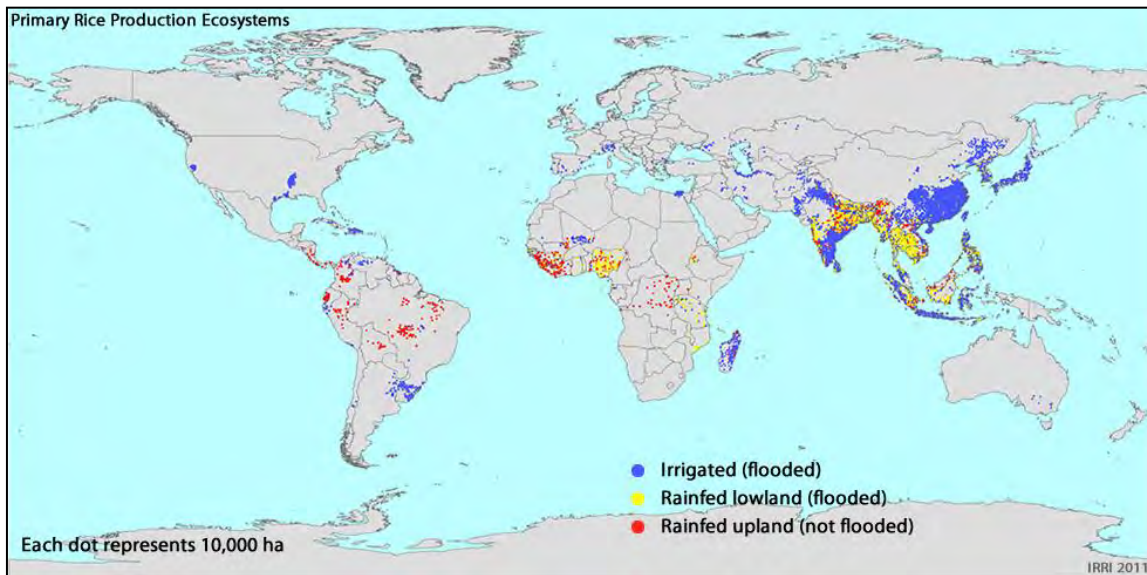
Figure 4. Map of the main rice production ecosystems. Source: IRRI.

Apart from the hydrological practices, the rice cultural practices in the world are characterized by:

- Method of planting: direct sowing or transplanting. In the case of direct sowing, rice seeds, which are often germinated, are sown on fields which are wet but not flooded. In the case of transplanting, the rice seeds are sown densely in a nursery, where they will grow for 15 to 30 days before being transplanted into fields covered with a thin (few cm) layer of water. Transplanting can be manual, in areas where labor is abundant, or mechanical, and therefore with a very regular alignment, in the areas where machines are available. In many countries, and particularly in Vietnam, manual transplanting, which is the traditional planting method is gradually being replaced by direct sowing in because of the increase in the labor cost.

- The number of rice cropping seasons per year depends on several factors, including climatic conditions (temperature, solar radiation, and precipitation), hydraulic development, hydrological practices, manpower, and the possibility to use new

hybrid rice cultivar with short growth cycle. Figure 5 shows an example of the global map of rice cropping density based on statistics and EO (MODIS) data.
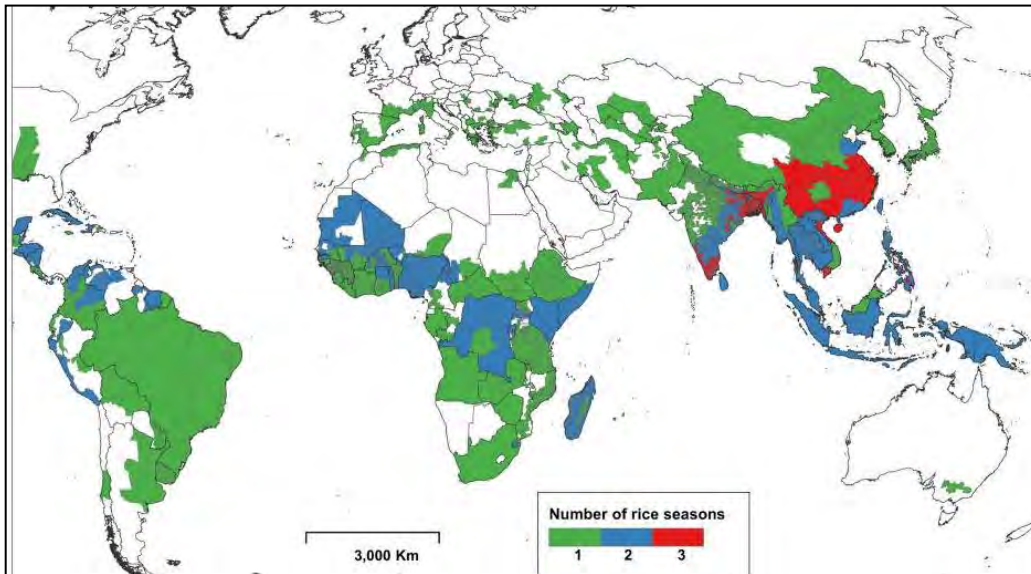
Figure 5. Map of cropping density or number of rice seasons per year (Laborte et al., 2017).

2.3. Rice growth cycle

Rice (*Oryza sativa*), native to India and China, traditionally comes in two main cultivars, indica and japonica. Indica rice has long, narrow grains and is cultivated in the humid tropics and sub-tropics. The japonica rice, with oval or round grains, grows in the tropics or temperate regions. From the mid-sixties, cultivar hybrids were created. They have higher yields and a shorter growth cycle, which allows obtaining several rice harvests a year, up to 3 in irrigated areas in the tropics.

Depending on the varieties used and climatic conditions, the crop cycle rice can range from 90 to over 150 days. After sowing or transplanting, the rice plants go through three phases:

(1) The vegetative phase extends from germination to floral initiation. It is characterized by a significant emission of tillers (secondary stems arising at the base of the main stem), an increase in the height of the plant, and the development of leaves at regular intervals. The duration of this phase depends on the variety adapted to the climatic conditions. About 20 days after transplanting, the clumps completely cover the spaces between plants. Throughout this period, the structure of the plant remains erectophile: tillers are almost vertical and the leaves have a low insertion angle (5 to 20°), as illustrated in the Figure 6.

Figure 6. Illustration of the vertical structure of rice plant at vegetative phase (Source: Ricepedia.org).

(2) The reproductive phase includes the heading / flowering stages: decrease in the number of tillers, development of panicle leaf, formation and flowering of panicles. It lasts 25 to 35 days. The height of the plants stabilizes and the angle of insertion of the leaves increases to 30-40°, causing the plant to lose its vertical appearance (as illustrated in the Figure 7). However, in modern varieties, leaves emerge from the panicles layer.

Figure 7. Illustration of the plant structure of rice at reproductive phase (Source: Ricepedia.org).

(3) The ripening phase results in the ripening of the grains and the drying up of the plant, and lasts from 25 to 40 days.

The evolution of the rice plant structure along its growth cycle will affect the backscatter characteristics of the rice fields.

2.4. Rice productivity

In the world, rice production is more than 754 million tons annually (470 million tons of milled rice) in 2016 (IRRI, AfricaRice and CIAT). About 90% of the rice in the world is grown in Asia (nearly 640 million tons), with China and India as the largest rice producers. Although its area harvested is lower than India's, China's rice production is greater due to higher yields because nearly all of China's rice is irrigated, whereas less than half of India's rice is irrigated. In 2016, the largest three exporting countries in 2016 are Thailand (26% of world exports), Vietnam (15%), and the United States (11%), while the largest three importers are Indonesia (14%), Bangladesh (4%), and Brazil (3%). Elsewhere, the most important production centers are in the United States (California and the southern states near the Mississippi River), which produced 9.0 million tons of paddy on average in 2006-2008. The leading European producers are Italy, Spain, and Russia. Australia used to be an important producer, but its output has declined substantially in recent years because of recurring drought (*Rice Almanac*, 2010).
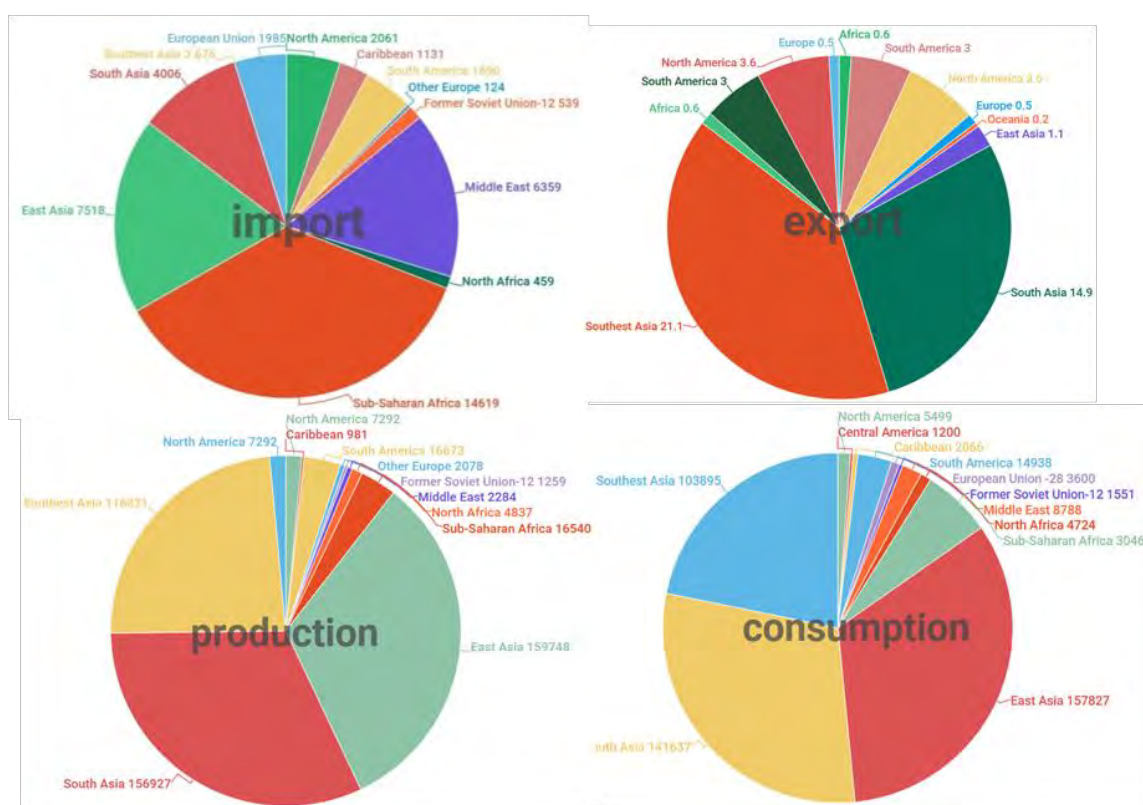
Figure 8. Import, export, production and consumption of rice in 2017 (milled rice equivalent – '000 tons) (Data from FAO, 2018).

Figure 8 shows the latest statistics from FAO on rice import, export, and production of rice in 2017.

✚ Rice yields

Yields range from less than 1 ton/ha under very poor rainfed conditions to more than 10 tons/ha in intensive temperate irrigated systems. The highest rice yields have traditionally been obtained from planting in high-latitude areas that have long day length and where intensive farming techniques are practiced, or in low-latitude desert areas that have very high solar energy (with available water for irrigation). Southwestern Australia, Hokkaido in Japan, Spain, Italy, northern California, and the Nile Delta provide the best examples. The productivity of upland rice is the lowest, only reaching 2,4 -3,0 tons/ha per planting season (*Rice Almanac*, 2010).

As stated previously, more than 90% of the world's rice is produced and consumed in Asia (IRRI, 2013). At the economic level, world rice trade is volatile due the uncertainty in the Asian demand, particularly in countries like Indonesia, the Philippines or Japan, where national production can vary as much as 20% from year to year. Accordingly, prices can fluctuate considerably.

Within this context, it is important to have a tool for early estimation of rice production. For this purpose, a large research community has been working on the rice growth models aiming at predicting the final yield well before harvest. These rice growth models were developed to simulate the potential production in optimum conditions of light and temperature and water. These conditions together with given varietal characteristics for phenological, morphological, and physiological processes determine the growth of the crop.

The new generation versions of these models, such as ORYZA2000 which will be used in this study, allow an explicit simulation of crop management options, such as irrigation and nitrogen fertilizer management. It can also be used in application-oriented research such as the analysis of the effects of climate change on crop growth.

2.5 Global emissions from rice fields

The importance of lowland rice fields as a source of atmospheric CH_4 was realized in the 1980s (Holzapfel-Pschorn and Seiler, 1985). Anaerobic decomposition of organic material in flooded rice fields produces methane (CH_4), which escapes to the atmosphere primarily by diffusive transport through the rice plants during the growing season. In inundated rice fields, CH_4 is produced by methanogens through anaerobic decomposition of organic matter, and part of the CH_4 is oxidized by methanotrophic bacteria in aerobic regions of the soil (i.e. the surface soil layer and the rice rhizosphere). Methane stored in soil can be

emitted to the atmosphere via three pathways: diffusion through flood water, ebullition, and transport through rice plants. Of these pathways, transport through rice plants is the most important: several studies have estimated that about 90% of CH4 emission during the rice growing season occurred through rice plants (Schutz et al., 1991; Butterbach-Bahl et al., 1997). The Intergovernmental Panel on Climate Change (IPCC, 1996) estimated the global emission rate from paddy fields at 60 Tg/yr, with a range of 20 to 100 Tg/yr. This is about 5-20 per cent of the total emission from all anthropogenic sources. This figure is mainly based on field measurements of CH4 fluxes from paddy fields in the United States, Spain, Italy, China, India, Australia, Japan and Thailand.

The measurements at various locations of the world show that there are large temporal variations of CH4 fluxes and that the flux differs markedly with soil type and texture, application of organic matter and mineral fertiliser (Neue and Sass, 1994). The wide variations in CH4 fluxes also indicate that the flux is critically dependent upon several factors including climate, characteristics of soils and paddy, and agricultural practices, particularly water regime. The parameters that affect methane emissions vary widely both spatially and temporally. Changing management of water resources also has likely contributed to reduced emissions from rice agriculture. Field studies indicate that mid-season drainage reduces CH4 emissions by 15–80% (Wassmann et al., 2000). Combining this information with regional statistics on management practices, Li et al., (2002) estimated that the practice of midseason paddy drainage in China could have lowered CH4 fluxes by about 5 $TgCH^4yr^{-1}$ from 1980 to 2000.

2.6. Summary on Earth Observation requirements for rice monitoring

Because of the complexity of rice ecosystems, and the diversity of cropping density, cultural practices, and the need of inputs for rice production models and methane emissions from rice fields, the requirement on Earth observation system can be summarized as follows:

o Monitoring of rice from remote sensing requires cost effective SAR data at high resolution (10-30 m) and temporal resolution of the order of 10 days.

o Mapping of rice extent requires multi-temporal SAR data and robust methods to be developed to deal with a diversity of multi-cropping, crop calendar and cultural practices in a region.

o Monitoring of rice phenology requires multi-temporal data, and the development of methods dealing with a diversity of rice varieties and cultural practices.

o For rice production estimation and prediction, and for methane emissions estimations, research needs to be conducted on the effective use of remote sensing data as inputs or validation means for rice yield prediction and methane emission models.

In particular, the information about crop calendar and rice planted and harvested areas and early production estimates are required in global initiative such as GEOGLAM (Group on Earth Observations Global Agricultural Monitoring) in which the Asian Rice Crop Estimation and Monitoring initiative (Asia-RiCE) is a component dealing with rice crop in Asia.

<div align="right">

Chapter 3

Study region and material

</div>

Contents

This chapter aims to present our study region and the data sets used through this thesis. The first section will present the general characteristics of the study sites. Then, in the second section, the ground data collection will be described. Finally, in the third section, the remote sensing data set and the images pre-processing chain for the data used through this thesis will be presented.

3.1. Study region

The test region selected for this study is the Vietnam Mekong Delta, in which an important diversity of rice crop cultivation is represented. In this region can be found single, double, and triple crop systems (i.e. number of crops per year), planted with short or long cycle rice, with shifted crop calendar between provinces and intra-provinces. Cultivation

practices include the traditional method with transplantation and continuous flooding (CF) and the modern method with direct seeding and Alternate Wetting Drying (AWD).

3.1.1. The Mekong Delta
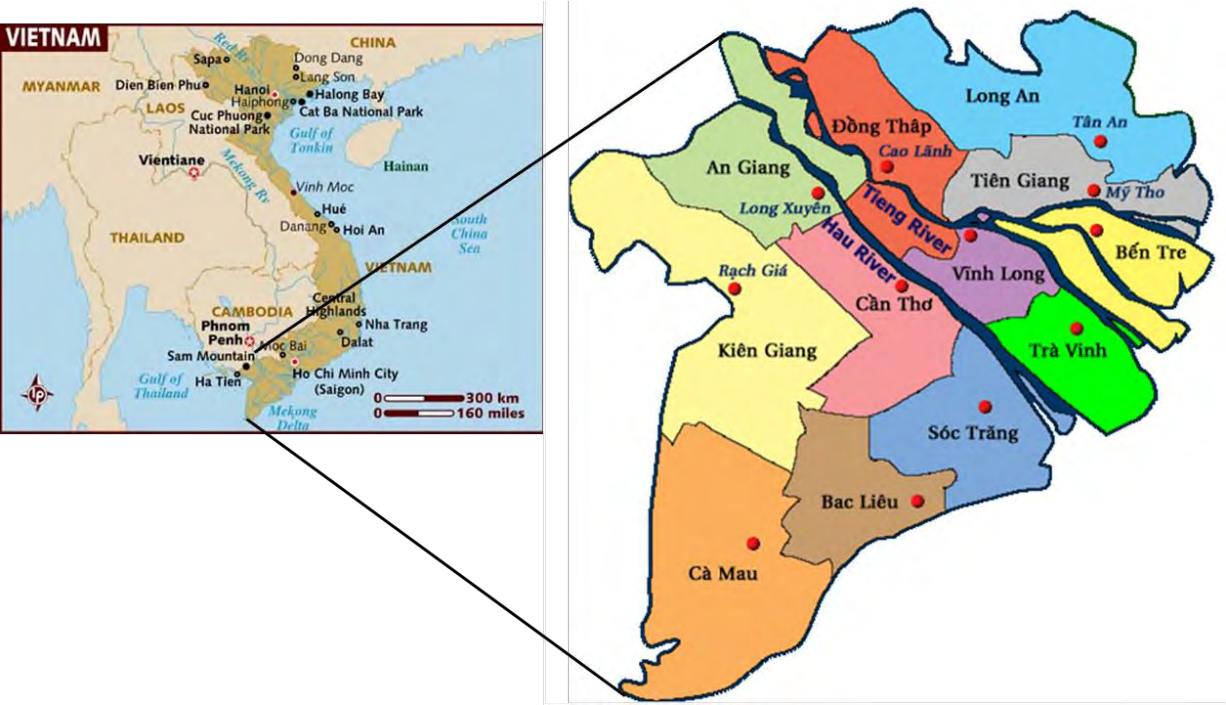
Figure 9. The Study region and map of 13 provinces in the Mekong Delta, Vietnam

The Mekong Delta, popularly known as the "Rice Bowl" of Vietnam, covers an area of about 40,000 km² between 8.5°−11.5°N and 104.5°−106.8°E in the southern part of Vietnam. A total of 12 provinces and 1 municipality constitute the Mekong Delta inhabited by about 17.4 million people, accounting for 20% of the population in the country. Geographically, the Mekong Delta is the last part of the Mekong River before it flows to the sea through a network of nine main distributaries. The topography of the region is extremely flat, with most areas lying just above sea level (0.7-1.2m in height). The climate of the Mekong Delta is monsoon tropical semi-equatorial with two well distinguishable seasons: the rainy season (June-November) and the dry season (December-May). Seasonal floods occur in a large part of the area, starting in August in the upper Delta, and then spreading to the lower Delta, peaking in September-October and lasting until the beginning of December. The floods bring large amounts of silt that contribute to the fertilization of the soil. The land is dedicated mostly to agriculture (63%), aquaculture (17.7%) and forestry (8.9%) (General

Statitics Office of Vietnam) with the agricultural land comprising predominantly rice paddies (66% in area of annual crop), sugarcane, fruit tree plantation (particularly mango).

The Mekong Delta is the main national rice producer. At the national level, the Mekong Delta accounts for only 11% (4.06 M ha) of Vietnam's area but contributes up to 54% of national rice production (General Statistics Office of Vietnam, 2017). The Mekong Delta has mostly irrigated rice ecosystems with three major cropping seasons: Winter-Spring, Summer-Autumn and Autumn-Winter cropping season.

(1) Winter-Spring season has the highest productivity (20.5% higher than the average yield of the region). Rice is planted at the end of the rainy season (Nov-Dec) and the increased solar radiation and irrigation in the later cropping season from February-April provide good conditions in rice reproductive and ripening phases ensuring high productivity.

(2) Summer-Autumn cropping season has the largest rice cultivation area, accounting for 54% of the total rice cultivation area of the region. Rice is planted in April-May. However, it rains during the second part of the season and the rice is harvested in July-August before being devastated by floodwaters. Because of the lack of solar radiation, during the rainy period, the productivity is lower than for Winter Spring rice.

(3) Autumn-Winter crop during rainy season has the lowest productivity. Rice is planted in July-August, and harvested in December-January. Rice area is the lowest in this rainy season, as almost 50% of the total area of the delta (4 million ha) is flooded, in particular in the northern part of the delta due to the overflowing of the Mekong River in the upper reaches. However, dyke systems were built starting in the early 90's in order to protect the fields from flood water and allow the third crop in certain parts of the Delta.

(4) In parts of the Delta not prone to floods, and without irrigation infrastructure during dry season, traditional rainfed rice still subsists. Rice is transplanted in July-August and harvested in November-December.

At a given site, the number of crops per year, from one to three, depends on the water management, including irrigation during the dry season and levee and dyke construction to stop flood waters during the rainy season. The crop calendar can vary every year, depending on the onset of the rainy season, and the calendar can be specific to each of the 13 provinces, depending on the geographical conditions and on provincial regulations.

Table 2 shows the main rice seasons and their typical calendar in the Mekong Delta. There is a recuperation period of approximately one to two weeks between cropping seasons,

31

with the exception of the 1 to 2-month seasonal flooding period. Rice seeds are directly sown on wet soil by drilling (precision equipment) or broadcasting (hand), or transplanted (manually or with transplanting machine). The sowing methods depend also on the rice varieties and farm strategies.

Table 2. Main rice seasons in the Mekong Delta

Rice crop season	Jan.	Feb.	Mar.	Apr.	May	June	July	Aug.	Sep.	Oct.	Nov.	Dec.
Winter-Spring	mid-season	mid-season	harvest								sowing	sowing
Summer-Autumn				sowing	mid-season	mid-season	harvest	harvest				
Autumn-Winter							sowing	sowing	mid-season	mid-season	harvest	harvest
Rainy season	harvest						sowing	sowing	mid-season	mid-season	harvest	

sowing **mid-season** **harvest**
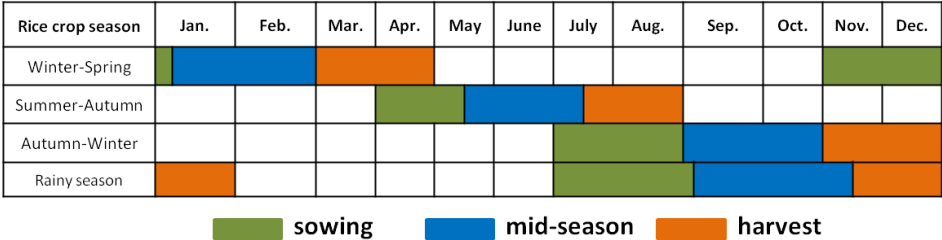
The water management is different between regions. A system of canals and dikes to bring irrigation water and control floodwater has been built in the recent decades to complement the existing canal system that operated mainly as an irrigation source. In the rice fields surrounded by irrigation canals and dykes system, irrigation is performed using sluices and pumping apparatuses attached within the dykes of the paddies, as can be seen for example in the An Giang and Dong Thap provinces. Moreover, besides the traditional continuous flooding method, modern water management has been developed in the last years, consisting in intermittent drainage between two irrigation operations (AWD) as described in section 2.2. In both cases of water management, the rice fields are flooded from 1–2 weeks until 3-4 days before the date of sowing in order to prevent self-propagating vegetation and pests. At the end of the season, the fields are drained two weeks before rice harvest.

With regard to fertilisers, no base fertiliser is applied, but top-dressing fertilisers are applied after sowing with 3-6 applications during a season, and rice fields are flooded when the fertilisers are applied. To avoid yield loss, insects, snails, diseases and weeds are controlled with approved pesticides. After the harvest, the straw is used in several ways: incorporated into the soil, utilised as compost for vegetable or flower cultivation, utilised as mushroom beds by rice farmers, burned, or utilised as feedstuff for livestock.

It is important to note that the Mekong Delta is often affected by climate change-related events. For example, since the end of 2015, El Niño has strongly affected South East Asia, leading to severe drought, in particular in Vietnam's Mekong Delta. River water levels were at the lowest recorded in 90 years in many places, causing more severe and earlier salt water intrusion than in the previous years.

3.1.2. Extension to national scale

In this thesis, the methods developed in the Mekong Delta are also extended to national scale in two countries, Vietnam and Cambodia.

⬥ Vietnam

Vietnam is the world's 5th rice producer and the 3nd largest (after India and Thailand) exporter worldwide (USDA, 2018). Vietnam is located in the southeast of Indochinese Peninsula and covers an area of more than 330,000 square kilometers. The topography in Vietnam is very diverse with mountains, hills, plains, coasts and continental shelf. Vietnam's climate is suitable for paddy production. The cultivated land of paddy covers 4.2 million ha (43% of total agricultural land area) within 9.3 million households planting of paddy (65% of rural households). The rice area harvested changed from 6.8 million ha in 1995 to 7.8 million ha in 2014 and has an average productivity of 5.6 ton per ha in 2016 (General Statistics Office of Vietnam, 2017).

Rice growing season and cultivation practices change from South to North with the most important and densely distributed paddy areas being in the low-lying deltas of the Mekong River in the South and Red River in the North. Besides the Mekong Delta described in section 3.1.1, the Red River Delta (RD) is the second rice producer in Vietnam, accounting for 17% of Vietnamese rice production. The RD is more densely populated, has smaller landholdings and has double-crop, with a small part of single crop rice cultivation. At the national scale, two to three major cropping seasons are distinguished more generally into spring, summer and autumn seasonal periods, for the three regions North, Center and South as shown in Table 3.

Table 3. Crop calendar in three main regions (North, Center and South) in Vietnam. For each season, the planting, mid-season and harvest stage correspond to the lighter-darker colors.
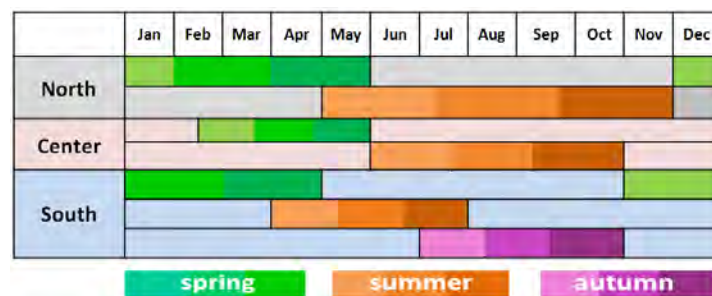
Cambodia

The second test at national scale in this study, Cambodia is located in Southern Asia, bordering the Gulf of Thailand, between Thailand, Vietnam and Laos. Cambodia can be divided into four geographical regions; the Mekong Plain Delta, Tonlé Sap Plain Delta, North and North-Eastern mountainous region and the coastal region. Cambodia's climate is dominated by monsoons and the rainy season is from May to October.

Rice is the main crop in Cambodia and rice production (GDP 13%) occupies 91% of the cropped area. In 2013/2014, the total rice-cultivated areas were about 3 million ha and 9.32 million tons were harvested. Cambodia became a rice-exporting country in the late 1990s and increased the export volume from 0.75 million tons in 2009/2010 to 1 million tons in 2013/2014. The sharp increase of rice productivity is closely related to the expansion of irrigation facilities, technology improvement and the rice price increase at the global market.

Rice in Cambodia is grown in four different ecosystems: rainfed lowland, rainfed upland, deepwater, and irrigated, with two main rice seasons: wet-season (short wet, medium wet and long wet season) and dry-season (Table 4).

Table 4. Crop calendar in Cambodia

3.2. Ground data

In line with the objectives of the thesis, the ground data collection was designed for:

(1) Analyzing radar satellite imagery to understand the temporal variation of the radar backscatter from the rice fields,

(2) Developing methodologies for mapping rice grown area, distinguishing long-cycle and short-cycle rice varieties, estimating and mapping rice phenological stage, sowing date, plant height and cropping intensity,

(3) Validation and accuracy assessment of the products developed in (2),

(4) Providing inputs and validation for rice growth simulation model ORYZA2000 for rice production estimation, and DNDC for Methane emission modelling.

For the three first objectives, the data collection was designed by CESBIO and Vietnam National Space Center (VNSC), in the frame of the GeoRice project (Le Toan et al., 2017). In line with labor availability, rice fields of different conditions within the An Giang province have been selected and data collection has been performed in collaboration with the team from the University of An Giang, Vietnam.

An Giang is one of the major rice producing provinces of Vietnam with 237,500 ha rice paddy over 278,800 ha (85%) of total agricultural land of the province (Figure 9). Similarly to the crop distribution in the Mekong Delta, rice crop is the dominant crop, the other crops which are sugarcane, maize, and vegetables (Phan *et al.*, 2018). The rice field samples have been chosen to be representative of rice-growing conditions in terms of cropping density, cultural practices (rice varieties, irrigation) and also accessibility of the area and availability of agricultural information (field map, irrigation schedule, rice variety, rice yield). In addition, the sampling strategy accounted for the different factors influencing the SAR backscatter when using Sentinel-1 (which will be described in Section 3.3).

The data has been collected over 60 sampling fields regularly during two periods: from April 2016 until April 2017, and from August 2017 to April 2018. Note that due to logistic reasons, most sampling fields have been changed during the second period, only 8 fields were surveyed during both periods. These fields have been chosen to cover a range of rice planting practices, rice varieties and crop calendar.

The data have been provided in GIS format for field delineation. The size of most fields varies from 40-60m in width and 100-120 m in length. 6/60 sampled rice fields are smaller (40 x 40m). For 60 rice fields, ground data were collected at the dates of Sentinel-1 overpasses, every 12 days and 6-9 times per seasons as shown in Figure 10.

35
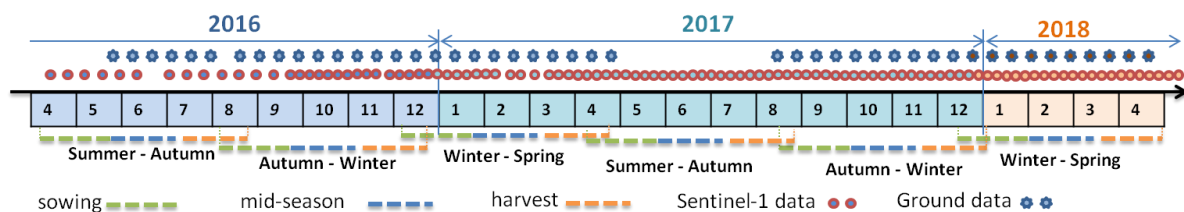
Figure 10. The time table of the study data sets: collected ground data and Sentinel-1 data, along with the rice crop calendar in the An Giang province, Mekong Delta, Vietnam.

The general information, i.e. gathered once for each sample field and each season, includes rice variety, planting method, seeding density, rice calendar, rice yield at harvest. An example of general information collected over sampled rice fields under study is given in Table 5.

Table 5. Example of general collection information of rice fields under study.

Sample ID	Variety	Planting method	Seeding density (kg/ha)	Sowing date	Harvest date	Yield (ton/ha)
1	50404	Direct sowing	20	14/8/2016	10/11/16	720
2	50404	Direct sowing	22	14/8/2016	10/11/16	700
3	50404	Direct sowing	20	14/8/2016	08/11/16	600
4	50404	Direct sowing	20	15/8/2016	08/11/16	650
5	50404	Direct sowing	25	15/8/2016	09/11/16	500
6	50404	Direct sowing	24	15/8/2016	09/11/16	800
7	50404	Line sowing	20	15/8/2016	11/11/16	650
8	50404	Line sowing	20	15/8/2016	15/11/16	500
9	Jasmine	Transplanting	8	14/8/2016	05/11/16	800

The detailed information, i.e. gathered at each visit in the field, comprise water layer thickness (cm), soil condition (1 for dry, 2 for wet, and 3 for water and mud) rice phenology, uniformity in plant height (1: yes; 2: no), plant height from the water or soil surface (cm). In all samples, photographs have been taken during the observation dates. An example of detailed rice plant parameters measured over sampled rice fields under study is given in Table 6.

36

Table 6. Example of rice plant parameters measured at some sample rice fields under study.

Sample ID	Water layer (cm)	Plant height (cm)	Uniformity	Soil condition	Phenological stage (1-12)
1	5	22	1	2	5
2	5.5	24	1	2	5
3	2.5	25	1	2	5
4	4	23	1	2	5
5	2	24	1	3	4
6	4	20	1	2	4
7	6	20	1	2	5
8	3	26	1	2	5
9	3	20	1	2	5

For the phenological stage, 12 growth stages scale have been observed during the rice growth cycle as follows:

1: seedling, emergence	5: stem elongation	9. milky stage
2: 2/3 leaves	6: booting	10. milky-hard stage
3: tillering start	7. heading	11. maturing
4: tillering max	8. flowering	12. maturity

This scale was used by local experts and the Vietnam agriculture services for field survey to record the phenological stage. However, the phenological stage could be expressed following the principal growth stages of the BBCH scale (Forestry, 2001). Depending on the required precision of the products and the temporal resolution of the EO data used to generate the product, the above stages can be simplified to a more reduce number of stages, for example 6 main stages instead of 12.

For validation of rice mapping results in the whole Mekong Delta, GPS check points were collected. The required information was: point coordinates, type of surface, current rice growing fields (labelled rice), rice field before or after the current rice season (before sowing and after harvest, labelled non-rice), other crop or other land use land cover classes (non-rice) and photographs. In total, five campaigns have been realized by the team from Vietnam National Space Center from July 2016 to April 2017: (1) from 3 to 8/7/2016, (2) from 2 to 4/9/2016, (3) from 15 to 18/11/2016, (4) from 18 to 19/2/2017 and (5) from 8 to 9/4/2017. For each of the campaigns, 100 rice fields corresponding to currently grown rice and 30 other types for each of the 3 main regions in the whole Mekong Delta have been collected, as shown in Figure 11.
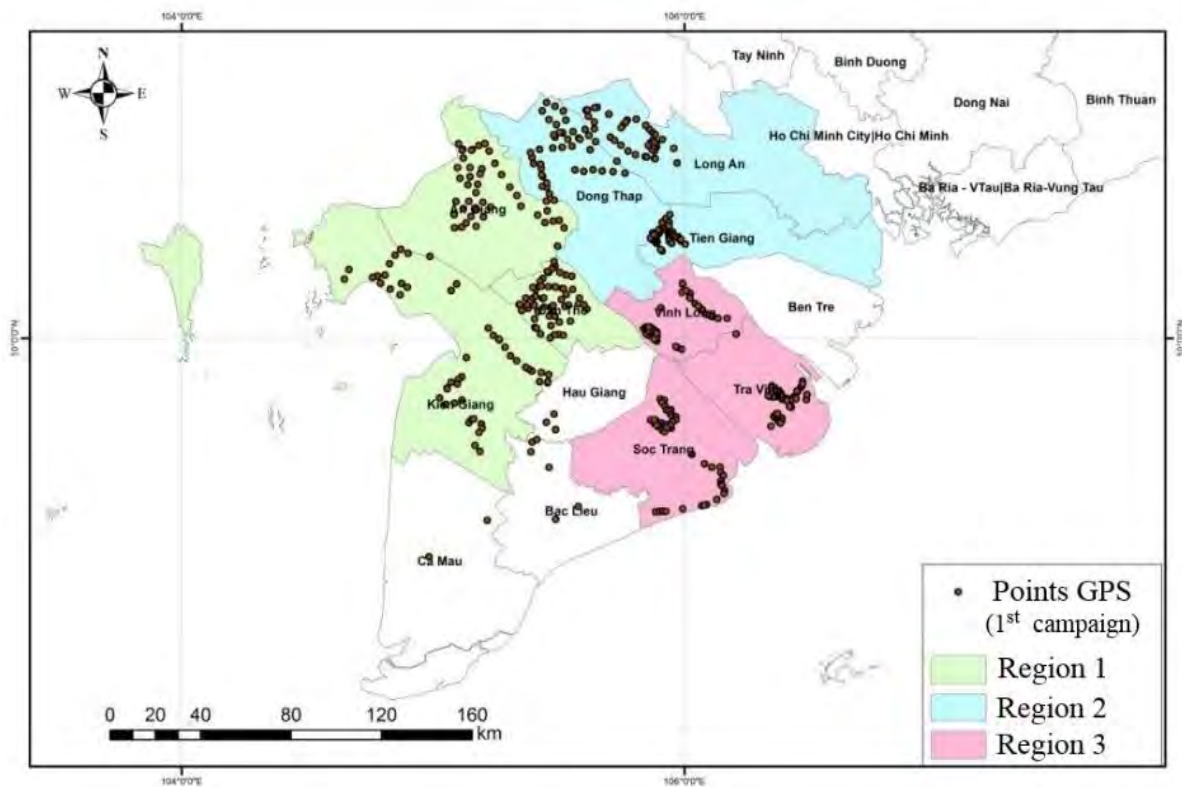
Figure 11. Example of check points for rice map product validation recorded during the 3-8 July 2016 campaign. Around 100 rice and 30 non-rice points for each of the 3 main rice regions.

It is noted that 3 main regions were chosen over 9 provinces in Mekong Delta to be accessible and the most favorable for the field trip.

> o Region 1: An Giang; Kiên Giang; Cần Thơ
>
> o Region 2: Đồng Tháp; Long An; Tiền Giang
>
> o Region 3: Sóc Trăng; Trà Vinh, Vĩnh Long

Figure 11 presents an example of the location of the check points recorded during the first campaign (3-8 July 2016), during the Summer-Autumn (April-August) rice season 2016. Figure 12 gives some photographs taken during the field trip of rice and non-rice samples in the Mekong Delta.

In addition, for rice production model and methane emission models (objectives 4 and 5), the study benefits from a collaboration with a team from the University of Tokyo and can make use of an existing database collected by this team. This dataset will be presented in Chapter 7.
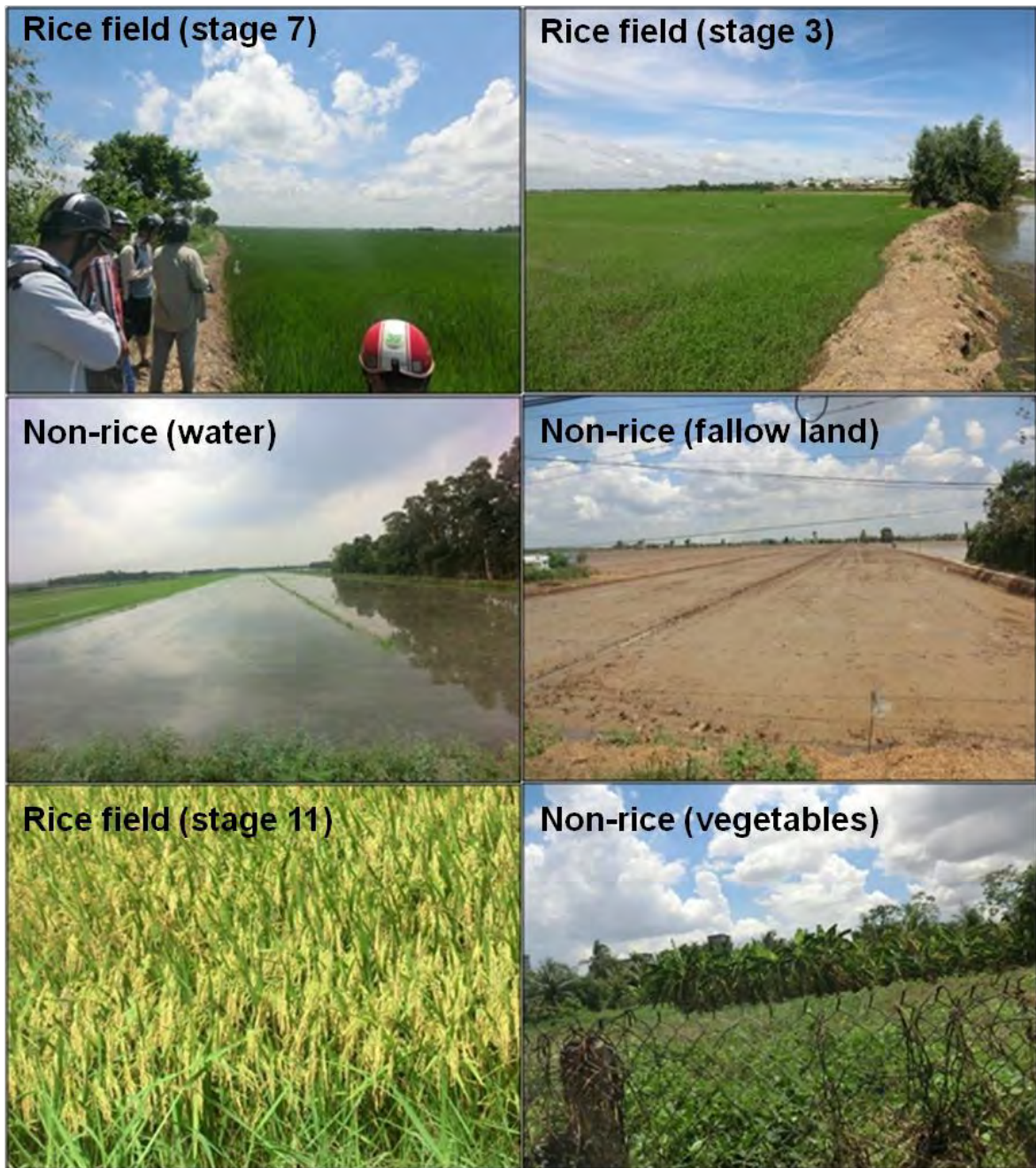
Figure 12. Example of the rice and non-rice sample photographs taken during the field trip in the Mekong Delta, Vietnam.

3.3. SAR data

This section aims to provide the basic knowledge on synthetic aperture radars (SAR) as well as the data used in this study. The first subsection provides an introduction of the SAR principle and theory, followed by an overview of the statistical properties of SAR

images. The rest of this section describes the data used in this thesis, from the Sentinel-1 data to the data preprocessing process.

3.3.1. SAR remote sensing introduction

3.3.1.1. Radar equation

RADAR (RAdio Detection And Ranging) is an active microwave observing system. A radar system consists fundamentally of a transmitter, a receiver, an antenna, and an electronics system to process and record the data. The electromagnetic energy propagates outward at light velocity, toward a target (object, surface). The radar measures the energy in the radar pulse which is reflected back towards the radar and is expressed as the radar backscatter (σ^0). The objects can be detected by measuring the time delay between the transmission of a pulse and the reception of the backscattered "echo" from different targets, which provides the information on magnitude, phase, time interval between pulse emission and return from the object, polarization and Doppler frequency.

The radar backscatter measurement is expressed by the radar equation. This equation describes the relationship between the received power (P_r) from the incident electromagnetic wave $\vec{E}^r$ and the transmitted power (P_t) for a single target in the form of the scattered wave $\vec{E}^t$, and can be written as:

$$P_r = \frac{P_t G_t \lambda^2}{4\pi R_t^2} \sigma \frac{A_r}{4\pi R_r^2} \tag{1}$$

Where P_r is the power detected at the receiving system, P_t is the transmitted power, G_t is the antenna gain, R_t is the distance between sensor and target, λ is the exploited wavelength. The term $\frac{P_t G_t}{4\pi R_t^2}$ is determined by the incident field $\vec{E}^t$ and it consists of its power density expressed in terms of the properties of the transmitting system. On the contrary, the term $\frac{A_r}{4\pi R_r^2}$ contains the parameters concerning the receiving system: the effective aperture of the receiving antenna A_r and the distance between the target and the receiving system R_r. The last term in (1), σ, is the radar cross-section of the target which determines the effects of the target on the balance of powers established by the radar equation, and is given by:

$$\sigma = 4\pi R^2 \frac{|\vec{E}^t|^2}{|\vec{E}^r|^2} = 4\pi |S|^2 \tag{2}$$

where $|\vec{E}|^2$ represents the intensity of the electromagnetic field and $|S|$ is the complex scattering amplitude of the object. The complex scattering matrix describes the

transformation of the two-dimensional transmitted (e.g., incident) plane wave vector $\vec{E}^t$ into the received (e.g., scattered) wave vector $\vec{E}^r$ (two-dimensional in the far field of the scatterer) performed by the scatterer [15], [35], [36]:

$$\vec{E}^r = \frac{\exp(-ikr)}{r}|S|\vec{E}^t \tag{3}$$

$$\begin{bmatrix} E_H^r \\ E_V^r \end{bmatrix} = \frac{\exp(-ikr)}{r} \cdot \begin{bmatrix} S_{HH} & S_{HV} \\ S_{VH} & S_{VV} \end{bmatrix} \begin{bmatrix} E_H^t \\ E_V^t \end{bmatrix} \tag{4}$$

The elements of [S] in (3) are corresponding to the four complex scattering amplitudes $\begin{bmatrix} S_{HH} & S_{HV} \\ S_{VH} & S_{VV} \end{bmatrix}$ in (4) where the subscripts horizontal (H) or vertical (V) indicate associated received and transmitted polarization. A radar system using H and V linear polarizations can thus have the following channels: HH for horizontal transmit and horizontal receive, VV for vertical transmit and vertical receive, HV for horizontal transmit and vertical receive, and VH for vertical transmit and horizontal receive. HH and VV polarizations are referred to as like-polarized or co-polarized, because the transmit and receive polarizations are the same. HV and VH polarizations are referred to as cross-polarized because the transmit and receive polarizations are orthogonal to one another. Different levels of polarization complexity can therefore be established: single polarized (HH or VV or HV or VH); dual polarized (HH and HV, VV and VH, or HH and VV); four (Quad) polarizations (HH, VV, HV, and VH).

For extended target, the average value of the individual sub-targets cross-sections in (2) (or received energy by the sensor σ_i) per unit area is defined as differential **scattering coefficient** σ^0 (sigma zero):

$$\sigma^0 = \left\langle \frac{\sigma_i}{\Delta A_i} \right\rangle = \frac{4\pi R_r^2}{A_0} \frac{\langle|\vec{E}^t|^2\rangle}{|\vec{E}^r|^2} \tag{5}$$

The backscatter cross-section is usually expressed in dB, which is given by:

$$\sigma^0(dB) = 10 log\sigma^0 (m^2 m^{-2}) \tag{6}$$

The resulting coefficient σ^0, reflect backscatter properties of the surface, which are determined by the geometrical (e.g., surface roughness, geometric structure, and orientation) and dielectrical (e.g., dielectric constant, moisture content, and conductivity) characteristics of the surface, and the radar observation parameters (i.e., frequency, polarization, and incidence angle of the electromagnetic waves emitted) (Ulaby et al., 1982). Such signal characteristics can be used to obtain a number of important geophysical and biophysical parameters.

3.3.1.2. SAR images characteristics

Synthetic aperture radar (SAR) satellites collect swaths of side-looking echoes at range resolution and along-track sampling rate to form an image. Range resolution depends on the bandwidth or pulse duration of transmitted signal and is determined by the pulse length (or 1/bandwidth) and the **incidence angle**:

$$\delta_r = \frac{C_0 \tau_r}{2} = \frac{C_0}{2B_r} \tag{7}$$

Where τ is the pulse length and equal $\frac{1}{B_r}$ (B_r: bandwidth of the radar), C_0 is the speed of light. The factor of 2 accounts for the 2-way travel time of the pulse. Ground range resolution is geometrically related to the slant range resolution by $\delta_g = \frac{C_0 \tau_e}{2 sin\theta}$ with θ is the look angle.

Azimuth resolution describes the ability of an imaging radar to separate two closely spaced scatterers in the direction parallel to the motion vector of the sensor.

$$\delta_a = \theta_a \cdot r_o = \frac{\lambda}{d_a} \cdot r_o \tag{8}$$
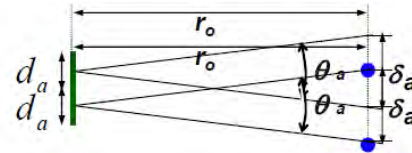
Real Aperture Radar (RARs) has an azimuth resolution determined by the antenna beamwidth, so that it is proportional to the distance between the radar and the target (slant-range). For RAR, azimuth resolution can be improved only by longer antenna or shorter wavelength. The use of shorter wavelength generally leads to a higher cloud and atmospheric attenuation, reducing the all-weather capability of imaging radars. Synthetic Aperture Radars (SAR) was developed as a means of overcoming the limitations of (RAR). SAR images have several characteristics that make it unique:

- It provides high-resolution two-dimensional images independent from daylight, cloud coverage and weather conditions.
- It is predestined to monitor dynamic processes on the Earth surface in a reliable, continuous and global way with no effects of atmospheric constituents (multi-temporal analysis).
- The amplitude and phase of the backscattered signals are sensitive to dielectric properties (water content, biomass, ice), to surface roughness (ocean wind speed), to target structure and subsurface penetration.
- It provides accurate measurements of distance (e.g. for interferometry).

In space-based remote sensing, the capability to penetrate through precipitation or into a surface layer is increased with longer wavelengths. The shortest wavelengths (Ka, Ku) are strongly attenuated in the lower layers of neutral atmosphere (troposphere). Long wavelengths (P) in turn are subject to strong scattering while passing through the ionosphere (layer F). The intermediate bands (X, C, S, and L) are therefore the most widely used.

3.3.1.3. Statistical properties of SAR images

A particular effect to be observed in SAR images is the so-called **speckle**, which is caused by the presence of elementary scatterers with a random distribution within a resolution cell (for example, in a resolution cell of forest land, the scatterers are the leaves, stems, the trunks, objects on the ground etc.). The coherent sum of their amplitudes and phases results in strong fluctuations of the backscattering from resolution cell to resolution cell. Consequently, the intensity and the phase in the final image are no longer deterministic, but follow instead an exponential and uniform distribution, respectively (C. Oliver & S. Quegan, 2004). The total complex reflectivity for each resolution cell is given by:

$$\phi = \sum_i \sqrt{\sigma_i} \exp(i\varphi_i^{scatt}) \cdot \exp(-i\frac{4\pi}{\lambda}r_{0,i}) \tag{9}$$

where i is the number of elementary scatterers within the resolution cell.

Although it is commonly referred to as noise, speckle cannot be reduced by increasing the transmit signal power, since it has a multiplicative character, i.e., its variance increases with its intensity. To mitigate speckle a technique known as **multi-look** is utilized, which is basically a non-coherent averaging of the intensity image (John C. Curlander, 1991, C. Oliver & S. Quegan, 2004). The exponential distribution of a single look intensity image is given by:

$$p(I) = \frac{1}{2\sigma^2} e^{\frac{-I}{2\sigma^2}} \tag{10}$$

With L is the number of look, the multi-look intensity is given by:

$$I_M = \frac{1}{L}\sum_{i=1}^{L} I_i \tag{11}$$

The mean value $\bar{I}_M = \bar{I}$, and the variance $var(I_M) = \frac{\sum_{i=1}^{L}\sum_{i=1}^{L}\rho_{ii}varI}{L^2}$

In SAR intensity data, the speckle variance is proportional to the mean intensity squared. The **Equivalent Number of Looks** is:

$$ENL = \frac{L^2}{\sum_{i=1}^{L}\sum_{i=1}^{L}\rho_{ii}} = \frac{(mean\ intensity)^2}{\sigma} \tag{12}$$

If the ENL is large, the spread of values due to speckle is small. Although multi-look can cause a degradation in the image resolution, it greatly improves the interpretability of the

SAR image. Additionally, the effect of speckle tends to weaken for very high-resolution systems, since the number of elemental scatterers within a resolution cell decreases.

Since the multi-look processing deteriorates the spatial resolution of SAR images, many filtering methods aimed at reducing the effect of speckle to increase the radiometric resolution have been developed (Lee et al., 1980, Frost et al.,1982, Kuan et al.,1985). The goal of these filters are to process the whole image pixel by pixel using a sliding window, on which the signal is supposed to be stationary and which constitutes a neighborhood to estimate locally a certain number of statistical quantities (average, variance, correlation). Most wisely used filters are Frost, Lee and Kuan linear filters which are applied to only one image at a time, so-called mono-channel filters. The simplest of them is the spatial averaging filter, which attributes to each pixel the average of the intensity of the pixels located in the window centered on it. This filter, used most often without structure detection, is effective on homogeneous zones but does not preserve the details of the image. Another approach combining several images from the same scene in order to provide optimal reduction of speckle has been developed which is **multi-channel filters** (multi-temporal and/or multi-polarization and/or multi-frequency) (Bruniquel and Lopes, 1997; Quegan and Le Toan, 1998; Quegan and Yu, 2001). These filters minimize speckle while preserving the radiometry and spatial resolution of the individual channels (polarization, image). They consist in performing pixel-to-pixel linear combinations of M intensity images I_i, in order to obtain M images J_k, such that the intensity information is preserved while minimizing the speckle. For uncorrelated images with the same number of looks L, the optimal linear combination is:

$$J_k(x,y) = \frac{\langle I_k(x,y) \rangle}{M} \sum_{i=1}^{M} \frac{I_i(x,y)}{\langle I_i(x,y) \rangle} \tag{13}$$

with $J_k(x,y)$ radar intensity of output image k at pixel (x,y)

$I_i(x,y)$ radar intensity of input image i at pixel (x,y)

$\langle I_i(x,y) \rangle$ local mean intensity of input image i at pixel (x,y)

The theoretical value of the ENL of the output filtered images is given by:

$$ENL = \frac{M \times N \times L}{M + N - 1} \tag{14}$$

where L is the initial number of looks, M is the number of images (or polarisation) using a fixed window size of N pixels (N is 49 if the window size is 7×7 pixels). The size of the spatial window can therefore be chosen to meet a required ENL value.

3.3.2. Sentinel-1 Data

In this study, the Sentinel-1 C-band (5.405 GHz) SAR data is used. The first Sentinel-1 satellite (Sentinel-1A), was launched on a SOYUZ rocket from Europe's Spaceport in French Guiana on 3 April 2014 and was followed by the second (Sentinel-1B) the 25 May 2016. These two satellites are the first series of earth observation satellites of the Copernicus Initiative. Each Sentinel-1 satellite is expected to acquire Earth observation data for at least 7 years and have fuel on-board for 12 years. The Sentinel-1 mission is the European Radar Observatory for the joint initiative on environment and security between the European Commission and ESA, in sea-ice monitoring and maritime surveillance, land monitoring of forest, water, soils and agriculture, monitoring of land surface motions, and mapping to support environment, crisis and natural disaster management.
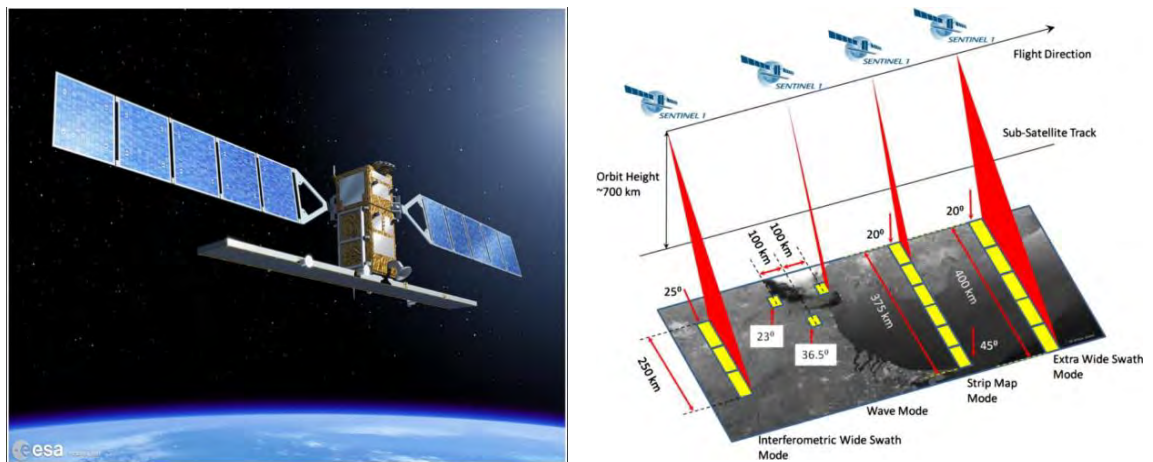
Figure 13. Sentinel-1 satellite and acquisition mode (Source https://sentinel.esa.int/).

Sentinel-1 is a sun-synchronous, near-polar circular orbit at a height of 693 km and an inclination angle of 98.18°, follows polar orbits with ascending and descending flight directions with respect to North (right looking geometry). It provides continuous all-weather, day-and-night imagery at C-band (5.405 GHz) with the incidence angle roughly between 31° and 45°. With Sentinel-1A and Sentinel-1B operating, Sentinel-1 offers a 6-day repeat cycle at the equator (depending of the data type and the region in the world). Sentinel-1 provides

dual polarisation capability (HH, VV, HH+VV, VV+VH), with different resolution (down to 5 m) and coverage (up to 400 km).

Sentinel-1 operates in four exclusive acquisition modes: Stripmap (SM), Extra-Wide swath (EW), Interferometric Wide swath (IW), and Wave mode (WV) (Figure 13). Each mode can produce products at SAR Level-0, Level-1 single look complex (SLC), Level-1 ground range detected (GRD) and Level-2 Ocean (OCN). Level-1 data are the generally available products intended for most data users for basic land cover classification (forest, agricultural crops, urban areas, etc.). Level-1 SLC products have been focused and geo-referenced using satellite altitude and orbit data, and are provided in zero-Doppler slant range geometry. Level-1 GRD products are detected, multi-looked and projected to ground range using an Earth ellipsoid model, and phase information is lost. GRD products can be in one of three resolutions: Full Resolution (FR), High Resolution (HR) and Medium Resolution (MR). The resolution and swath of SAR images is a critical parameter for SAR users as it defines how well different surfaces can be classified and how large it can cover for mapping applications.

Table 7. Sentinel-1 operative modes.

Mode	Swath (km)	Resolution (m×m)	Polarization
Stripmap	80	5×5	Dual
Extra WS	20	5×5	Dual
Interferometric WS	250	5×20	Dual
Wave	400	20×40	Single

Table 7 presents the Sentinel-1 operative modes together with their swath, resolution and polarization parameters. The IW mode allows combining a large swath width (250 km) with a moderate geometric resolution (5 m x 20 m) while Extra-Wide swath mode provides a large swath width of more than 400 km but with low resolution (20m x 40m). Stripmap (SM) mode acquires data with an 80 km swath at 5 m x 5 m spatial resolution. Finally, the Wave mode is composed of single stripmap operations (5 m x 5 m) in 20 km by 20 km vignettes at 100 km intervals. To conclude, IW mode satisfies most of user requirements in terms of resolution, swath width and polarization.

Figure 14. An example of the archived observation scenario maps of the Sentinel-1 mission (05/2017). This map contains information of orbit pass, revisit frequency, coverage frequency and polarization scheme globally. (Modified from https://sentinel.esa.int/).

To summarize, the Sentinel-1 SAR constellation represents an unprecedented data source for an application such as rice mapping and monitoring, thanks to its high resolution, cost free and rapid product delivery at a time interval of 6 or 12 days. The dense time series of Sentinel-1 offer a unique opportunity to systematically monitor rice crop at a weekly repeat cycle. In addition, the continuity of Sentinel data is guaranteed up to 2030 and the next generation of Sentinel is planned beyond 2030, allowing long-term environmental monitoring.

3.3.2.1 Data Available for the Study

The data used in this study are Sentinel-1 (S1-A and S1-B) operating in Interferometric WideSwath Mode (IW) at level-1 Ground Range Detection (GRD). In this mode, images are provided at 10 m spatial resolution (single look) with a 250 km swath (within 3 sub-swaths) at VV and VH polarizations. Over the swath, the incidence angle ranges from 29.1° to 46°. The data covers the Mekong Delta every 12 days from October 2014 with S1-A, and every 6 days from October 2016 with S1-A and S1-B, with rapid and free of charge data delivery on https://peps.cnes.fr or https://scihub.copernicus.eu/.

47

Figure 15 shows an example of Sentinel-1 images covering the Mekong Delta.

Swath width	250 km
Incidence angle range	29.1°-46.0°
Sub-swaths	3
Resolution	5 x 20 m
Polarisation	Dual VH + VV
Radiometric stability	0.5 dB (3σ)
Radiometric accuracy	1 dB (3σ)
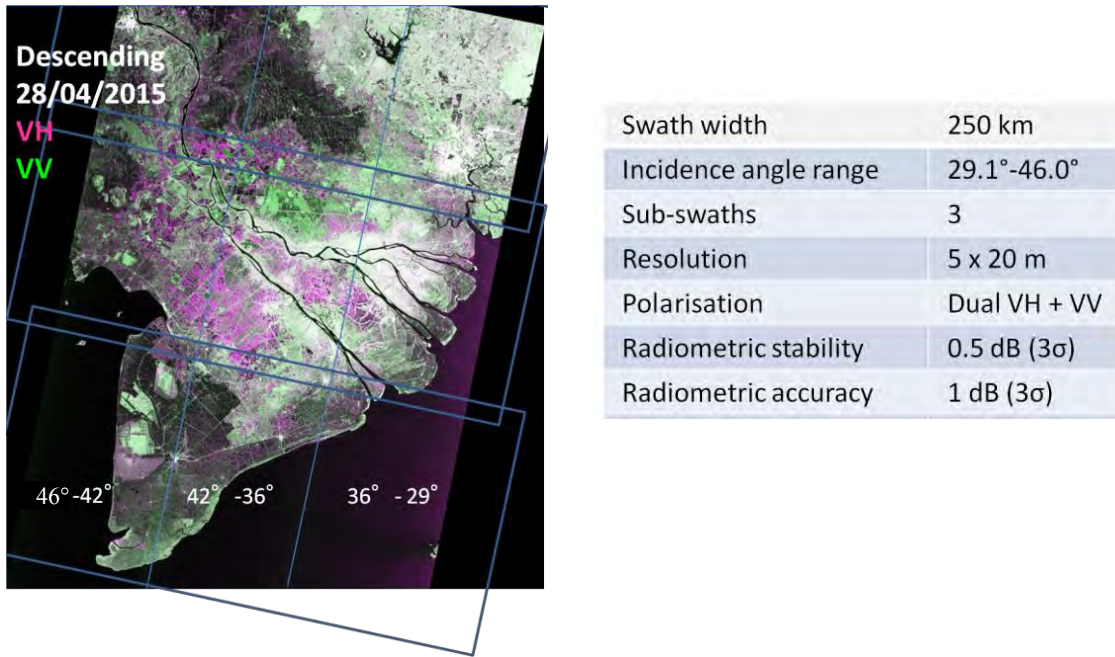
Figure 15. Example of Sentinel-1 image (descending pass) on 28/04/2015 to cover the whole Mekong River Delta, Vietnam (left) and Sentinel-1 image characteristics (right). The three incidence angle ranges are noted on the image.

As mentioned before, the methods developed in this thesis will be tested in the Mekong Delta and then also applied to national scale in two countries, Vietnam and Cambodia.

For the Mekong Delta, the temporal series of Sentinel-1 data from 06/10/2014 to 23/08/2018 has been downloaded. As seen in Figure 15, 3 Sentinel-1 images per acquisition are required to cover the whole Mekong Delta. As a result, a total of 507 descending images (169 acquisitions × 3 images) and 132 ascending images (44 acquisitions × 3 images) have been downloaded for data preprocessing.

For the national coverage, the Sentinel-1 data has been downloaded from October 2015 to March 2016 for the whole Vietnam and Cambodia to test the methodology. Figure 16 shows the Sentinel-1 data scheme over 4 strips for a full coverage of Vietnam and Cambodia. 4 strips data have been acquired at different dates (5 day shift) with the different time intervals (12 and 24) between acquisitions and incidence range (29°-46°) in descending orbit. Over one year, for the Sentinel-1 datasets with an average of every 12-day revisit, a total of approximate 720 GB data were downloaded and preprocessed, as shown in Figure 16.
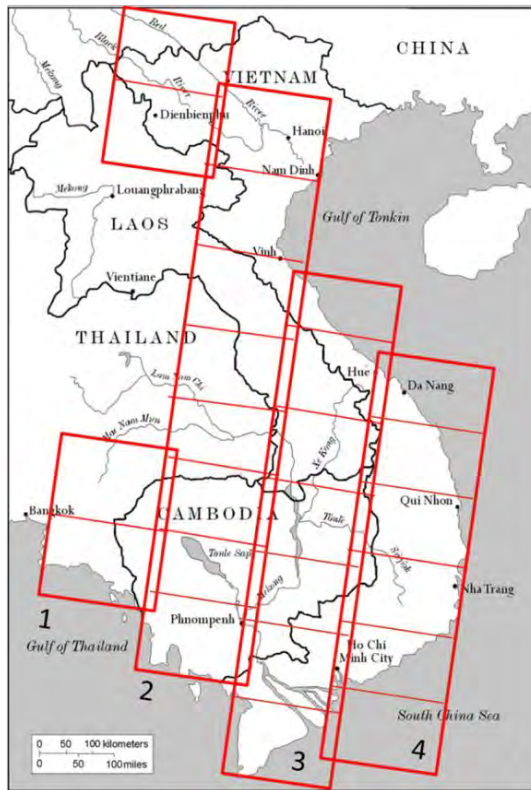
Acquisition over swath 2&3: 6/12 days

Acquisition over swath 1&4: 12/24 days

To cover 2 countries:

~24 GB data/acquisition

Average of a 12-day revisit:

30 acquisitions x 24GB = **720** GB

Figure 16. Sentinel-1 data schema over 4 strips coverage Vietnam and Cambodia.

3.3.2.2. Sentinel-1 Preprocessing

The Sentinel-1 images downloaded from the website (Peps.cnes.fr) are at the level 1-A (Level-1 Ground Range Detected (GRD) products consisting of focused SAR data that has been detected, multi-looked and projected to ground range using an Earth ellipsoid model such as WGS84). These data need to be preprocessed and quality assessed before the analysis.

SNAP software was utilized to preprocess the Sentinel-1 images (Sentinels Application Platform, http://step.esa.int/main/download/). The Sentinel-1 images preprocessing comprises the following steps:

- Multi-looking: to reduce the effect of speckle noise, spatial averaging is applied. However, multi-looking also decreases the spatial resolution of SAR images. For that reason, this step is only applied for the data used at the national scale in order to reduce the volume of the data, by averaging a window of 2x2 (20 m space pixels) (for the dataset in the Mekong Delta, multi-looking was ignored to keep original spatial resolution of 10 m).

49

- Calibration: conversion to the radar backscattering coefficient sigma nought (σ^0) from the digital numbers, which follows the procedure specified by the European Space Agency (ESA, 2017);

- Geo-correction: Due to the topographical variations of a scene and the tilt of satellite sensor, distances can be distorted in the SAR images. Terrain Correction is used to compensate for these distortions so that the geometric representation of the image will be corrected;

- Filtering: A multi-temporal filter as described in subsection 3.3.1 was applied to reduce the speckle noise in SAR images and thus increase the original number of looks in the image to a higher ENL (equation 14), without reducing the spatial resolution.

The required ENL can be assessed in order to meet a given probability of error in the rice/non-rice classification problem, as will be described in Section 5.3. This multi-temporal filter has been developed at CESBIO and implemented using Matlab software.

Analysis and interpretation

Contents

This chapter presents the analysis and interpretation of the experimental data which lead to the derivation of SAR indicators to be used in the rice monitoring methods. In the first section, which is based on the collected ground data, a detailed analysis of rice parameters with respect to cultural practices is carried out. In the second section, the SAR data time series are analysed as a function of ground data, followed by a physical interpretation of the temporal and polarization behavior of the radar backscatter, taking into account the effect of rice variety and cultural practices. Finally, based on the analysis and interpretation results, several indicators are derived for rice monitoring applications.

4.1. Ground data analysis

A total of 300 field samples (60 x 5 crop seasons) have been analyzed in terms of rice crop calendar, rice variety, cycle duration, rice yield, plant height, phenological stage and water management. The following characteristics of rice fields under study can be summarized:

(1) **Rice crop calendar**: Table 8 shows the sowing period and the harvest period of 60 rice field samples over 5 rice cropping seasons. The sowing period of each rice season could be expanded over 15 days (Autumn-Winter 2016), and up to 36 days (Summer-Autumn 2016). Meanwhile, the harvest dates of each rice season can differ between the sampling fields by up to 45 days (Autumn-Winter 2016). Overlapping among the fields has been found between the sowing period and the harvest period of two consecutive rice growing seasons, as shown in Figure 17.

Table 8. Ground survey of the sowing dates and harvest dates of 60 rice field samples under study over 5 rice cropping seasons.

Rice Seasons	Sowing period	Harvesting period
Summer - Autumn 2016	29/03/2016 to 06/05/2016	29/06/2016 to 12/08/2016
Autumn - Winter 2016	05/08/2016 to 20/08/2016	01/11/2016 to 14/12/2016
Winter - Spring 2017	29/11/2016 to 26/12/2016	05/03/2017 to 15/04/2017
Autumn - Winter 2017	16/08/2017 to 10/09/2017	15/11/2017 to 20/12/2017
Winter - Spring 2018	15/12/2016 to 06/01/2018	18/03/2018 to 25/04/2018

The calendar can be changed for the same rice season in different years, for example it was observed that the rice crop calendars of the rice seasons in 2017/2018 were delayed compared to the same rice season of in 2016/2017 (Figure 17).

Rice season of Autumn-Winter 2016 was started from 05/08/2016 to 20/08/2016, and harvested from 01/11/2016 to 14/12/2016, while Autumn-Winter 2017 rice season was started from 16/08/2017 to 10/09/2017 and harvested from 15/11/2017 to 20/12/2017, about more than 10 days later than the previous year calendar. Similarly, the sowing dates of Winter-Spring 2018 (from 15/12/2017 to 06/01/2018) were found later than the sowing dates of Winter-Spring 2017 (from 29/11/2016 to 26/12/2016).

One of the main reasons of the changes in local crop calendar is the effect of El Niño year in 2015/2016. Because of severe drought and saline intrusion in the region in 2016, the province authorities recommended to change the calendar in 2017. On the other hand, as mentioned in the section 3.2 on ground data collection, 52/60 sampled rice fields have been

52

replaced by 52 other rice fields for Autumn-Winter 2017 rice season, and this could also contribute to this difference in field specific crop calendar.
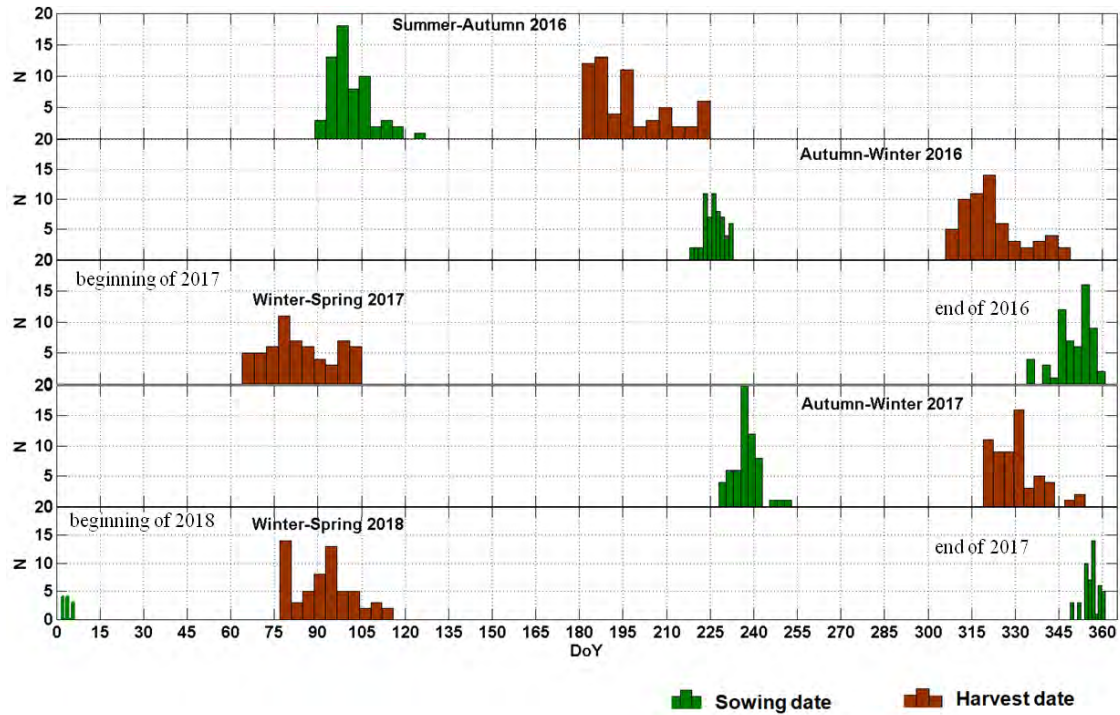
Figure 17. The histogram of sowing date and harvest date of 60 rice field samples during 5 rice cropping seasons. N represents the number of fields, DoY is the Day of the Year.
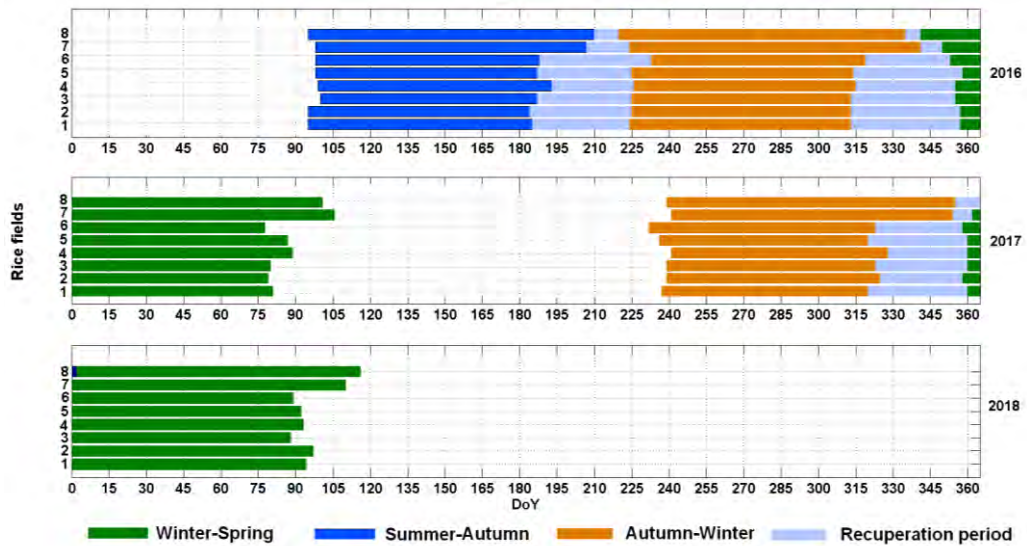
Figure 18. The crop calendar (sowing dates, harvest dates and cycle duration) of 8 same rice field samples over 5 rice cropping seasons.

However, Figure 18 shows a similar delay in the crop calendar of the 8 rice fields that did not change over 5 seasons.

It can be seen that the time between two consecutive rice growing seasons is spanned from a week up to 45 days, depending on the rice variety and the crop season. Long rice cycle variety (fields 7 and 8) has a much shorter recuperation period (about 7-10 days) compared to short cycle rice (fields 1 to 6). The recuperation period between Summer-Autumn and Autumn-Winter is observed shorter than the one after Autumn-Winter season, because of the flooding season (from October to December).

(2) **Rice varieties, cycle duration and yields**:

Table 9. Summary of the number of surveyed fields by rice varieties, planting methods, seeding density, and rice cycle duration of the 60 sampled rice fields under study over 5 rice cropping seasons.

Rice Seasons	IR 50404	OM 5451	Glutinous	Jasmine	Taiwan	Others	Total
Summer - Autumn 2016	32	4	5	2	11	6	60
Autumn - Winter 2016	34	3	4	4	11	4	60
Winter - Spring 2017	33	2	5	10	9	1	60
Autumn - Winter 2017	5	21	22	8	0	4	60
Winter - Spring 2018	25	0	26	7	0	2	60
Total	129 (43%)	30 (10%)	62 (20.67%)	31 (10.3%)	31 (10.3%)	17 (5.67%)	300
Planting method	Direct seeding	Direct seeding	Direct seeding	Transplanting	Transplanting	Direct seeding	
Seeding density (kg/ha)	22-30	20-30	25-30	10-12	8-15		
Rice cycle duration (day)	85-100	90-100	90-103	97-110	100-120	85-100	

Table 9 summarize the number of sampled fields per rice varieties, planting method, seeding density, and rice cycle duration of 60 sampled rice fields over 5 rice cropping seasons in the An Giang province.

The dominant varieties in 300 rice samples were short-cycle rice varieties including IR 50404 (43%), OM5451 (10%), and Glutinous (20, 67%), and long-cycle rice varieties account for 20.6% (Jasmine and Taiwan) in line with the rough estimate of the percentage of the long and short cycle rice in the region.

The short-grain rice variety such as IR 50404 or OM5451 have a short cycle duration from 85 to 100 days. The long–grain, long growth cycle varieties (Taiwan and Jasmine) have cycle durations from 100 to 120 days. As seen in Figure 18, rice fields 7 and 8 have been using the same long rice cycle variety (Jasmine) over the 5 rice seasons, so that the recuperation period is very short (7 to 10 days).

The long and short cycle rice fields differ in planting practices: transplantation for long cycle rice and direct sowing for short cycle rice. In transplanting, the seedlings are prepared and then transplanted to the inundated fields to provide regular spacing between the plants, with a seeding density of 10-15 kg/ha. For the direct sowing, the seeds are thrown

to the wet fields by hand or machine with the variable seeding density from 20-30 kg/ha, resulting in intra-field and inter-fields spatial heterogeneity. It can be seen that transplanting crop saved more than 50% of the seeds. However, 80% of farmers were using the direct seeding in order to eliminate the laborious process of planting seedlings by hand and greatly reduce the land preparation time and the crop's water requirements. However, the market price is much higher for long-cycle rice, because of the rice grain quality (FAO, 2017). As a consequence, the long-cycle rice, long time abandoned, is more and more used in the region (Phan *et al.*, 2018).

In terms of rice yields, the statistics of final yields of 300 rice fields show that it varies between rice varieties and between rice seasons. Figure 19 shows the histograms of final yields of the IR50404 samples (short cycle) and Jasmine and Taiwan (long cycle), and that of the total 60 rice fields over 3 consecutive rice cropping seasons in Summer-Autumn 2016, Autumn-Winter 2016 and Winter-Spring 2017.
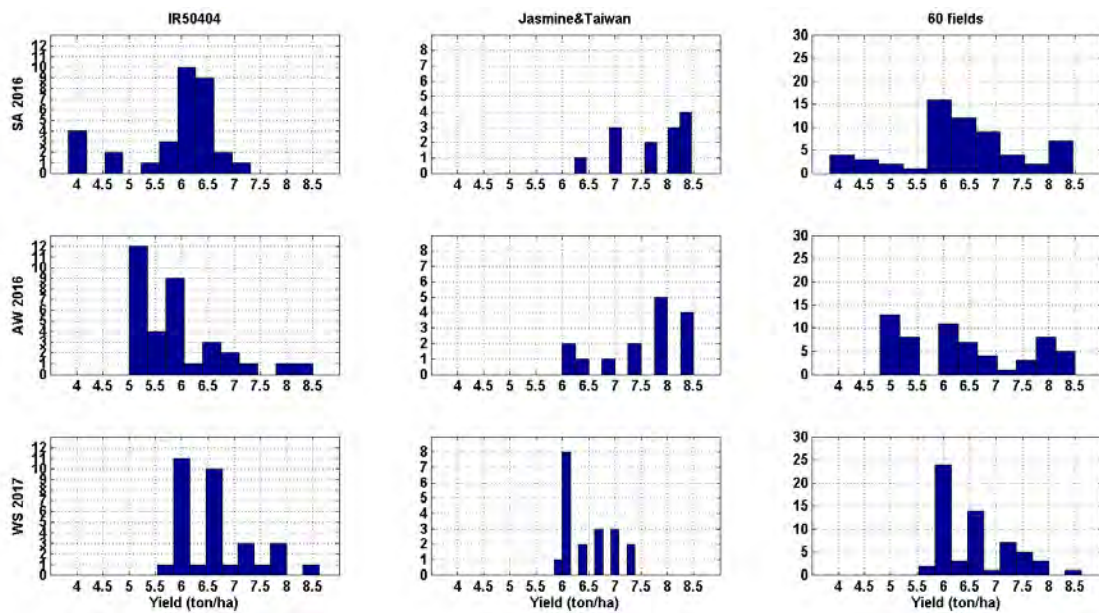
Figure 19. Histogram of final yields of IR50404 (the first column), Jasmine & Taiwan (the second column) and of all 60 rice field samples (the third column) over 3 consecutive rice cropping seasons in Summer-Autumn 2016 (the first row), Autumn-Winter 2016 (the second row) and Winter-Spring 2017 (the third row). The vertical axis represents the number of fields.

The yield ranges are quite large. However, a difference of rice yields is observed between two groups of short cycle rice variety (IR 50404) and long cycle rice variety (Jasmine & Taiwan). Long cycle rice variety had higher yield compared to short cycle rice

variety. The yield for 99 sampled fields of IR50404 was 4–8.5 ton/ha (average 6.5 ton/ha). 47 sampled fields of Jasmine and Taiwan had yield ranging from 6-8.5 ton/ha (average 7.6 ton/ha).

Figure 20 shows the histogram of final yields of 60 rice fields collected over 2 rice cropping seasons in Autumn-Winter 2017 and Winter-Spring 2018. The yield range showed a difference between the two rice seasons. It is clearly seen that Winter-Spring 2018 (7–9 ton/ha) had higher rice yields than that in Autumn-Winter 2017 (4.5-6 ton/ha). This is in line with the knowledge that Winter-Spring season has the highest productivity and Autumn-Winter has the lowest productivity as mentioned in section 3.1.

However, there is no distinction among rice variety groups. At the same rice season, long-cycle rice variety (Jasmine) had the same rice yield range than short-cycle rice variety (IR50404 & OM5451) and Glutinous.
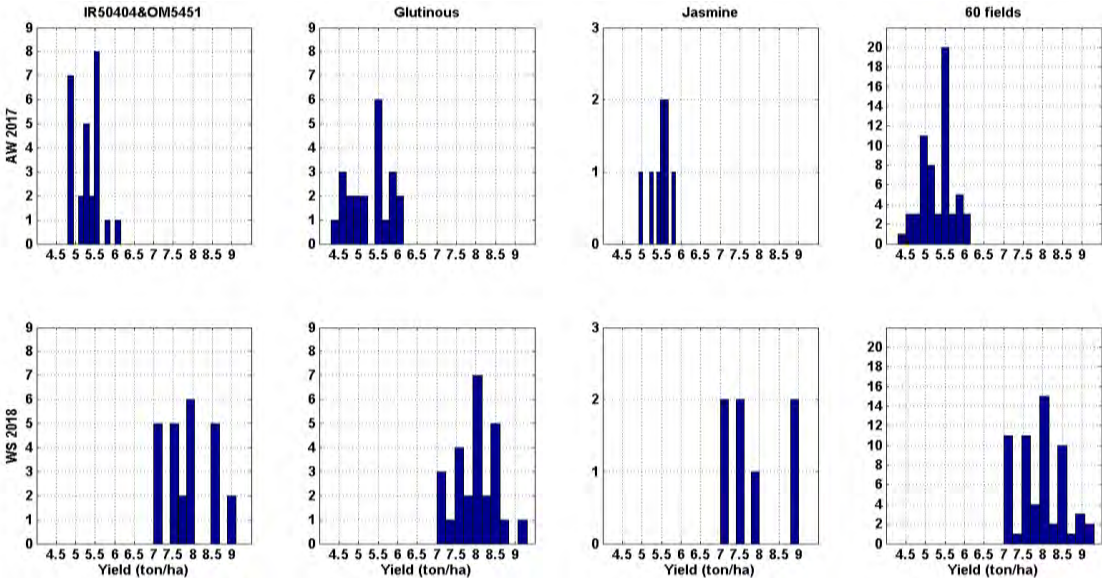
Figure 20. Histogram of final yields of IR50404 & OM5451 (the first column), Glutinous (the second column), Jasmine (the third column) and of all 60 rice field samples (the fourth column) over 2 consecutive rice cropping seasons in Autumn-Winter 2017(the first row) and Winter-Spring 2018 (the second row).

For the same rice seasons over two years (AW 2016 and AW 2017, WS 2017 and WS 2018), although the rice samples are not the same, it can be seen that the yields differ between two years. AW 2016 had much higher rice yields than AW 2017 in both long-cycle and short-cycle rice variety. Moreover, Jasmine rice had the lowest yield in AW 2017 (lower than 6 ton/ha) compared to 4 other rice seasons (higher than 6 ton/ha). In the contrary, WS 2017 had lower rice yields than WS 2018. This could be a result of the differences in cultural

practices, water management and also due to the effect of environmental conditions (flooding year, drought year).

For consistency, the ground data of the two last seasons (Autumn-Winter 2017 Winter-Spring 2018) will be used to analyze the detailed parameters including plant height and phenological stage, because the sampled rice fields were different in the previous rice seasons.

(3) **Plant height**:

Figure 21 shows the temporal variation of the plant height of one group of short cycle rice and one group of long cycle rice. The analysis is applied separately to long cycle rice (15 samples of Jasmine) and short-cycle rice (51 samples of IR50404, OM5451).

Long-cycle rice varieties
15 samples of Jasmine
$y = -0.006x^2 + 1.6x - 1.1$
$R^2 = 0.9345$
$\varepsilon_{rel} = 2.23\%$
RMSE = 6.72 (cm)

Short-cycle rice varieties
51 samples of IR50404, OM5451
$y = -0.0078x^2 + 1.7x - 4.2$
$R^2 = 0.9525$
$\varepsilon_{rel} = 1.16\%$
RMSE = 4.91 (cm)
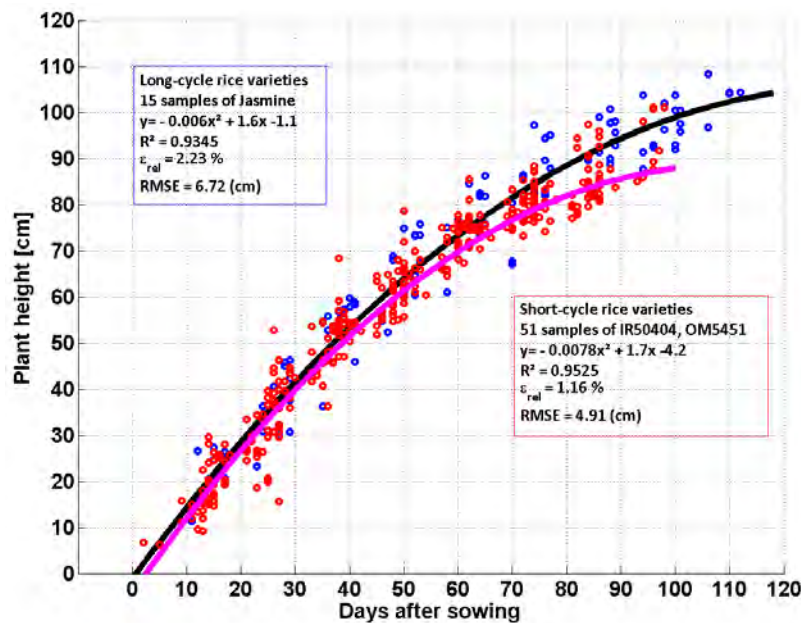
Figure 21. Temporal variation of plant height (versus days after sowing): 15 sampling fields for long-cycle rice plants (blue points and black polynomial regression); 51 sampling fields for short-cycle rice plants (red points and pink polynomial regression) of 2 consecutive rice cropping seasons in Autumn-Winter 2017 and Winter-Spring 2018.

The same increasing trend is observed until 80 days at 80–90 cm for both groups. This trend has been observed in previous studies monitoring paddy rice fields (Phan *et al.*, 2018, Ndikumana *et al.*, 2018).

From 60 days after sowing (beginning of reproductive phase for short cycle rice), the short cycle rice variety shows a smaller increase rate until 95 days, while long cycle rice variety continues until 110 days. Two empirical polynomial regression curves of plant height have been derived and used. A coefficient of determination $R^2 = 0.93$ and a RMSE of 6.72

57

cm was obtained for long cycle variety group and R² = 0.95 and a RMSE of 4.91 cm for short cycle variety group.

(4) **Phenological stage and water management**:

Figure 22 shows the phenological stage, from 1 to 12, as a function of the days after sowing. The distribution of sampled data at each stage is represented by a box plot based on five representative quantities: minimum, first quartile, median, third quartile, and maximum. Outliers are also singled out. This analysis also makes use of two groups of short cycle rice (51 samples) and long cycle rice (15 samples).
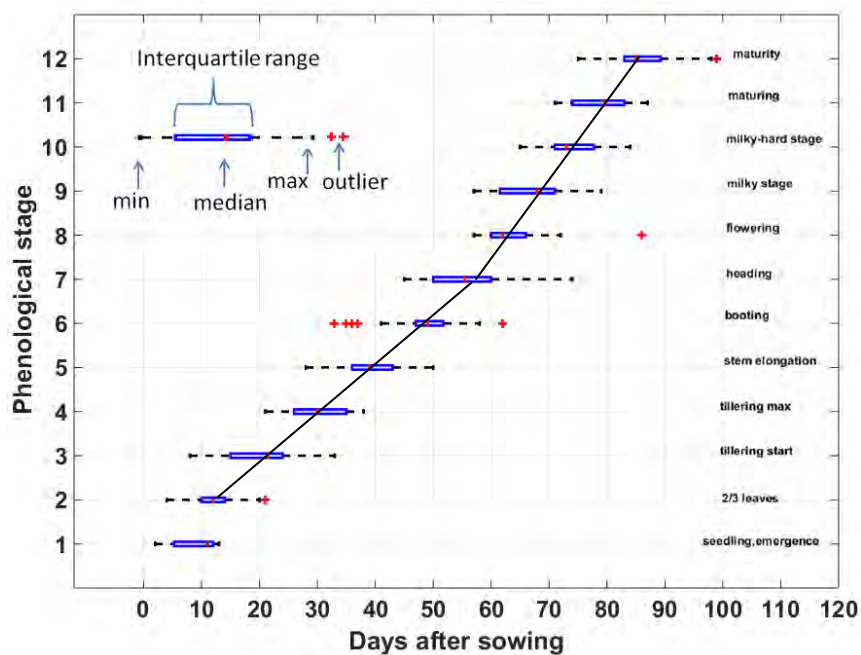
Figure 22. Box plot of phenological stage (from 1 to 12, corresponding to the stage name on the left part of the figure) of 51 short-cycle rice sampling of Autumn-Winter 2017 and Winter-Spring 2018 rice seasons.

Figure 22 shows the box plot of 12 phenological stages of 51 short-cycle rice sampling of Autumn-Winter 2017 and Winter-Spring 2018 rice seasons. Two periods can be distinguished: from 1 (emergence) to 7 (heading), rice grows reaching the following stage every 10 days; and from 7 (heading) to maturity (12), rice grows reaching the following stage every 3 – 5 days.

Similarly, Figure 23 shows the box plot of 12 phenological stages as a function of plant age of 15 long-cycle rice samples of Autumn-Winter 2017 and Winter-Spring 2018 rice seasons (days after sowing of long cycle rice means days after transplanting).

58
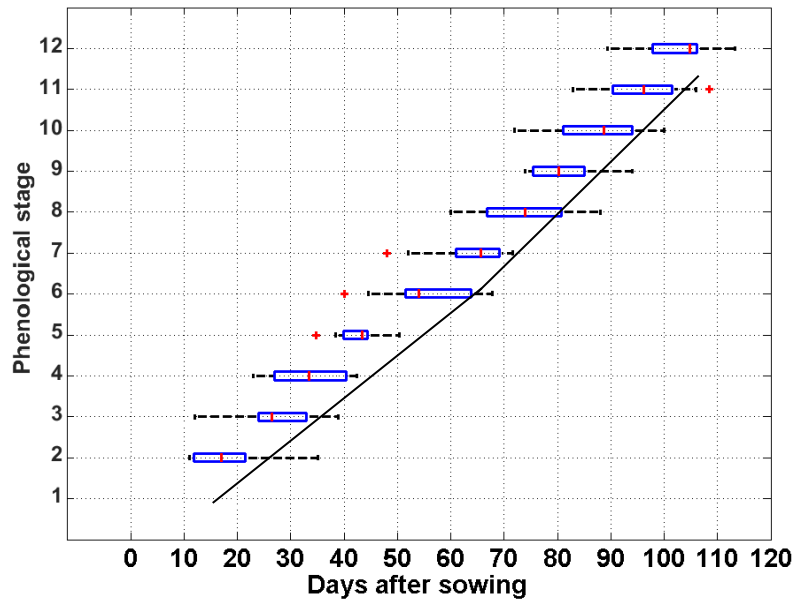
Figure 23. Box plot of phenological stage of 15 long-cycle rice sampling of Autumn-Winter 2017 and Winter-Spring 2018 rice seasons.

Figure 24 shows the histogram at each phenological stage of all the rice fields over two rice seasons.
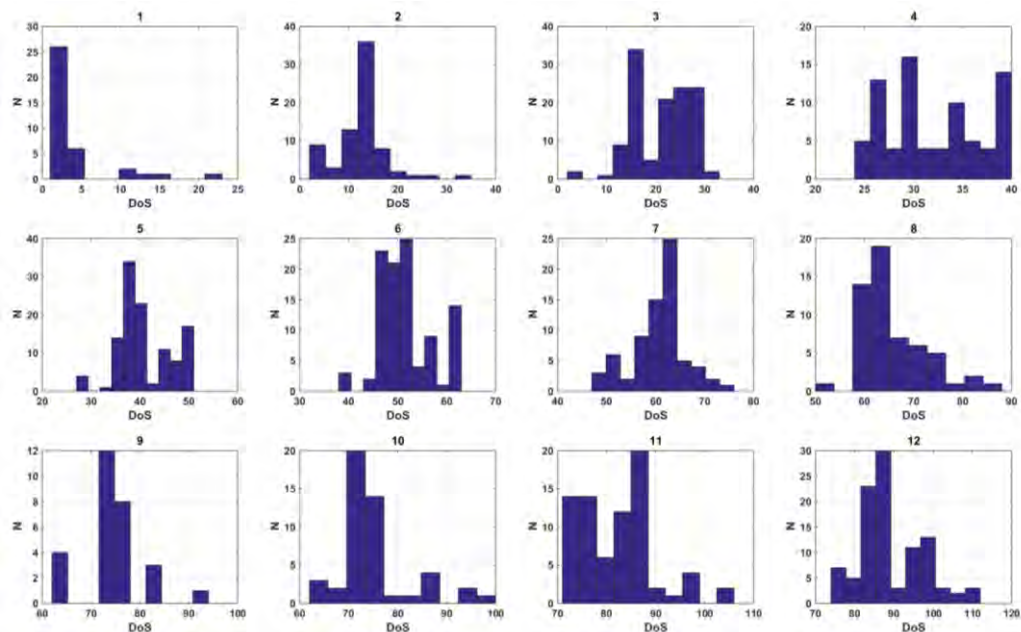
Figure 24. Histogram at each phenological stage of 120 rice samplings (60 sampling of Autumn-Winter 2017 and 60 sampling of Winter-Spring 2018 rice seasons).

A large inter-fields variability is observed as a result of the difference on rice varieties, planting practices and field and water management. From stage 1 to stage 7, the

inter-field variability (about 20 days) is smaller than that from stage 8 to stage 12 (from 30 to 40 days). The growth stages of short and long-cycle rice follow the same trend until stage 7 (heading of short cycle rice). From stage 8 onwards, short cycle rice grows reaching the following stage every 3 – 5 days while long cycle rice continues to grow reaching the next stage every 7-10 days (Figure 22 and Figure 23).

Based on the analysis of collected ground data and on the farmer survey, the phenological stage of rice development as well as the associated water management in the region under study can be summarized as follows:

- For **short cycle rice**:

➢ 1-2 weeks before the sowing, the fields were flooded in order to prevent self-propagating vegetation and pests. The fields were drained 1-2 days before sowing. Rice seeds were directly sown on wet soil by drilling (precision equipment) or broadcasting (hand). 3-4 days after sowing, the fields were irrigated (2-3 cm) just for 1 day then drained to ensure sufficient moisture on the field surface to facilitate seed germination.

➢ 10 to 15 days after sowing (stage 2, plant height at about 15-20 cm, 2-3 leaves). The fields were inundated during this period for the roots to grow smoothly.

➢ 15 to 25 days after sowing (stage 3, plant height at about 20-35 cm, beginning of tillering). During the tillering period, the rice grows rapidly and strongly in roots and leaves. This period is the key in the development of leaf area and number of effective tillers, number of leaves (and number of future panicles). The duration of the tillering depends on the variety, cultivation methods and environmental conditions. In favorable solar radiation and nutritional conditions, this period lasts about 20-25 days. The fields were irrigated 2-3 times for about 5-10 cm and water kept for 2-3 days each time. It is important to note that about 20 days after sowing, the rice plant loses its vertical structure.

➢ 25 to 35 days after sowing (stage 4, the plant height is at about 35-45 cm, and the plant reaches the end of tillering). Farmers keep only 3-5 effective tillers per plant and eliminate the others to optimize the nutrition consumption as well as avoiding pest infestation. The fields were irrigated during fertilizing for a couple of days then drained to kill pest.

Alternate wet/dry irrigation (AWD) was applied from this stage to save water irrigation, the intermittent drying of the rice fields instead of keeping them continuously flooded as described in section 2.2.

- 35 to 48 days after sowing (stage 5, plant height is at about 45-58 cm, and the plant reach stem elongation). Plant is growing straight up and denser.

- 48 to 58 days after sowing (stage 6, the plant height is at about 58-70 cm, the plant is at booting stage). The first step is the process of differentiation and formation of reproductive organs, and this process directly affects the rice yield. In this period, rice has significant changes in morphology, leaf color, physiology, and resistance to external circumstances.

   The initial panicle has been formed and prepared for heading. From the panicle initiation stage, three more leaves have been formed.

   Until this stage, the rice plants finish the vegetative phase (tillering, elongation, and booting) which is characterized by an increase of the plant height, an increase of the number of tillers, and a development of leaves.

- 58 to 65 days after sowing (stage 7, heading). When the booting period is finished, the heading starts the reproductive phase. The entire panicles are heading from the leaf sheath. The process is finished within 4-6 days.

- 65 to 75 days after sowing (stage 8, plant height at about 70 – 80 cm, flowering). It takes about a week for the flowers on the same panicle to blossom. After 10 days, all the flowers are fertilized and begin to develop into seeds.

   During the reproductive phase (heading, flowering) the plant is characterized by a decrease of the number of tillers, the development of panicle leaf, the panicles formation and development. After heading, the growth (height, biomass) stops and the leaves change their orientation, to be no more erectophile.

- 75 to 85 days after sowing (stages 9, 10, milky stage). The biomass of grains strongly increases during this period, reaching 70-80 % of the final grain biomass. The heavy panicle curls down.

- 85 to 100 days after sowing (stage 11, 12): maturity stage.

   During the ripening phase (grain filling, milk, and maturity), a decrease of leaf and stem moisture content and a decrease of the number of leaves are observed. The irrigation is stopped during the latter part of this period until harvest.

- For **long cycle rice**, the vegetative phase development was similar to the short rice cycle until stage 6. From stage 7, rice develops with a 3-4 days longer at each stage compared to short rice cycle to end its cycle duration of 110-120 days.

To summarize, the analysis of the ground data shows that the crop calendars are not uniform within the region, leading to difficulties in obtaining information on the timing of the crop growth stages, in particular sowing and harvest dates.

The analysis shows that during the rice cycle development, the plant structure changes at key phenological stages. This can be used to understand and interpret the temporal and polarization behavior of the radar backscatter. In particular, the changes at the beginning of tillering, and the booting-heading (about 20 days and 60 days after sowing), independently to the rice variety, can lead to the development of backscatter indicators for rice phenological stages.

4.2. Radar backscatter analysis & physical interpretation

4.2.1. Radar scattering mechanisms of rice fields

The SAR data have proven ability to distinguish rice from other land cover types because of the specific response of the radar backscattering of vegetation with vertical structure over inundated or wet soil. The interaction between a radar electromagnetic wave and vegetation involves mainly three mechanisms: the scattering from the ground attenuated by the vegetation canopy (surface scattering), the volume scattering, and the multiple scattering between the volume and the ground (volume-surface scattering).
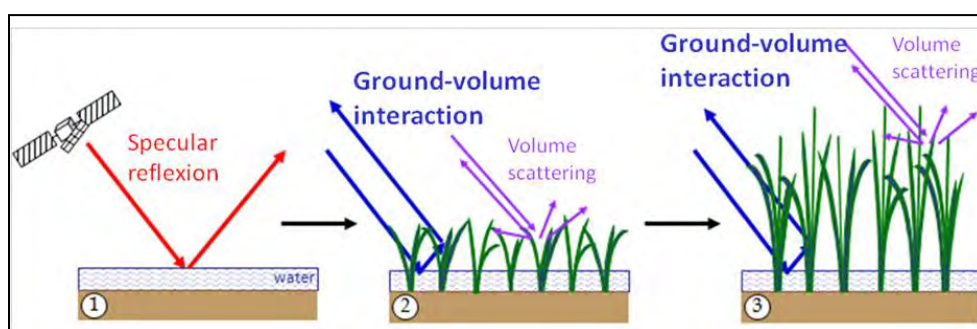
Figure 25. The backscattering mechanisms involved in rice fields at the flooding stage in traditional cultural practices, before transplanting (left), early vegetative stage (center), and late vegetative stage (right).

The volume-surface scattering term usually brings a negligible contribution compared to the two others in the usual case of vegetation growing over non-flooded soils. However, in the case of flooded fields or fields with wet soil such as rice paddies, this term

becomes dominant when the plants develop because of the double-bounce between the water surface and the plant stems, which are the dominant scatterers in the volume. The different backscattering mechanisms are illustrated in Figure 25.

As described in Chapter 2, for traditional cultural practices, the rice fields are covered with a blade of water during most of their growth cycle. For modern alternate wetting and drying (AWD) practices, the fields are inundated only during certain periods, and the soil is wet for the rest of the season. For transplanted rice, radar backscatters from inundated fields before transplanting are low due to specular reflectance from the water surface. However, with the direct sowing, seeds are sown on wet soil and the backscatter at sowing dates has no more low characteristic values. During the growing period from the vegetative stage, to reproductive stage, radar backscatter increases rapidly which is the consequence of a rapid increase in rice plants height and biomass. The following reproductive phase includes the panicle initiation, heading, and flowering processes. During this phase, the plants stop increasing in height, biomass, and the leaves start to wither and die. Ripening is the final stage with its milk, dough, and mature grain processes.

Electromagnetic models have been used to explain the temporal variation of rice backscatter at X band (Le Toan et al., 1989), C band (Le Toan *et al.*, 1997) and L band (Wang et al., 2005). Most studies simulated the backscatter at HH and VV polarization, and the simulation results indicate that 1) the double bounce backscatter is dominant during a large part of the rice cycle, in particular at C and L-band, 2) the strong increasing temporal variation of rice backscatter during the vegetative phase, 3) the large attenuation in VV polarization due to the vertical structure of rice plant, leading to high HH/VV ratio. Those studies have led to the selection of the backscatter temporal change and the polarization ratio as indicators for detection of rice grown area (Bouvet et al., 2009) (Bouvet and Le Toan, 2011).

However, the previous studies had provided simulations for VV, and HH (e.g. to interpret ERS and ENVISAT ASAR C-band data). Sentinel-1 offers a cross-polarised intensity together with a co-polarised intensity in its dual-polarisation products. Theoretical modelling studies are required for a better understanding of the backscatter in HV or VH polarization. In this study, MIPERS (Multistatic Interferometric Polarimetric Electromagnetic model for Remote Sensing) has been used to simulate the HV backscatter. MIPERS developments have been initiated at ONERA (Villard, 2009) during a PhD work and are being pursued at CESBIO. The data used for detailed description of rice plants until heading stage were from Ribbes et al., (1998), and Le Toan et al., (1997) (for logistical

reason, it was difficult to conduct detailed measurements of rice plants at different growth stages in the study region).

The model distinguishes the four scattering mechanisms illustrated in Figure 25:

(1) Volume contribution: simple reflection onto volume scatterers (belonging to the vegetation layer).

(2) Double bounce contributions: considering wave-plant-ground or wave-ground-plant interactions. Specular reflections onto the ground surface are accounted for using the modified Fresnel coefficients.

(3) Triple bounce contribution: coupling terms with the ground surface are accounted twice, so that two specular reflections are considered on the ground surface.

(4) Ground direct contribution: simple reflection onto ground scatterers.

The model simulations were used to interpret the VH backscatter of rice fields in the An Giang province measured over a rice field which follows traditional cultivation (long cycle rice, transplanting and continuous flooding).
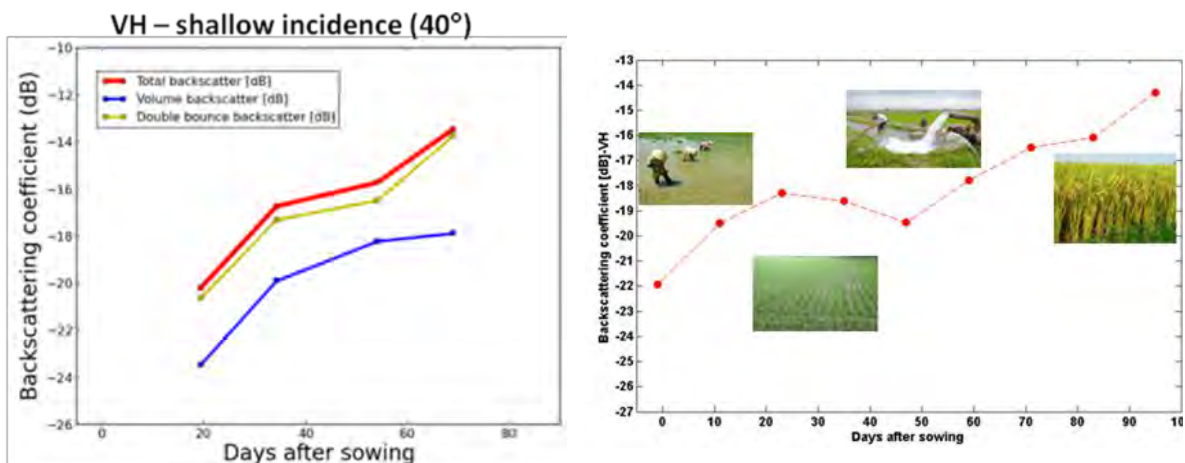
Figure 26. Simulation results from MIPERS (left), compared with Sentinel-1 backscatter profiles (right), for the VH backscatter of a rice field following traditional cultivation (transplanting, continuous flooding,long cycle rice).

The simulation showed that at a shallow incidence (40°, which corresponds roughly to the incidence at the center of the Sentinel-1 IW data), the cross-polarised backscatter is also dominated by the double-bounce interaction between the scatterers and the ground, similarly to the co-polarised backscatter, as shown in Figure 26. This result brought a new insight to the earlier knowledge, which often assigned cross-polarisation backscatter to volume scattering. The result also revealed that the double bounce backscatter shows a lower rate in its increase at 55 days after sowing, resulting in a small decrease in VH backscatter

64

at that stage, and this was interpreted as due to higher attenuation at the booting-heading stage. The experimental data show similar trends to the simulations, despite that the input data describing the plant growth were not derived from the description of the plants observed in the experiment. The work needs to be completed with a dedicated campaign measuring geometric and dielectric properties of the components of the rice canopy under study at different dates during the rice season, in order to interpret in details the scattering mechanisms that occur at different growth stage.

4.2.2. Sentinel-1 times series analysis

4.2.2.1. Times series analysis at different polarizations

The time series of 126 Sentinel-1 images from 06/10/2014 to 31/03/2018, with a 12-day revisit until 25/09/2016, then a 6-day revisit period afterwards, have been used to analyse the temporal behavior of radar backscatter over rice fields. The images were preprocessed as described in the previous section before being used to extract the radar backscatter coefficients ($\sigma°$) of the 60 sampling rice fields.

Figure 27 shows the VH and VV and VH/VV ratio of backscatter coefficients extracted from the 60 sampled fields. For comparison with optical data, instead of Sentinel-2 data which are often affected by cloud cover, the Proba-V NDVI (Normalized Difference Vegetation Index) product has been used. All the NDVI images employed in this work were downloaded from http://www.vito-eodata.be/. Figure 27 contains the NDVI time series from January 2016 to December 2017. The NDVI values are averaged for the rice fields under study from pixels of 100 m × 100 m of Proba-V NDVI (1-2 pixels per sample).

The data time series from 6/10/2014 to 19/11/2017 clearly show characteristic temporal behavior of the backscatter at VV, VH, and VH/VV for each rice season, with a clear similarity between seasons.

From the start to the end of a rice season (indicated by vertical bars in Figure 27), neither VH nor VV exhibit a 'bell curve', as often suggested in past studies. Instead, VH/VV follows well the bell curves, but the curves have their minima not at the start and the end of season but shifted about 20 days after the start of season. This large increase in VH/VV can be interpreted as caused by the differential contribution of the double bounce scattering, and the differential attenuation in VH and VV. As a consequence, the ground contribution is minimised in the ratio, and it is expected that the backscatter ratio has higher correlation

with the plants parameters such as biomass or LAI, as reported by (Mattia et al., 2001, Bernardis et al., 2016, Veloso et al., 2017, Begue et al., 2018). This behavior is to be compared with the NDVI curve, with minima ±6 days after at the sowing date and ±6 days before the end of season.
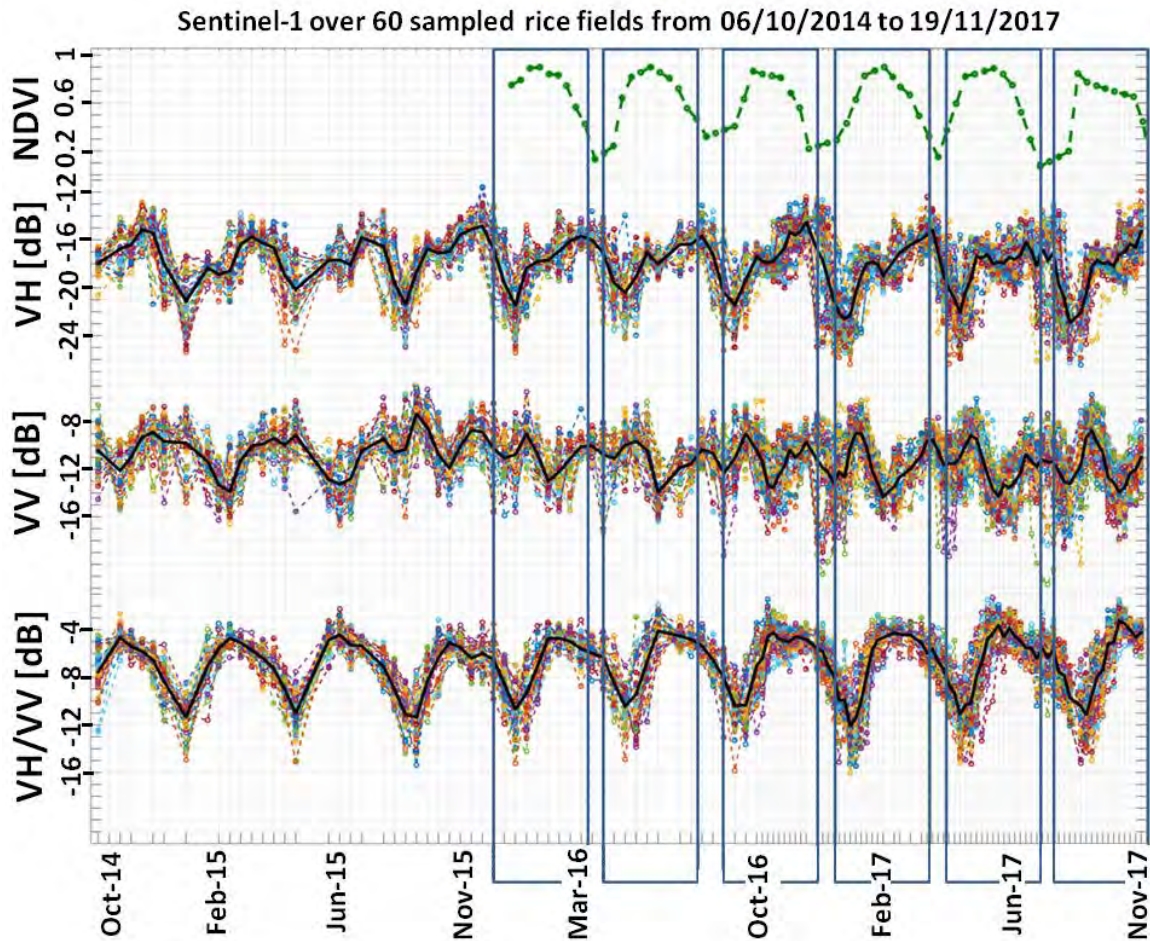
Figure 27. VH and VV backscatter coefficients and their ratio VH/VV extracted for the 60 sampled fields from Sentinel-1 images from 06/10/2014 to 19/11/2017. It is noted that the revisit time of the Sentinel-1(A+B) from 26/09/2016 is every 6 days. The black curves are the averaged quantities for all 60 fields. The green curves is the NDVI time series of the rice fields under study from January 2016 to December 2017.

Figure 27 also shows the difference in the curves with 12 days or 6 days (after 10/2016) acquisition intervals. In the second case, inter-season variation is better captured (in VV and VH), and the minimum backscatter values for each season are lower. Figure 27 shows that the maximum temporal variation (difference between maximum and minimum backscatter) is high: for the mean curve (averaged over 60 fields) the maximum temporal change is about 5-6 dB for VH, 4-5 dB for VV, and 6-7 dB for VH/VV. The characteristic

66

temporal behaviour of the backscatter is expected to reflect the changes in plant morphology (and/or in water management), along the different phenological stages of the plants.

For a given date, the inter-field variation of the backscattering coefficient of the 60 fields can be very large, up to 20 dB, notably at the beginning of the season when the fields have a diversity of status, from bare fields, flooded or not, to rice plants at early and late growth stages. Moreover, the planting calendar was different among the 60 rice fields, with different rice varieties, planting practices and management. Figure 28 shows an example of RGB combinations of three dates from Sentinel 1 images over rice fields in the An Giang Province using the VH polarization. In this region entirely constituted by rice fields (98%), a mere combination of 3 dates provides a distinction of a high number of 'rice classes', which makes it not adapted to the use of traditional classification methods to map rice fields. In this context, physical based methods are required to deal with the diversity of rice field conditions.
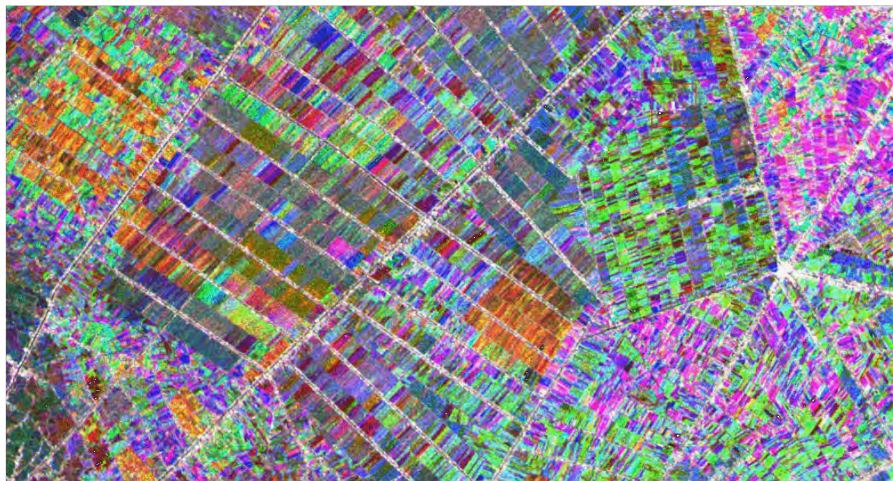
Figure 28. Example of RGB combinations of different dates (R:26/10/2016, G:01/11/2016, B: 07/11/2016) from Sentinel-1 images, VH polarization over rice fields in the An Giang province.

4.2.2.2. Times series analysis at different incidence angles

The data used in this study are Interferometric Wide-Swath (IW) mode to cover the whole Mekong Delta region with a 250 km swath. Because IW mode captures 3 sub-swaths of different incidence angle ranges from 29.1° to 46° (Table 10), it is necessary to assess the variability of the rice backscatter temporal profiles across the incidence range.

Table 10. The incidence angle (in degrees) of the IWS data corresponding to the 3 different sub-swaths of different incidence angle ranges from 29.1° to 46°.

	IW1	IW2	IW3
Min orbit altitude	30.86° - 36.59°	36.47° - 41.85°	41.75° - 46.00°
Max orbit altitude	29.16° - 34.89°	34.77° - 40.15°	40.04° - 44.28°

To analyse the effect of incidence angle on the radar backscatter, the training rice samples have been selected over the Mekong Delta, with 7 samples at each 2 degrees from 31° to 46° (a total of 56 samples).
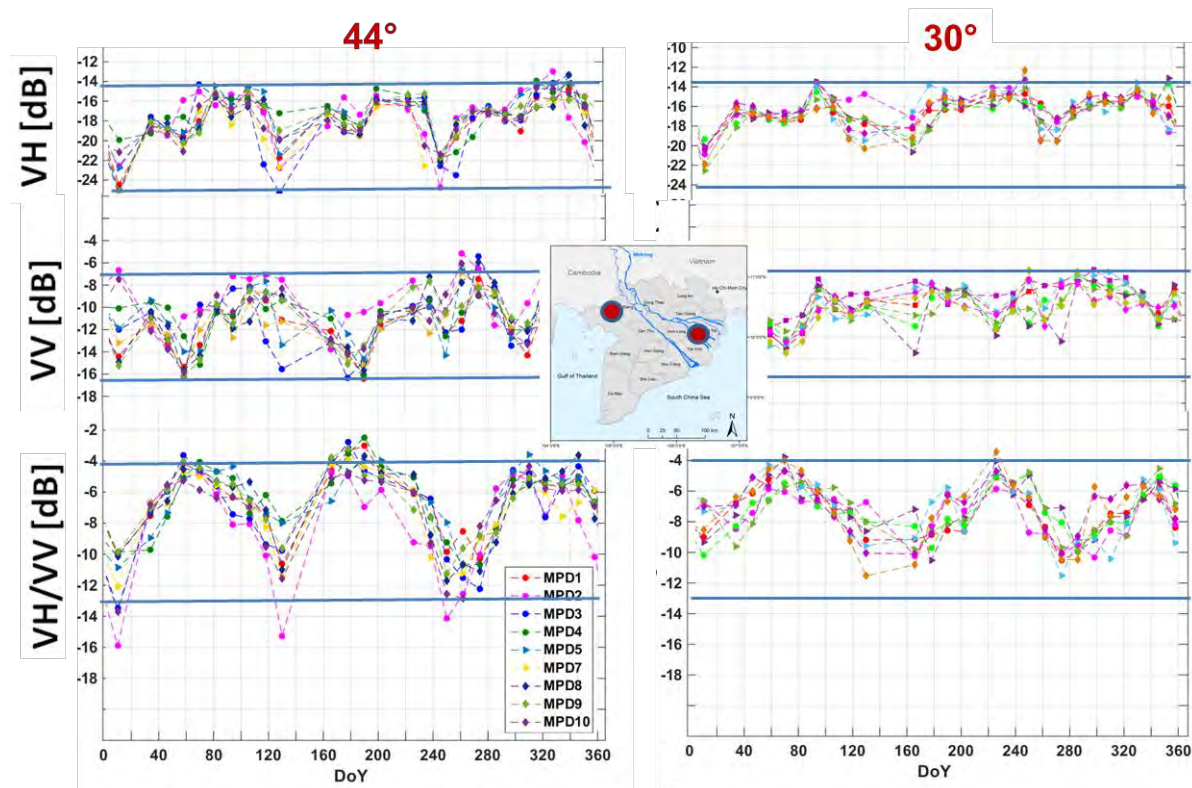
Figure 29. Example of the temporal variation of VH, VV and ratio VH/VV backscatters over rice fields in 44° (An Giang) and 31° (Ben Tre) in the Mekong Delta.

Figure 29 shows a comparison of the temporal variation of the backscatter VH, VV, and VH/VV from rice fields located at 44° incidence angle (in the An Giang province) and from rice fields located at 31° (in Ben Tre province). The first difference between the backscatter at 44° (left column) and at 31° (right column) is the lower dynamic range (difference between maximum and minimum) in the lower incidence angle curves. The

reduced dynamic range appears to be caused by higher minimum backscatter values (of 3-4 dB) at 31°, and a slightly lower maximum backscatter values (1 dB or less).

However, the analysis needs also to further take into account of the differences in cultural practices at different places in the Mekong Delta, from East to West.

The maximum temporal increase of VH has been analysed as a function of the incidence angle range from 31° to 46°. Figure 30 shows that the maximum temporal change for one rice season increases with the incidence, from about 6 – 8.5 dB in nearest range to about 9 - 12 dB beyond 38°.

It can be understood that the incidence angle in the range from 30° to 45° has different effects on the volume, double bounce and surface scattering. The surface scattering which corresponds to the minimum backscatter changes significantly from 30° to 45°. At 45° the specular scattering over smooth water surface is expected to produce much lower backscatter than at 30°, where the radar scattering pattern gives rise to higher backscatter. The reduced backscatter maximum temporal change from 45° to 30° can be assigned mainly to this decrease in surface scattering backscatter. Regarding the maximum backscatter, which occurs at 65-70 days after sowing, passing from 45° to 30° decreases the double bounce term, and the volume scattering should have only a slight increase (if the variation follows cos (θ), the difference between 30° and 45° corresponds to a decrease of 0.8 dB).
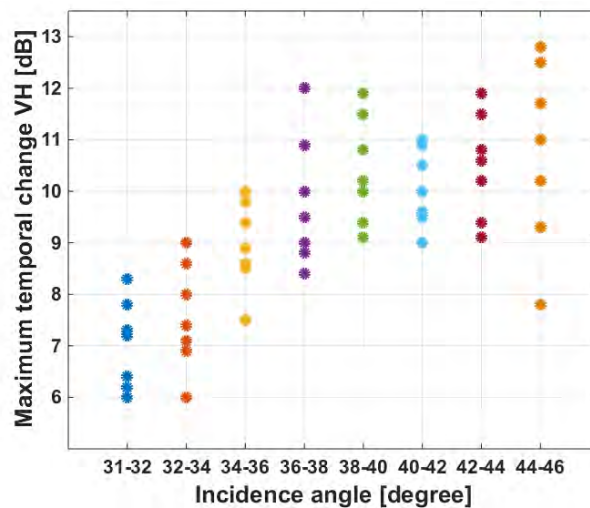
Figure 30. Maximum temporal change of VH backscatters over rice fields versus incident angle of Sentinel-1 data in the Mekong Delta.

The resulting overall maximum temporal change varies from 6-8 dB to 9-12 dB as shown experimentally in Figure 30.

The effect of the incidence angle on the backscatter is also tested over small water bodies. Figure 31 shows that the VH and VV backscatter coefficients are both decreased of 3-4 dB with increasing incidence angle from 30° to 45°.
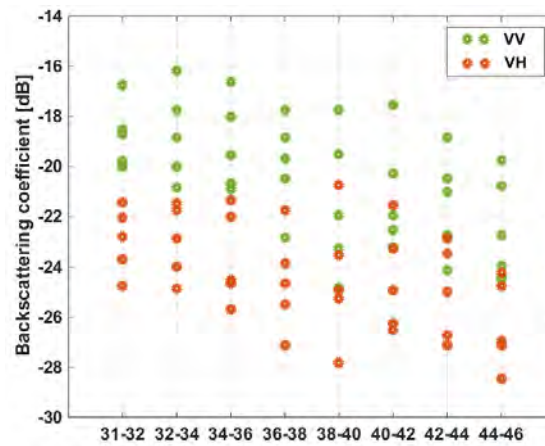
Figure 31. Temporal change of VH and VV backscatters over water bodies versus incident angle of Sentinel-1 data in the Mekong Delta.

However, in Figure 30 and Figure 31, it can be noticed that the angular behavior could have discontinuities which correspond to the three sub swaths, 30°-35°, 35°-40° and 40°-45°. In this case, additional variations should be due to the processing to compensate for the incidence angle effect.

4.2.2.3. Times series analysis at ascending and descending orbits

Sentinel-1 SAR system has both ascending and descending orbits. This gives an expectation to combine ascending and descending data in order to reduce the time interval between acquisitions over an area of interest. However, it is noted that ascending and descending measurements are done along different line-of-sight (LOS) thus a given field is observed at two different incidence angles and cannot be combined simply using averages. An analysis of Sentinel-1 time series makes use of 32 ascending images and 32 descending images in the Mekong Delta. This time series was from 13/03/2017 to 01/04/2018, a 12-day revisit time within 1 day difference in Europe time in the acquisitions between two orbits. However, the descending orbit passes around 23 pm (i.e. 6 am the next day over the Mekong Delta) while the ascending orbit acquires around 11 am (i.e. 6 pm the same day over the Mekong Delta), resulting at the same date in the acquisitions for both orbits for the region under study. Figure 32 shows the temporal variation of VH, VV backscattering coefficient,

and polarization ratio VH/VV over a rice field sample and water sample extracted from S1-A time series at ascending and descending orbits.
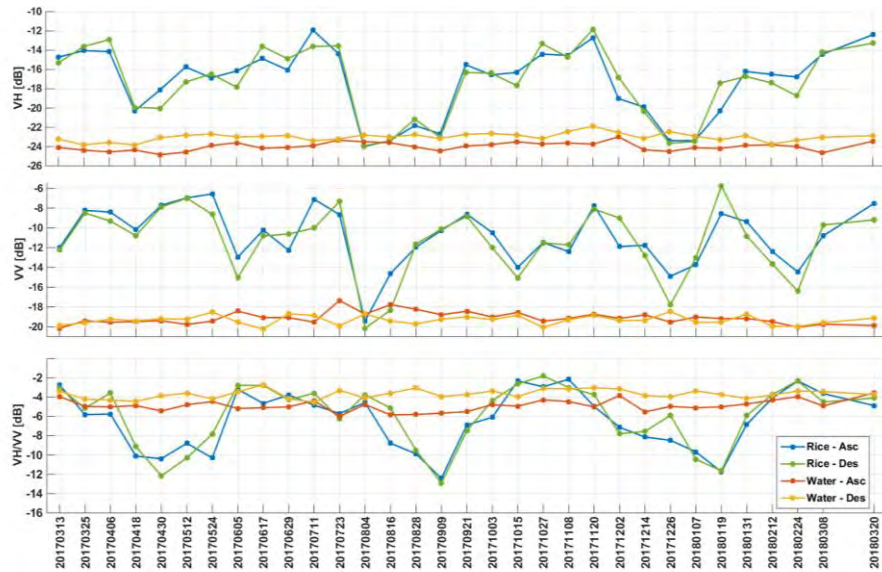
Figure 32. Variation of VH, VV backscattering coefficient, and polarization ratio VH/VV over rice fields and water sample extracted from S1 images at ascending and descending orbits.

The samples are located at incidence angle of 37° and 43° at ascending and descending orbits, respectively. It can be seen that the difference between ascending and descending orbit over the time series is more important for VV than VH, however in most cases less than 2 dB for rice fields and water samples. This is in agreement with the differences which can be observed at these two relatively close incidence angles (Figure 30 and Figure 31). It can be noted that, the effect of the environmental condition (wind, rain) between the morning (descending) and the afternoon (ascending) can also contribute to the difference.

This analysis needs to be completed by comparing fields at more important differences in incidence angle and across seasons. Nevertheless, the relatively small differences shown in Figure 32 indicate a potential to combine the ascending and descending acquisitions to increase the frequency of data acquisitions. However, the availability of both orbits depends on the region of interest and the Sentinel-1 acquisition scenario (Figure 14). For example, in, the Mekong Delta, the descending orbit has been acquired at every 12 days from October 2014 and every 6 days from October 2016, while the ascending orbit has been acquired from March 2017 at every 12 days.

4.2.3. Seasonal variation with regard to the phenological stages

To understand the seasonal variation of the backscatter with regard to the phenological stages of rice plant and field condition, the backscatter time series are analysed as a function of plant age (days after sowing).

Figure 33 shows the VH, VV and VH/VV backscatter of 30 rice sampled fields in the Autumn-Winter 2016 rice season in An Giang province. These 30 samples have been chosen to have close sowing dates, the same planting practices, same rice variety, in order to avoid the effect of cultural practices in the trend analysis.

At the early stage (stage 1), rice is directly sown on wet soil. Low radar backscatter values at VH and VV polarizations are observed, with large inter-field variation due to the different field conditions (wet bare soil with variable roughness, smooth surface with clods, mud or water pockets, etc. (Zribi et al., 2006, Baghdadi et al., 2016). At 10 days after sowing, the fields are flooded and the water layer remains during the period of 10-15 days. VH and VV remains low, with VV starting to increase with the vegetation growth.

From 10 days to 20 days, at the beginning of tillering, (stage 2 to stage 3), VV increases steadily of 5-6 dB, whereas VH shows a small increase (less than 2 dB) due to the increase of the volume and double bounce backscatter and reaches the maximum value at around 20 days.

From 20 to 30 days (stage 3 to 4, maximum of tillering) VV having reached its maximum, starts to decrease, whereas VH still increase.

From stage 4 to 6 -7 (end of stage 6, booting, beginning of stage 7, heading), the plant is characterized by an increase of the plant height, an increase of the number of tillers, and the full development of leave, and by a clear vertical plant structure. The rice canopy becomes denser, leading to an increasing attenuation in double bounce and in volume backscatter, enhanced by the vertical structure of the plant in VV. VV shows a very strong decrease, i.e. from -8 dB to -16 dB, in about 1 month, whereas VH shows also a decrease, but much smaller (2 dB). During this period, the attenuation by the plant increases, reducing the VV and also the VH backscatter, as observed in the model simulation (Figure 26).
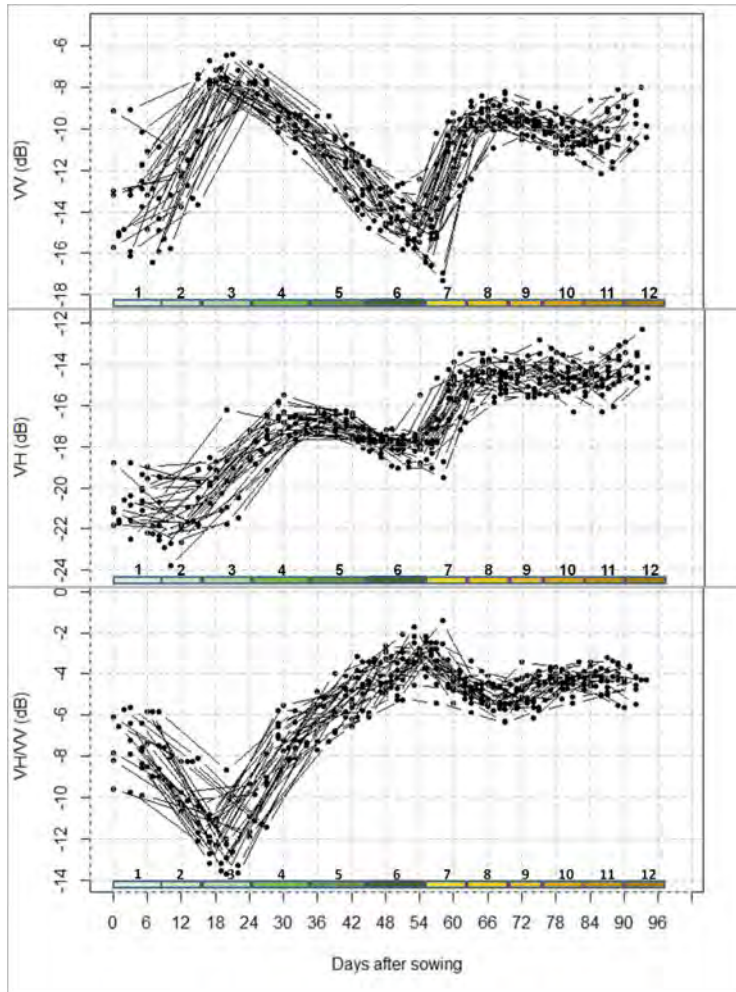
Figure 33. Variation of VH, VV backscattering coefficient, and polarization ratio VH/VV of the 30 sampled fields extracted from S1 images versus the days after sowing. On the horizontal axis, phenological stages from 1 to 12 are indicated.

During the reproductive stage from 55 days to 70 days (heading, stage 7 and flowering, stage 8), the plant is characterized by a decrease of the number of tillers, the development of panicle leaf, the panicles formation, and the increases in biomass, contributing to an increase of the volume scattering. The radar backscatter therefore increases at both VH and VV polarizations, with a stronger increase in VV (6-7 dB vs 2-3 dB).

From 70 days to maturing stage (stage 8 to 11), the leaves and stem biomass decreases and the grain biomass increases to reach 70-80 % of the final values. A small decrease of VV is observed whereas VH remains stable.

At the end of the cycle, stage 11 to 12 (maturity stage before harvest) when the grains reach the maximum of biomass and the leaves and stems biomass continue to decrease, a small increase (of 2 dB) is observed for both VV and VH.
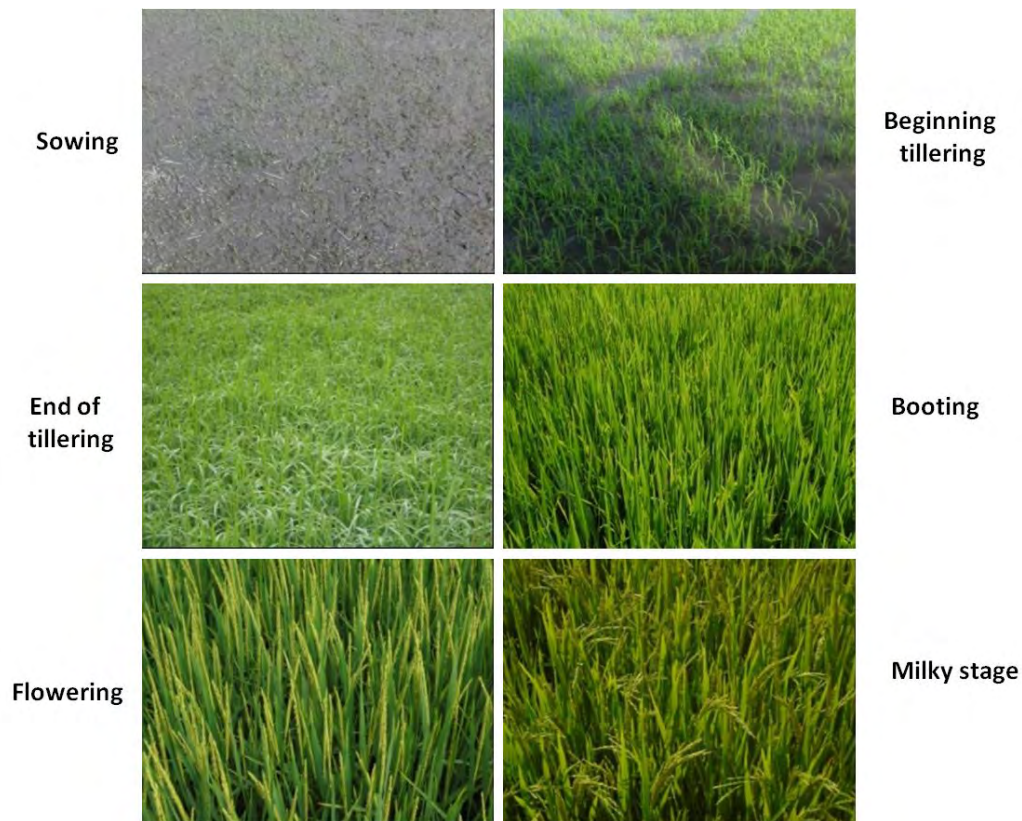
Figure 34. Illustration at some phenological stages in the rice field under study.

The ratio VH/VV, resulting from the behavior of VH and VV, exhibits the following specular trend:

- From stage 1 to stage 3, a decrease to reach the minimum value at stage 3 at 20 days. This corresponds to the strong increase of VV as compared to that of VH.
- From stage 3 to stage 7, the ratio increases following two rates: from stage 3 to stage 4, during the tillering stage, the increasing rate is more important, about 4 dB in 10 days; as compared to 3-4 dB in 30 days, from stage 4 to stage 7.
- From stage 7 to stage 8, from heading to flowering, the ratio decreases slightly (about 2 dB), before remaining stable until stage 12.

4.2.4. Effect of short/long cycle duration, effect of water management

In the previous section, the temporal behavior of VH, VV and their ratio has been analysed for short cycle rice, in relation with the rice phenological stages. In this section, the long cycle and short cycle rice are compared at different rice seasons and different years. To do that, the 8 sampled rice fields that did not change over two years of ground data collection (as discussed in section 4.1) were used.
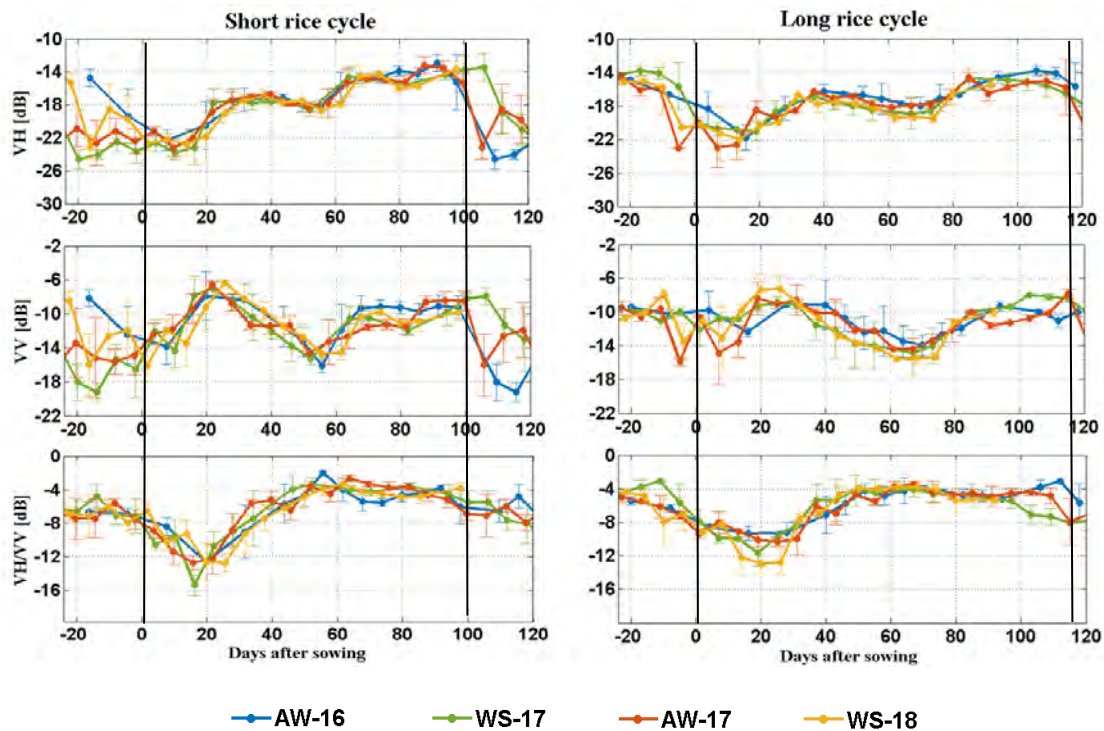
Figure 35. Temporal evolutions and standard deviation of VH (the first row), VV (the second row), and VH/VV (the third row) of short rice cycle (the first column) and long rice cycle (the second column) over 4 rice cropping seasons Autumn-Winter 2016 (AW-16), Winter-Spring 2017 (WS-17), Autumn-Winter 2017 (AW-17) and Winter-Spring 2018 (WS-18).

Figure 35 shows mean VH, VV and the ratio VH/VV along with their standard deviation of long/short cycle rice fields in Autumn-Winter and Winter-Spring rice season over two years 2016/2017 and 2017/2018.

The main differences of the temporal evolution of VH, VV and the ratio VH/VV of short cycle rice (100 days duration, direct seeding) and long cycle rice (118 days duration, transplanting) can be noticed as follows:

- For the period before the start of season, VV and VH differ notably due to field preparation. For direct seeding, fields are usually inundated for a few days to eliminate weeds, before drainage occurs, and direct seeding is done on wet soil. For long cycle rice, fields are inundated just before transplantation. Moreover, as discussed in the previous section, the sampled rice fields of long cycle rice had very short recuperation periods (7-10 days) between two consecutive rice growing seasons. The maturity stage of rice of the previous rice season was explained for the high backscatter values of long cycle rice in the period of -20 days to -10 days before the sowing date compared to short cycle rice where the rice fields were already harvested.

- About 60 days after sowing, a difference between long and short cycle rice at VH and VV backscatter can be observed. For short cycle rice, VH and VV start increasing after 60 days while for long cycle rice, they continue to decrease until 75 days then start increasing again.
- About 100 days after sowing, VV and VH backscatter of short cycle rice decreases drastically, whereas the backscatter of long cycle rice continues its course.
- For VV/VH, the two rice types show quite similar temporal variations.

This effect of long and short cycle rice on radar backscattering is found consistent with the analysis of ground data in section 4.1 with regard to phenological stages.

The possibility to detect rice field inundation state is important to assess the water used in irrigated rice, and to estimate the GHG emissions. Moreover, it is expected that the detection could be done with Sentinel-1 based on the more important double bounce scattering mechanism when the fields are inundated.

Figure 36 shows the backscatter temporal variation at VH, for 2 fields: the first is planted with long cycle rice (transplanted, continuous flooding), the second with short cycle rice (direct seeding, AWD).
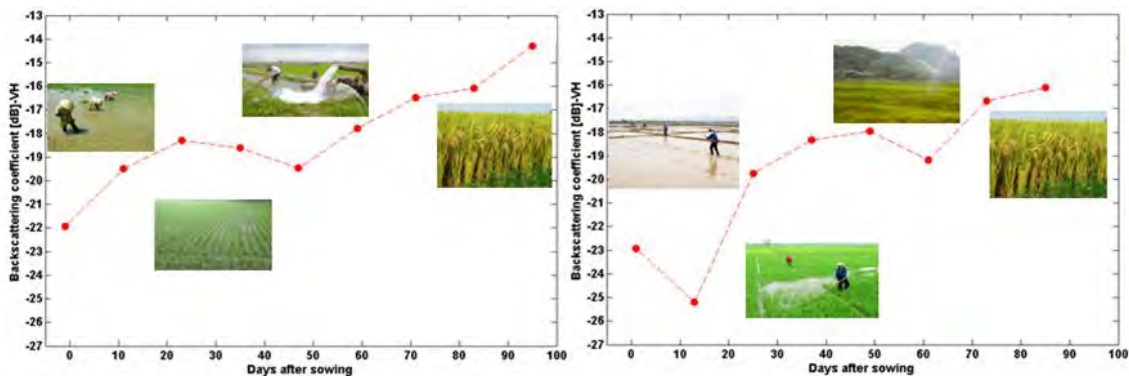
Figure 36. VH backscatter as a function of plant age (days after sowing) of two rice fields under study: long cycle rice (transplanting, continuous flooding) on the left and short cycle rice (direct seeding, AWD) on the right.

In the direct seeding method associated to short cycle rice, the wet soil was prepared before broadcasting. After 10-20 days, the fields were filled with water for few days. When the rice fields are at the reproductive phase the fields should be irrigated again using drip irrigation or overhead sprinkler. As noted before the crop is not continuously flooded, the farmer uses the AWD technique with fewer pumping operations.

However, the differences between the backscatter curves of the two fields in Figure 36 are difficult to identify either due to inundated status or to rice varieties. For AWD, the

duration of field inundation periods during the rice season is relatively short: 4-5 days at the beginning of the season, and before flowering. For the first flooding period, when the plants are small, the minimum backscatter is detected, as in Figure 36 (right), but for the second period, when the plants are fully grown, the difference in backscatter with or without inundation is small (1-2 dB) and difficult to interpret. Moreover, with a repeat cycle of 6 day, it is not clear if Sentinel-1 can capture the field inundation states. For the long cycle rice (Figure 36 left) which is continuously flooded, at the start of the season, the plants are already at 10-15 cm at transplantation, the minimum backscatter should be observed before the date of planting. It is noted that the increase of the backscatter has been interpret as that of the double bounce scattering, and the small decrease at 50 days was interpreted as due to attenuation at booting-heading stage (Figure 26 in Section 4.2.1)

In this study, the water management is derived from the identification of long and short cycle rice, based on the cultural practices in the Mekong Delta. However, more work should be conducted for the detection of inundation status.

4.2.5. Inter-season and inter-annual variations

Time series analysis of Sentinel-1 images has been carried out over 3 years from October 2014 to November 2017 to study the inter-season and inter-annual variations of rice fields in the Mekong Delta. Figure 37 (a, b, c) shows temporal variations of different rice cropping system in the Mekong Delta, from 1 crop per year to 3 crops per year.

Three rice crops per year were observed in the An Giang, Dong Thap province, where the dykes system was built, as shown in Figure 37(a).

Figure 37(b) shows 2 rice crops per year with rotation of rice-rice-vegetable, mostly in the provinces near the coast.

More recently, farmers near the coast have diversified their rice systems by also growing shrimp, either concurrently or in rotation with the rice, as shown in Figure 37 (c). The temporal variations of VH, VV and VH/VV backscatters of the rice crop are similar to the trends analysed in the previous section.
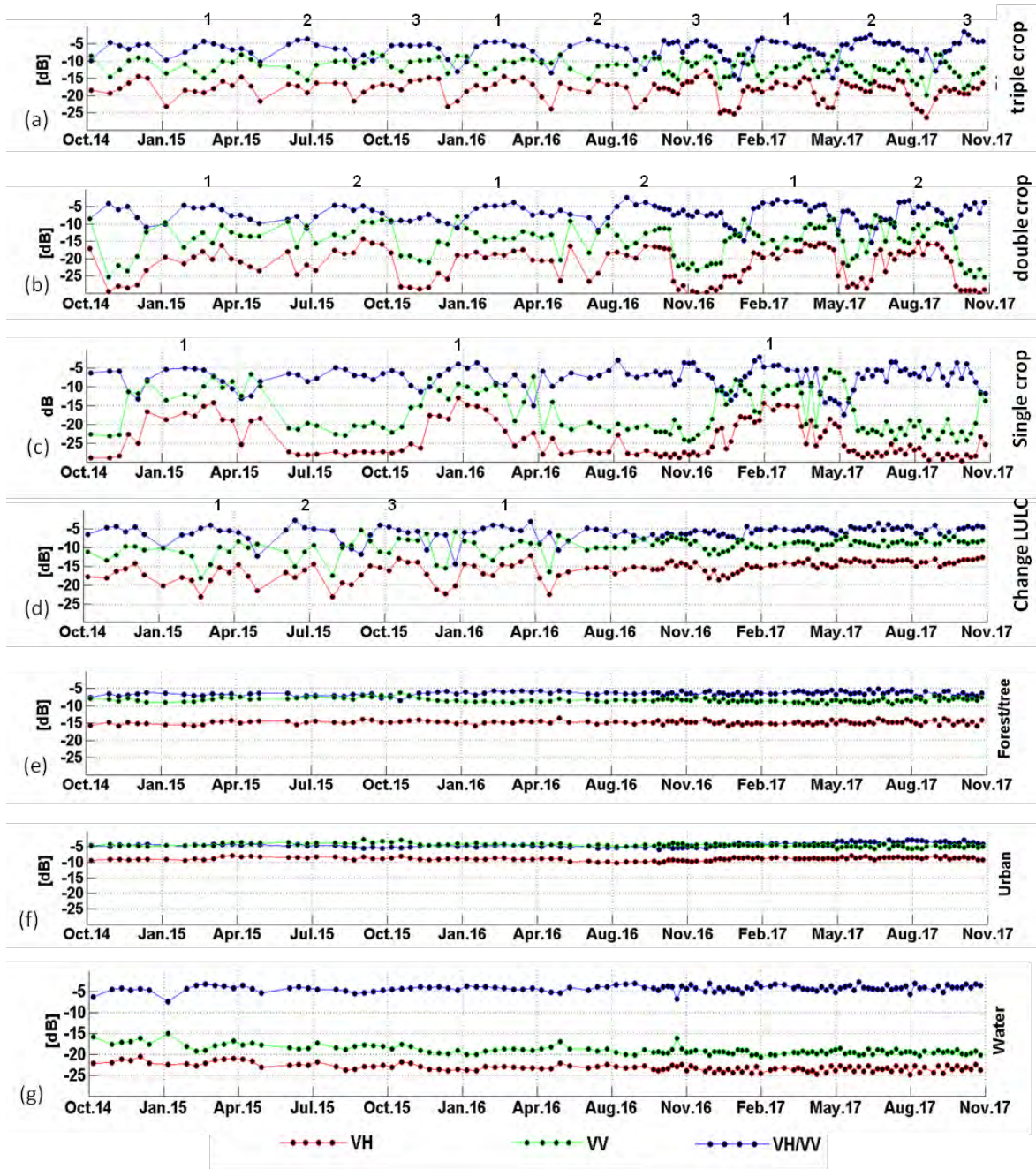
Figure 37. Temporal evolutions of VH, VV, and VH/VV backscatters of Sentinel-1 time series over rice fields, of triple crop (panel a), double crop (b), single crop (c), 3 rice crops a year followed by aquaculture (d), forest/tree (e), urban (f) and water body (g), from October 2014 to November 2017.

To distinguish rice from other land use land cover type, it is important to understand the backscatter and its temporal variations for the other cover types. Figure 37 (e, f, g) shows the backscatter of the main other land use classes present in the Mekong Delta, here, forest, water, and urban areas, which have much more temporal stability, and which have very different VH backscatter levels.

78

4.3. Derivation of Indicators for rice mapping and rice monitoring

From the analysis results, we can derive several indicators for rice mapping, mapping of short-cycle and-long cycle rice, determination the sowing date and the phenological stage and plant height estimation:

(a) Rice mapping: to discriminate rice fields from other LULC the temporal change of the VH and HH/VV ratio can be used. However, if the data acquisitions are not frequent, the data at the beginning or the end of a given rice season can be missed. In this case, polarization ratio VH/VV is a better indicator than VH for rice field mapping. In addition, indicators derived from the VH polarization (e.g., the maximum and minimum backscatter values in the VH time series) can be used to map other land use land cover classes (water, forest, and built up area).

(b) Determination of sowing date: Figure 33 shows the radar backscatter behavior of VH, VV and the ratio VH/VV as a function of sowing date. This trend has been confirmed by several rice seasons over several years (Figure 35) and then can be used as a reference curve (derived statistically from the experimental data) to estimate the sowing date. For VH and VV temporal variations, the confidence range of the reference curves is from 1 to 60 days after sowing where the radar backscatter behavior is the most stable. Meanwhile, the ratio VH/VV reference curve over the whole rice cycle appears repeatable from one rice season to the other, over the years of data analysis. The VH/VV time series are therefore used for sowing date estimation.

(c) Mapping of short/long cycle rice: in Figure 35, the backscatter of VH polarization of the short cycle at around 65 - 75 days after sowing has lower values (i.e lower than -16.5 dB) as compared to the long cycle rice. The indicator to be used is therefore the values of VH polarization during flowering stage (65 to 75 days after sowing).

(d) Phenological stage mapping: Once the sowing date of the rice field is estimated, the phenological stage can be derived. However, at each growth stage, VH, VV and VH/VV value should be used as indicators to confirm the rice growth development (as shown in Figure 33).

(e) Plant height: Two empirical polynomial regression curves of plant height derived in the section 4.1 (Figure 21) will be used for plant height estimation.

Based on the observed specific temporal behavior of the backscatter of rice fields over different rice seasons and different years, and considering the effects of rice varieties, radar incidence angles and ascending and descending modes, Sentinel-1 backscatter indicators have been developed for rice mapping, mapping of long and short cycle rice, determining sowing date, phenological stages, and plant height.

<div align="right">Chapter 5</div>

Methodology development

Contents

This chapter describes the methods developed for rice mapping and monitoring using Sentinel-1 SAR data. The aim of this work is to derive methods based on the knowledge of the temporal development of the rice plants and rice fields under different conditions, and on the understanding of the related temporal variation of the radar backscatter in order to introduce a simple approach that is robust, repeatable and suitable for rapid rice mapping over large extents with cost-effective field work.

Methodologies have been developed based on the indicators described in the previous chapter for mapping of rice area, rice varieties, rice cropping intensity and for retrieval of rice parameters (sowing date, phenological stage and plant height).

An overview of the rice mapping and monitoring workflow is given in Figure 38.
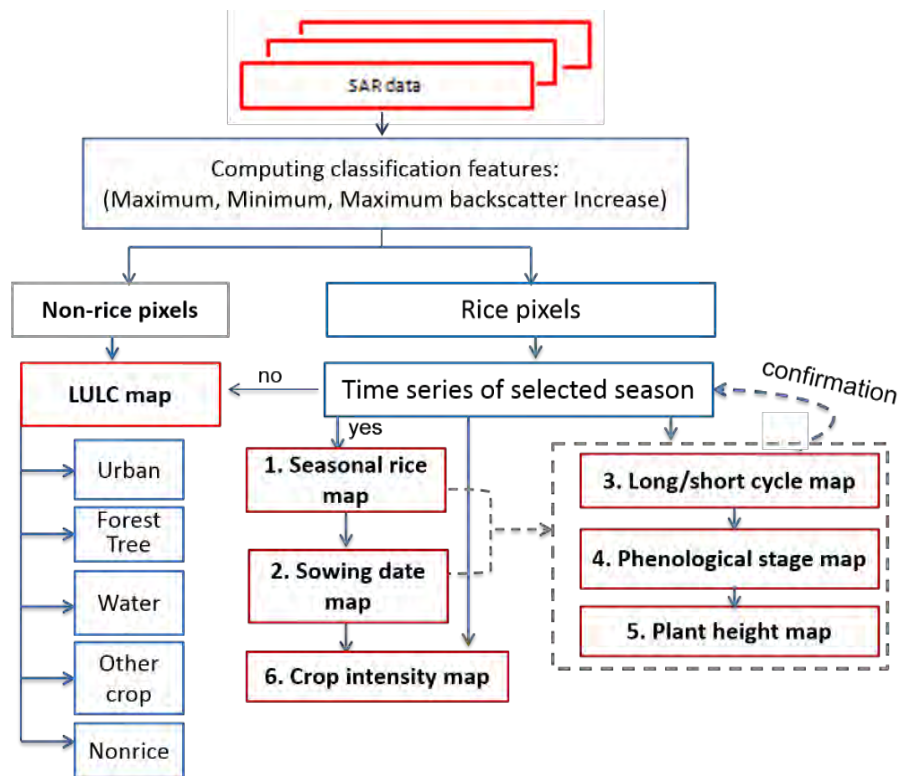
Figure 38. Workflow of rice monitoring method using Sentinel-1 data.

- As a first step, a time series of preprocessed Sentinel-1 data is used to calculate the classification features at the pixel level. By using the rice/non rice classification feature which is the maximum temporal change, all non-rice pixels will be classified as other land covers (water, urban, forest, tree or other crops). The remaining pixels will be considered as potential rice pixels and used to make rice mapping products.

- Then, an algorithm will be applied to automatically select the time period covering a given rice season for the production of the rice seasonal map.

- Following this time period selection, the rice seasonal map and sowing date map will be produced, which are subsequently used to derive other mapping products (long/short cycle map, phenological map, etc.). It is noted that for a given Sentinel-1 date, rice field before sowing and after harvest will be labeled as non-rice, so that the rice map corresponding to each Sentinel-1 date will refer to the fields with the presence of rice plants. Whereas the rice seasonal map will include all the fields observed from the sowing date to the end of the season (the last phenological stage). The rice mapping and monitoring method are described in detail in the following sections together with the limitations of each approach.

82

5.1. Calculation of classification features

The rice/non-rice mapping algorithms in this research rely on a limited number of classification features which are statistical features computed from the Sentinel-1 time series. The main purpose of the first step is to mask out non-rice pixels and then create the LULC map (water, urban, forest/tree and other crop), the rest will be considered as potential rice pixels. For this purpose, a time series of all available Sentinel-1 images are used, preferably to cover a cropping season (from before sowing to after harvest). The maximum value, minimum value, mean value and maximum change in time series of Sentinel-1 at VH and VV polarizations are used to generate the rice/non-rice (LULC) maps.

Maximum value in time-series: VH_max, VV_max and VH/VV_max: The classification features VH_max and VV_max correspond, for each pixel, to the maximum value of the intensity at VH and VV polarizations within the time-series of this pixel for the period that covers the area of interest (AOI). **VH/VV_max** is the maximum value of VH (dB) – VV (dB) for each pixel in time series.

Minimum value in time-series: VH_min, VV_min and VH/VV_min: Likewise, the classification features VH_min and VV_min correspond, for each pixel, to the minimum value of the intensity at VH and VV polarizations within the time-series of this pixel for the period that covers the AOI. **VH/VV_min** is the minimum value of VH (dB) – VV (dB) for each pixel in time series.
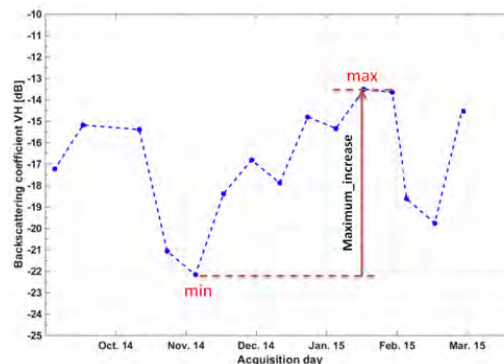
Figure 39. Example of maximum increasing of VH backscatter temporal change during rice growth cycle.

Maximum change in time-series: VH_max_inc and VV_max_inc: The classification features VH_max_inc and VV_max_inc correspond, for each pixel, to the maximum positive intensity change at VH and VV polarizations over the time-series of this pixel for the period that covers the AOI. In this study, **VH_max_inc** is used only.

83

In practice, it is calculated by identifying the minimum intensity in the time-series (which corresponds to the early stage of the rice field during its cycle) and the maximum intensity in the dates that follow the occurrence of this minimum intensity as illustrated in Figure 39.

5.2. Seasonal date selection

The time series of Sentinel-1 images are selected based on the knowledge of rice seasons in the region. In order to map a specific rice season, the time series needs to contain a date around the start or the end of the season, and a date approximately during the peak season (highest backscatter). However, for a large region, the crop calendar varies considerably with environmental conditions as well as farming practices. The overlapping between the sowing period and the harvest period of different rice growing seasons (as mentioned in the previous chapter) can affect the rice mapping products. This weakness has been discussed in (Nguyen *et al.*, 2015).

Table 11. Calendar of the Summer-Autumn rice season in 2016 in the 13 rice growing provinces of the Mekong Delta. Note that for Hau Giang and Tra Vinh, the calendar for 2015 and 2016 are shown to point out the change in crop calendar decided by farmers and local authorities motivated by the impacts of El Nino in 2015.

Summer-Autumn	1	2	3	4	5	6	7	8	9	10	11	12
Ben Tre												
Vinh Long												
Can Tho			22/3									
Tien Giang												
Long An												
Hau Giang												
Hau Giang 2016		9/2						10/8				
An Giang												
Ca Mau					1/5			30/8				
Dong Thap	16/1				15/5							
Tra Vinh 2015												
Tra Vinh 2016												
Bac Lieu						1/6			25/9			
Kien Giang												
Soc Trang												

Table 11 shows an example of the calendar of the Summer – Autumn rice season 2016 in the 13 provinces in the Mekong Delta. To cover this rice season for the whole Mekong Delta, the Sentinel-1 acquisitions could be selected from 16/1 to 25/9. By this method, it can detect the previous rice season in some provinces such as Ben Tre, Ca Mau and Bac Lieu (Table 11). To remove such error source, a careful date selection needs to be

adopted for each season in order to define the rice crop calendar before deriving other parameters.

In several studies, NDVI time series has been used to determine start of season (SoS) and end of season (EoS) (Boschetti et al., 2009; Son et al., 2013). In this study, the relationship between the seasonal curves of NDVI and Sentinel-1 backscatter (especially the VH/VV ratio) in rice fields is also shown and analysed in subsection 4.2.2 (Figure 27). However, in the effort of developing rice monitoring algorithms operational at the field scale (or the pixel scale), low resolution optical data is not suitable, not to mention the limitation due to cloud cover in the tropical regions. Hence, the goal of the seasonal date selection is to specify the range of acquisition dates of Sentinel-1 images which correspond to the rice season in order to maximize the robustness of the seasonal rice mapping algorithms without using optical data.

This algorithm is based on the ratio of radar backscatter at VH and VV polarizations, i.e. VH/VV. As shown in the previous chapter (Figure 33), the minimum of VH/VV is at about 20 days after sowing and the maximum of VH/VV is at about 60 days after sowing (as reported in chapter 4). The local maximum and the local minimum of VH/VV in the time series are calculated on a pixel basis. The local minimum is first determined, and then the local maximum following the occurrence of this local minimum is determined. Hence, a new time series will be created for a range from d_{SoS} to d_{EoS} where d_{SoS} is defined by the local minimum $-$ x (x is the number of acquisitions over about 20 days) and d_{EoS} is defined by the local maximum $+$ y (y is the number of acquisition over about 50 days). For the Sentinel-1 of 6-day revisit, x can be 3-4 images and y can be 8-9 images). In other words, d_{SoS} would be around the sowing date while d_{EoS} would be around the harvest date of a given rice cropping season. The start and end of this new time series can naturally be different for each pixel.

Finally, the rice mapping algorithm will be applied on a new time series $[d_{SoS}:d_{EoS}]$ without taking into account the out-of-season acquisitions. Therefore, the errors caused by rice pixels from other rice seasons will be minimized in the final seasonal rice mapping products.

For this algorithm, the basic knowledge of rice season in the AOI is required in order to predict the range of acquisition dates where the local minimum and the local maximum should be localised. For regions where the crop calendar is homogenous, this step can be ignored or can be used to update the local crop calendar. On the other hand, the number of days before the local minimum (about 20 days in this study) and after the local maximum

(about 50 days in this study) can be defined depending on the rice cycle duration and cultural practices at different regions. Despite its complexity, the proposed algorithm can be automatized, and it is expected to apply it to a diversity of rice planting systems.

5.3. The rice/non-rice mapping algorithm

In general, the retained rice mapping algorithm is composed of the three following rules:

$$\text{If VH\_max\_inc} > threshold_i \ (dB) \text{ then rice}$$
$$\text{Else if VH\_min} > threshold_j (dB) \text{ then trees/built-up areas} \qquad (15)$$
$$\text{Else if VH\_max} < threshold_k \ (dB) \text{ then water.}$$

The first rule describes the typical backscatter increase of rice fields in each rice season, from the early stage to the mature stage, as in analysis in section 4.2. The strong backscatter increase during rice growing season has been exploited in rice fields mapping algorithms at C band (Ribbes & Le Toan, 1999, Bouvet et al., 2009, Bouvet & Le Toan, 2011) and at X-band (Nelson *et al.*, 2014). In this research, the method has been improved taking into account the effect of incidence angle range and culture practices. This will be clarified in this section.

The second rule accounts for the fact that built-up areas and trees have a consistently high backscatter at cross-polarization compared to the other land use types in this area, as shown in Figure 37 (e), (f). Built-up areas and trees/forest can be distinguished by applying a $threshold_{j1}(dB)$ of VH_min for built-up areas and then $threshold_{j2}(dB)$ for trees/forest thanks to the fact that built-up areas has higher backscatter values than those of trees/forest.

The third rule is based on the fact that the backscatter of water bodies, though slightly variable, is consistently low as shown in Figure 37 (g).

Other rules using classification features from VV polarization can be added in order to limit the error from non-rice pixels in case of limited number of Sentinel-1 images. In this study, VH polarization alone is sufficient to generate rice/non-rice map thanks to the high revisit frequency of the Sentinel-1 data in the Mekong River Delta.

The next step is to define the optimal threshold for rice/non-rice discrimination. The rice/non-rice discrimination is ultimately based on an intensity ratio, as the VH maximum increase corresponds to the ratio r=VH_max/VH_min. An approach to calculate the probability error in threshold methods based on a SAR intensity ratio has been developed in

Bouvet et al., (2010). This theoretical probability of error has been carried out in this study to determine the optimal threshold for this approach and also to evaluate the temporal change mapping method. This was done using 40 non-rice samples (class A, with average intensity ratio r_A) and 40 rice samples (class B, with average intensity ratio r_B) in which a number of pixels were selected.
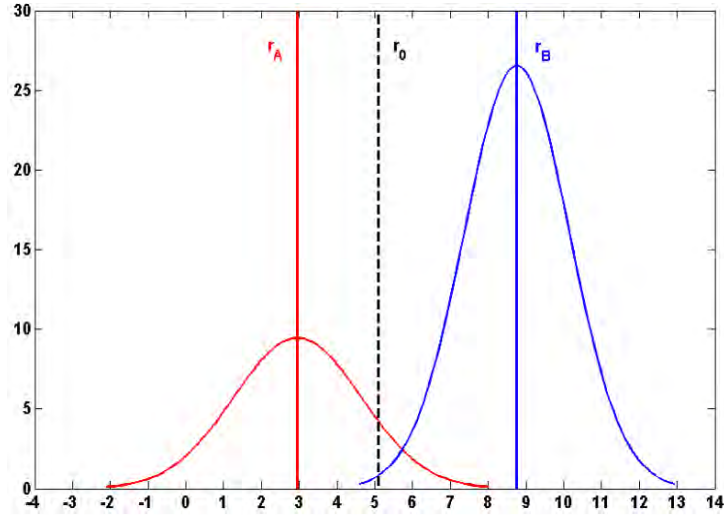
Figure 40. PDFs of the intensity VH_max_inc of (red line) class A and (blue line) class B with class parameters: $r_A = 2.95$ dB and $r_B = 8.76$ dB, $r_0 = 5.084$ dB and $\Delta r = 5.81$ dB for L = 4.4.

Figure 40 shows the PDFs of r=VH_max_inc of the two class A and B. $\Delta r = r_B / r_A$ represents the distance between the mean values of two distributions, and it is, therefore, a measure of the class separability. This parameter is more conveniently expressed in decibels (Δr) dB $= (r_B)$dB $- (r_A)$dB.

The class parameters (average intensity ratios) are represented by vertical lines (red and blue), and the chosen classification threshold r_0 is represented by a vertical dash line.

A multi-temporal filter described in section 3.3 was applied to reduce the speckle noise in SAR images and thus increase the original number of looks in the image to a higher ENL, without reducing the spatial resolution. In this study, for each rice cropping season, about 26 dates (26 acquisitions) were used with the original number of looks is 4.4, a 3×3 square window (9 pixels) is chosen for the multi-temporal filtering, resulting in an ENL of 33.2.

Figure 41 shows the probability of error PE as a function of Δr for different values of L when the classification threshold is r_0. Δr is the difference between the maximum of temporal change for the rice class and that of the non rice class. Figure 30 shows that the

maximum temporal change of rice can be from 6 dB to 13 dB, depending on the incidence angle. Among other non rice classes, forests and urban have low temporal variation, with maximum temporal change is about 1-2 dB. Other classes can have higher variations but lower than rice class (as shown in Figure 37, chapter 4).
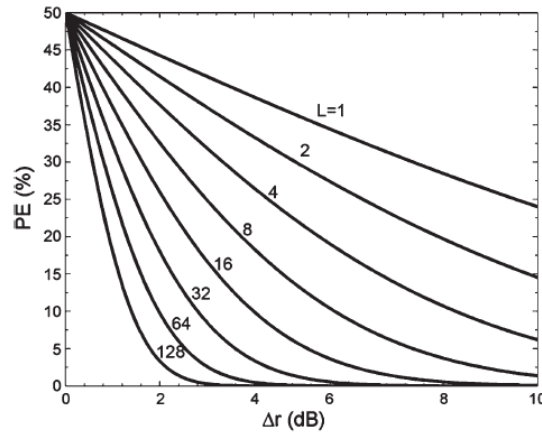
Figure 41. Probability of error (in %) of the ratio method as a function of the change in intensity ratio Δr (dB) between the two classes, for a number of looks L varying between 1 and 128 (Bouvet et al., 2010).

For example, for rice fields located at low incidence angle, the maximum temporal change is 6 dB, and assuming the maximum temporal change of non-rice classes is 3 dB, the Δr is 3dB. For a Δr of 3dB, in order to have a probability of error of < 10%, the ENL should be > 32. For rice fields located at higher incidence angle, where the maximum of temporal change is about 13 dB, Δr is 10 dB. For PE < 5%, the ENL should be > 8. The Sentinel-1 data in this study was applied multi-temporal filter window 3x3. For the data spatial resolution 10m, ENL=33.2, the error is expected to be lower than 1% at all regions.

Moreover, the threshold should be optimized considering the number of data acquisitions and other constraints such as local crop calendar, land use change, etc. (Lam-Dao *et al.*, 2009).

In this study, a $threshold_i$ = 6 dB for rice detection (this threshold can minimize the effect of the incident angle for the whole Mekong River Delta, since it covers the minimum threshold observed at the highest incidence angle of 29°), a $threshold_j$ = -20 dB for water detection and a $threshold_k$ = -10 dB for urban/tree detection were applied. Other pixels not selected by those rules will be classified as non-rice pixels which can be other type of crops (sugar cane, corn, and vegetable) and natural vegetation (grass, bushes).

5.4. Estimation of sowing date

According to the analysis in the previous chapter, the backscatter of VH, VV and especially the ratio VH/VV are found to have a unique behaviour over rice seasons (Figure 33). The theoretical curves of VH, VV and VH/VV can be used to estimate the sowing date. However, the inter-field variation of VH/VV temporal change is smaller than those of VH and VV polarizations. Therefore, in this study, a reference curve derived from experimental VH/VV curves of the 60 sampled rice fields is used. The mean values of the ratio VH/VV as a function of sowing date over these 60 fields in Summer-Autumn 2016 is created and then is smoothed by using a moving average function on Matlab software. The resulting curve as a function of sowing date from 0 to 100 days for both long and short cycle rice is created as shown in Figure 42.
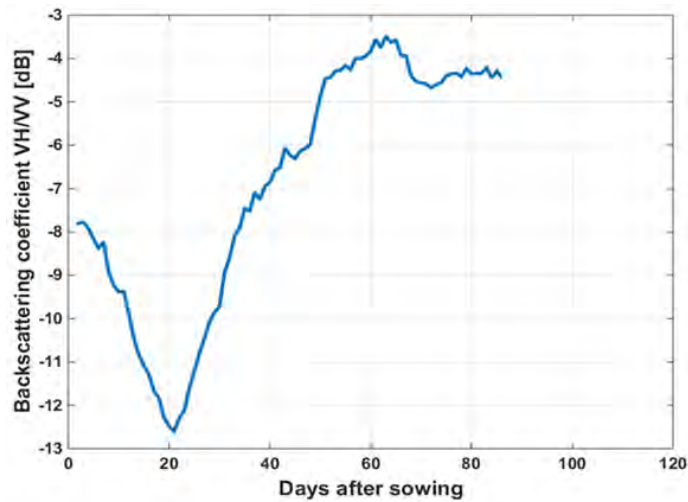
Figure 42. Experimentally derived curve of VH/VV used for sowing date retrieval.

Then, the sowing date estimation algorithm is applied on the time series of the ratio VH/VV in the range of d_{SoS} to d_{EoS}. As mentioned in 5.2, the dates d_{SoS} and d_{EoS} are selected in such a way that d_{SoS} is thought to correspond approximately to the sowing date. The sowing date is determined at each pixel by running a loop in which it is assumed that the sowing date occurs X days around d_{SoS}, with X ranging between -35 and +35. The ratio VH/VV from the time series in the range of d_{SoS} to d_{EoS} is plotted as a function of the assumed sowing date and then is compared with the 'reference' curve at each iteration of the loop to find the assumed sowing date that provides the best fit for the two curves as shown in Figure 43 (left). The root mean square (RMS) error gives a quality of the comparison. In particular, for each assumed sowing date, a RMS error is estimated by deriving the root mean

89

square distance (RMSD) between the VH/VV curve and reference curve, using the following formula:

$$RMSD = \sqrt{(VH/VV_{time\ series} - VH/VV_{reference})^2} \qquad (16)$$

For several assumed sowing dates, a set of RMSD is derived as shown in Figure 43 (right). The minimum RMSD gives the value of the sowing date which best fits the theoretical curve with the VH/VV curve of the time series.
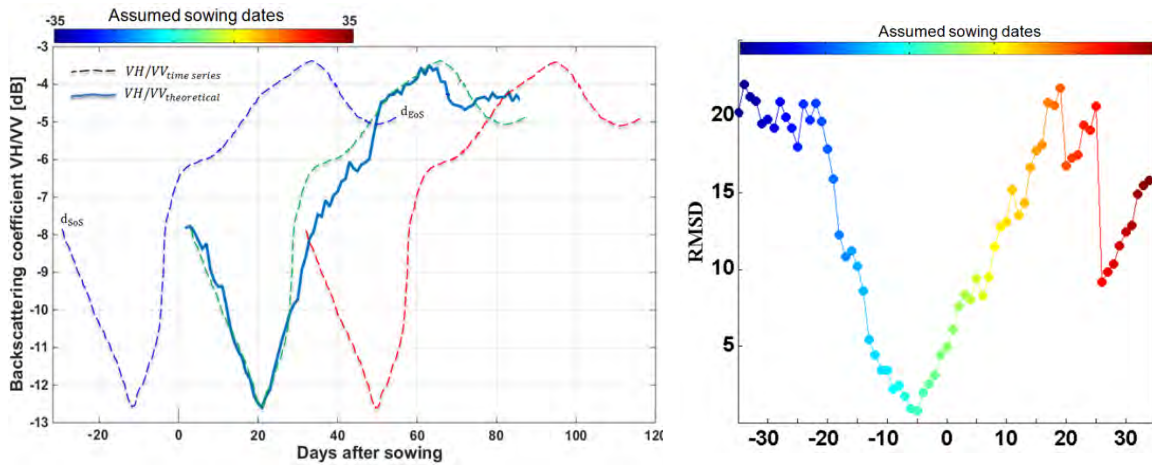
Figure 43. Illustration of sowing date retrieval estimation method.

The advantage of this algorithm is that it is based on the time series of Sentinel-1 over the rice growing cycle instead of exploiting a certain development stage of rice fields. This can minimize the effect of other parameters (incident angle, climate condition, culture practice, etc.). However, for this sowing date estimation approach, the assumed sowing date is crucial. The error of sowing date retrieval can come from the error of crop calendar information. Therefore, this algorithm should be used together with the seasonal date selection algorithm described in section 5.2, even in homogeneous regions.

This algorithm can also exploit the reference curves of VH or VV polarization. However, for VH and VV, the most accurate period of the reference curve should take from 20 to 60 days after sowing where the radar backscatter behavior is the most stable without effect of long/short rice cycle rice variety and practice methods.

5.5. Detection of long/short cycle rice variety

The algorithm of short/long rice mapping was based on the mean value of VH and/or VV during 65 to 75 days after sowing. A threshold is applied for the Sentinel-1 images during this period to distinguish long and short duration cycle rice varieties:

If $mean\_VH_{(65-75)} \geq$ -16.5 dB then short duration cycle rice

Else If $mean\_VH_{(65-75)} <$ -16.5 dB then long duration cycle rice

(17)

This method for discrimination of long/short cycle rice requires information of sowing date obtained by the method developed in the previous section, and the results are obtained only during the reproductive phase, from flowering stage to grain maturity phase. For this purpose, sowing date map and SAR images at around 70 days after the sowing date are required.

To apply this method to other regions with different rice varieties, rice cycle duration and cultural practices, the backscatter temporal behavior of the rice fields should be reassessed.

5.6. Detection of rice phenological stage at S1 acquisition

A phenological stage estimation algorithm is applied to the rice pixels after the rice mapping has been performed using the information of sowing date at two groups of rice variety: long cycle rice variety and short cycle rice variety. The algorithm is based on the relationship between phenological stage and the day after sowing of rice fields.

For short cycle rice, from the sowing date of each rice field, the information of phenological stage is derived as following:

Stage 1 (emergence): **0-10**   Stage 5 (stem elongation): **35-45**   Stage 9 (milky): **75-80**

Stage 2 (2/3 leaves): **10-15**   Stage 6 (booting): **45-58**   Stage 10 (milky hard): 8**0-85**

Stage 3 (tillering start): **15-25**   Stage 7 (heading): **58-65**   Stage 11 (maturing): **85-90**

Stage 4 (tillering max): **25:35**   Stage 8 (flowering): **65-75**   Stage 12 (maturity): **90-100**

For long cycle rice, the phenological stage is detected similarly to the short cycle rice until stage 6. From stage 7, it can be derived as following:

Stage 7: **58-68**   Stage 10: **90-100**

Stage 8: **68-80**   Stage 11: **100-110**

Stage 9: **80-90**   Stage 12: **110-120**

This identification needs to be confirmed by looking at the backscatter behavior at each stage. Especially, from stage 7 onwards, the development of rice can be confirmed by using a threshold on radar backscatter. The temporal change behavior of VH, VV and VH/VV can be used for this algorithm. In this study, the ratio VH/VV with $threshold_a = -7\ dB$ has been used to check the development of the rice fields:

91

- If at the date X the number of days after sowing is between d1 and d2 (identified above), and the VH/VV ≥ threshold$_a$ (dB) then the identification of phenological stage at date X is confirmed, and this condition is checked at each acquisition date until stage 12 or the last image in the stack.

- If at the date X the number of days after sowing is between d1 and d2, and the VH/VV < $threshold_a$ (dB), it means that the condition of radar backscatter is not satisfied, and that the rice has probably withered or failed. The pixel is then reclassified as non-rice.

Similarly, a reverse countdown can be applied to assess the phenological stages of dates X-1, X-2, and so on.

The algorithm developed in this research is based on the rice system in the Mekong Delta, Vietnam. To generalize the algorithms globally, more studies need to be carried out for diverse rice varieties and growth development from different region. To apply the method to other regions, the knowledge of the duration of the rice growing season and the phenological development of rice plants are required. The threshold used for this algorithm ($threshold_a$) needs to be adapted with the range of incident angle and cultural practices as described in section 5.3.

5.7. Estimation of plant height

The analysis of plant height as a function of the day after sowing showed that the relationship can be expressed by polynomial regression curves presented in the section 4.1 with a high correlation coefficient for both groups of rice varieties: long cycle rice and short cycle rice (as seen in Figure 21). Rice plant height of long and short cycle rice variety at the date M are retrieved from the equations bellow:

If rice=long rice

$$\text{plant height} = -0.006 \times x^2 + 1.6 \times x - 1.1$$

Else rice=short rice:

$$\text{plant height} = -0.0078 \times x^2 + 1.7 \times x - 4.2$$

where x is the day after sowing since date M.

Similarly to the phenological stage development, the plant height estimation should be confirmed by using the backscatter value of Sentinel-1 images or by observing the phenological stage once it is derived at date M. In particular, if at the date M, the phenological stage is within the range of 1 and 12, then the empirical polynomial regression curves can be applied. Otherwise, rice plants in the pixel are not in their growing cycle.

However, the main problem of plant height estimation taking into account the condition of the phenological stage is the propagating error source of the phenological stage map. Therefore, instead of using the phenological stage map, the threshold approach of VH, VV or VH/VV could be used to confirm the development stage of rice plant as described in section 5.6.

5.8. Estimation of crop intensity

The rice cropping intensity indicates the number of rice season(s) cultivated per year. For example, the rice cropping intensity of single rice, double rice, and triple rice was 1, 2, and 3, respectively. It can be easily estimated from the seasonal rice map (which is derived in the previous section) by combining the information contained in each rice pixel (i.e. the number of seasons for each pixel) for the different seasonal rice maps generated over a year. However, inaccuracies of the rice pixels from the seasonal rice map can induce errors in the final rice cropping intensity map.

Another algorithm developed in this section to estimate the rice cropping intensity is based on the variation of the radar backscatter of the Sentinel-1 time series. A moving smooth function has been applied on the time series of VH/VV for each pixel (only potential rice pixels which were defined from section 5.1 are used). Figure 44 shows an example of variation backscatter of VH/VV (dB) time series of rice field from 20/08/2016 to 19/12/2017 with an acquisition interval of 6 days (with some gaps due to missing data). The smoothing function returns a moving average of the elements of a time-series using a fixed window length (i.e. span) that is determined heuristically. The window slides down the length of the time-series, computing an average over the elements within each window.

The rice cropping intensity is defined by estimating the number of peaks in the VH/VV time series with a minimum period of time between each peak to cover the rice cycle duration. The peaks must also be above -6 dB which is the characteristic of cultivated rice fields (as analysed in chapter 4). The smoothing of the time-series using an averaging window helps to determine the number of peaks efficiently. However, the span of the smoothing moving window must be chosen carefully, as is illustrated in Figure 44. In this figure we can observe the original time-series smoothed with an increasing span of 5, 10 and 20-days (i.e. about 1 to 4 Sentinel-1 images of 6 days revisit). The VH/VV peaks are difficult to detect when the smoothing window is too large, as can be seen with the red curve in the Figure 44.
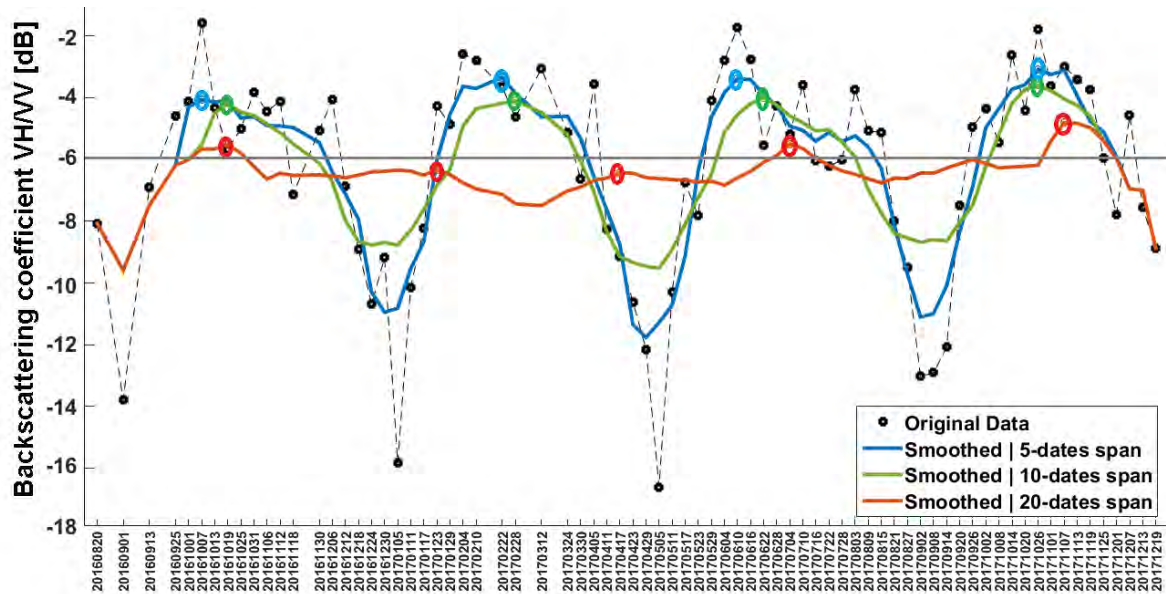
Figure 44. Smoothing function with VH/VV time series for rice cropping intensity estimation.

For the studied region, a rice cycle is about 90 to 120 days depending on the rice variety. Therefore, for short cycle rice, the distance between peaks can be around 90 days and 120 for long cycle rice.

5.9. Discussion and conclusion

The methods for rice mapping and monitoring developed in this study are based on the knowledge of the temporal development of the rice plants and the related temporal variation of the radar backscatter of different rice varieties and cultural practices over large areas. The methods used thresholds applied to the temporal variation of the radar backscatter, which is not only a simple and easily implemented approach but also robust, repeatable and suitable for rapid rice mapping over large extents. Furthermore, the methodological developments carried out also take into account the local rice crop calendar, the effect of long cycle rice and short cycle rice and the effect of incident angle of the Sentinel-1data.

However, to apply the algorithms to other regions under different conditions, for example rainfed, upland rice, etc., it is necessary to understand the backscatter temporal variations of the rice fields in order to refine the methods for their robustness across sites in other regions and countries.

94

<div align="right">Chapter 6</div>

Mapping products generation, validation and accuracy assessment

Contents

In this chapter, the products generated using the methodology described in Chapter 5 will be presented together with the product validation to assess their accuracy. The mapping products in the Mekong River Delta will be illustrated and validated in the same order as the methodology development in chapter 5 (rice map, sowing date map, long/short rice cycle map, phenological stage map, plant height map and rice crop intensity map). Additionally, the rice extent area mapping products at national scale will be demonstrated at two countries (Vietnam and Cambodia). To sum up, the discussion and conclusion of this chapter will be given in the last section.

6.1. Mapping products generation, validation and accuracy assessment

The product validation was carried out using the validation data bases described in chapter 3, which are summarized in the following:

1. Data regularly collected on the 60 surveyed fields in the province of An Giang over five rice seasons: One over five seasons has been used as training data for sowing date mapping algorithms and will not be used for product validation. As a consequence, 240 rice surveyed fields are used for validation and accuracy assessment of rice map, sowing date estimation, rice variety detection, phenological stage map and plant height estimation.

2. Data collected randomly for rice/non-rice validation in many other rice provinces in the Mekong delta: A total of 1500 GPS points for the rice class and 450 GPS points for the non-rice class are used. Those GPS points are distributed over the three main regions of the Mekong Delta as described in chapter 3.

3. Product validation at near real time: two campaigns in the Mekong Delta on 08/2015 and 10/2016 for validating the rice area and phenological stage. A number of 270 points were collected and validated in near real time conditions (within 2-3 days after Sentinel-1 acquisition).

4. The validation of rice planted area using the data from Statistics office of 13 provinces in the Mekong Delta.

For validation, the independent validation consists in performing a quantitative comparison between the EO derived products and the validation data base following the defined validation methods and metrics. Standard accuracy assessment measures were used i.e., kappa coefficient, overall accuracy, omission error, and commission error.

In order to distinguish rice from other classes at a given satellite acquisition date, the rice pixel is defined as stated previously, as the location where rice is currently planted, from sowing/planting to harvest. Fallow fields or fields with intermediate crops between two rice seasons, and fields before planting and after harvest will be labeled as non-rice.

6.1.1. Land use land cover map

As described in the previous chapter, non-rice areas are firstly masked out, in order to apply the rice mapping algorithms only in areas where rice can be potentially found. In addition, land use land cover maps have been produced: water, tree and urban have been created based on the maximum and minimum VH backscatter values of the time series.
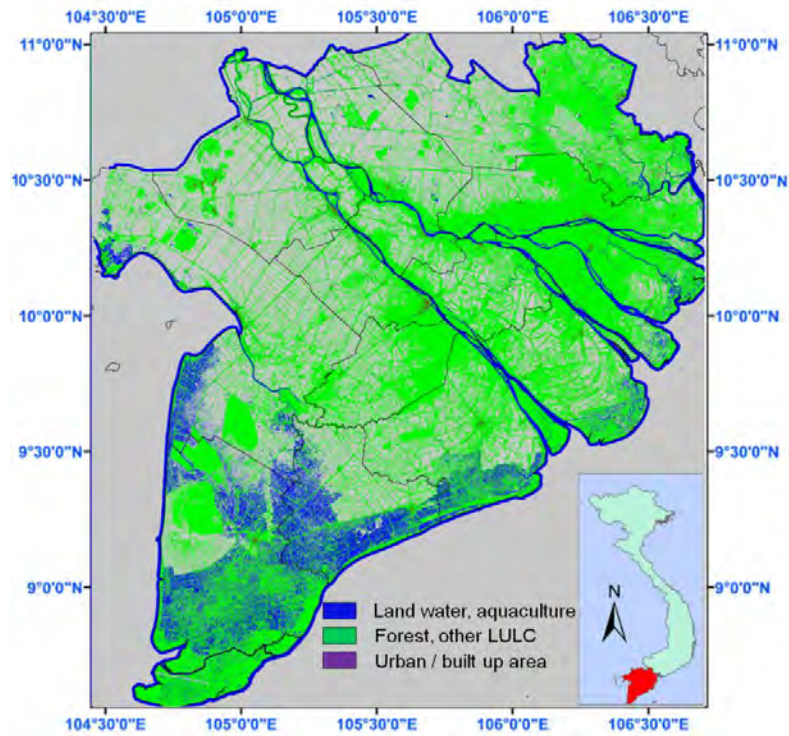
Figure 45. Mapping of main land use land covers including land water/aquaculture, forest/ trees, urban or built up area in the Mekong River Delta in 2018.
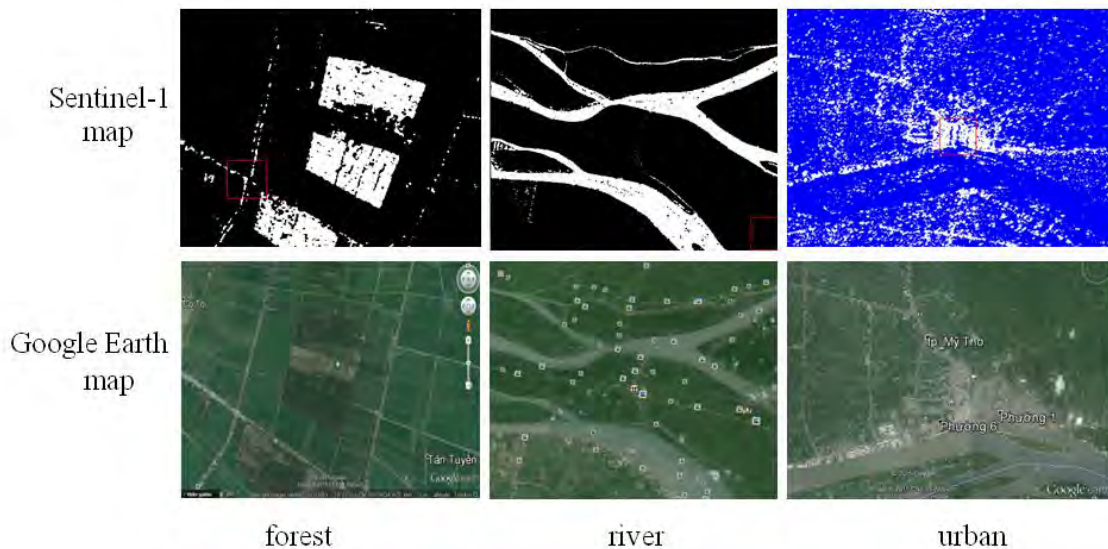
Figure 46. Comparison of land cover maps of forest, river, urban and rice by Sentinel 1 with the Google Earth map.

As seen in Figure 45, the province in the South of the Mekong River Delta, the main LULC was found including cultivated lands, aquaculture ponds, mangrove forest, natural water bodies and built up area. For geometric delineation of image features, the LULC map derived from the Sentinel-1 images are compared with good agreement to Google Earth map as shown in Figure 46.

97

6.1.2. Seasonal rice map

The rice mapping has been produced for all rice seasons in the Mekong River Delta from October 2014 to August 2018 comprising 10 rice cropping seasons. Figure 47 shows the rice map of Summer-Autumn 2018 in the Mekong River Delta, with a detailed rice map of the An Giang province as example.
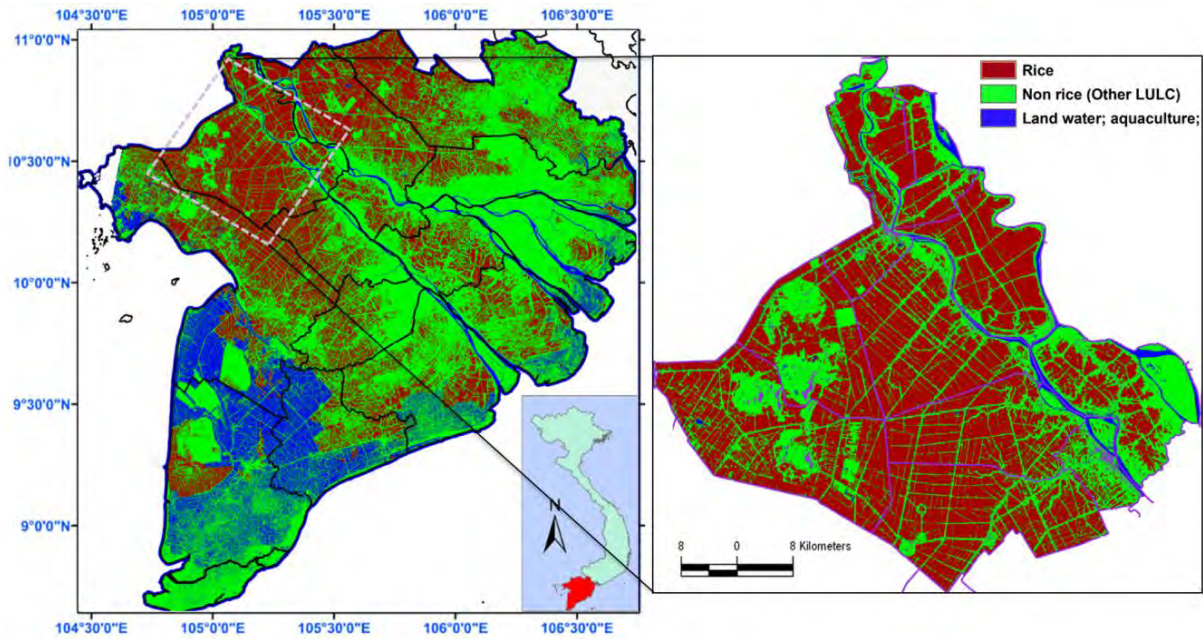
Figure 47. Rice map derived from 20 images of Sentinel-1 (10m spatial resolution) in Summer-Autumn 2018 in the Mekong Delta (left) and An Giang province (right).

All the seasonal rice maps in the whole Mekong Delta from October 2014 to March 2018 are shown in the Figure 48.
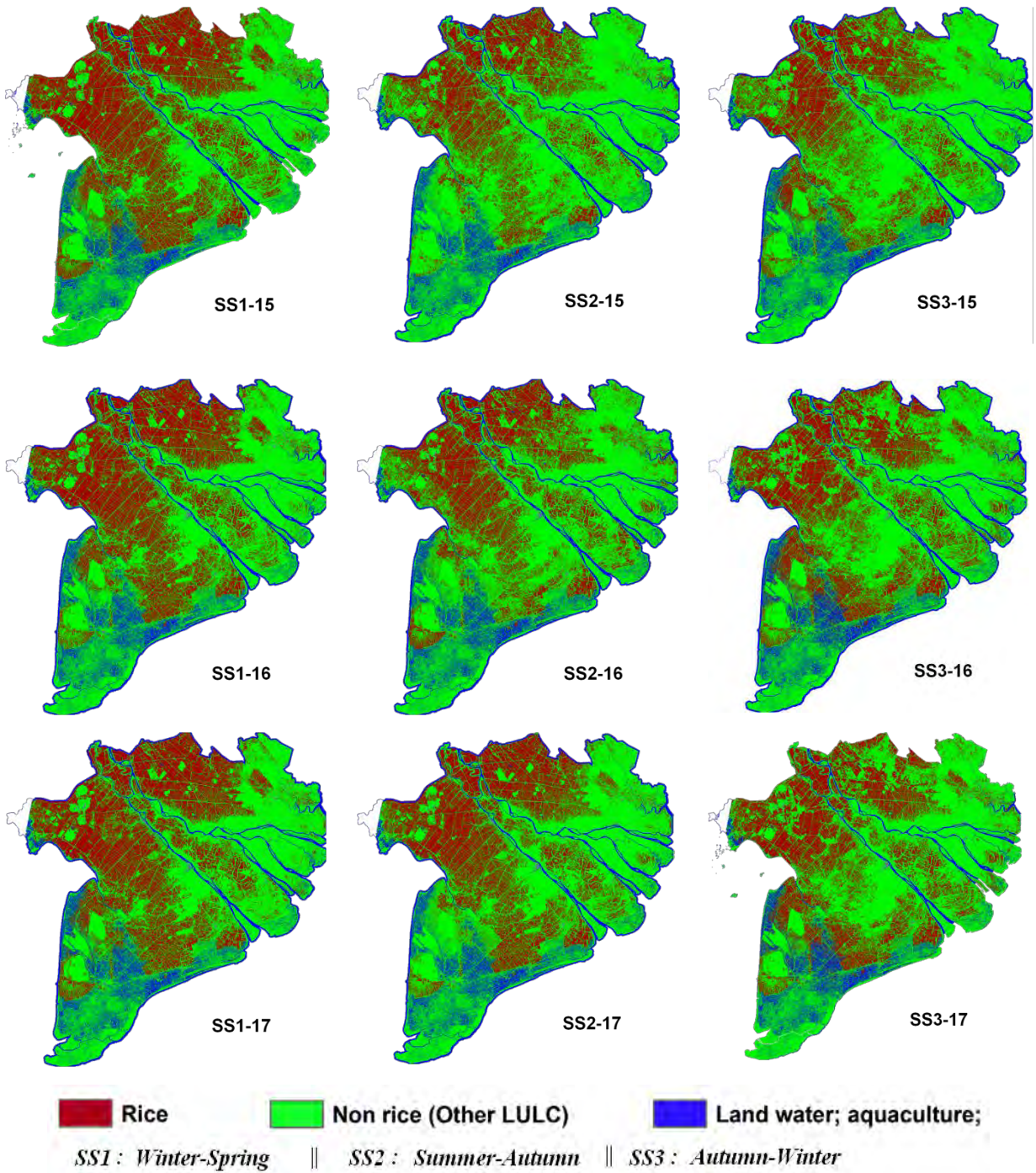
Figure 48. Seasonal rice maps over 3 years 2015, 2016 and 2017 in the Mekong River Delta, Vietnam.

♣ Inter-annual variation of rice planted area
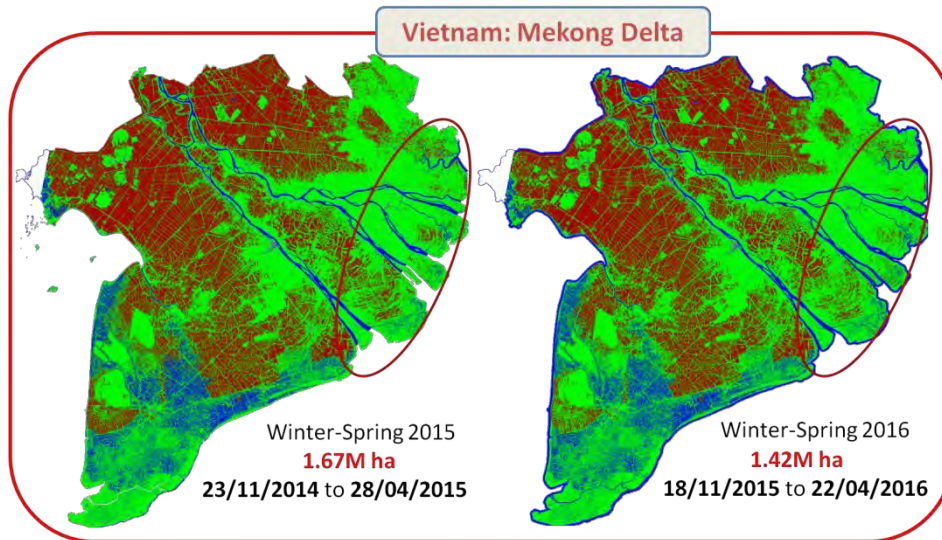
Figure 49. Rice mapping in Winter-Spring 2015 is compared to Rice in Winter-Spring 2016 in the Mekong Delta, Vietnam. Red: Rice, Blue: Water, Green: non-rice (forest, urban, etc.)

The mapping results have been used to assess the inter-annual variations of rice planted area. Figure 49 shows a comparison between rice mapping results in 2015 and 2016 in the Mekong delta. A decrease of rice areas in Winter-Spring in 2016 is detected and attributed to El Niño effect. The unusual decrease by the end of April 2016 in Spring season as compared to end of April 2015 is caused by shortage of water and saline water intrusion (decrease of 253000 ha or 16.7%; i.e. 1.42M ha vs 1.67M ha).

♣ Rice/ Non-Rice geometric accuracy

The GIS localization of the 60 surveyed rice fields in the province of An Giang and the independent GPS check points over the Mekong Delta are used to test both the rice/non rice performance of the method, and the geometric accuracy of the results, for correct delineating field boundaries.

Figure 50 (left) shows the overlay of 60 reference fields over the S1 derived rice maps displayed on the rice/non-rice product. In general, the fields correspond well to the rice class. However, the collected fields are very close to the road which can produce an error on the field boundaries pixels as shown by the subset images in Figure 50 (left).

This was also observed for the independent check points in 3 regions in the Mekong Delta (Figure 50 (right)). The error can be attributed to i) the mixed pixels at the field border (which leads to its classification as a non-rice pixel), ii) the precision of the GPS coordinates.
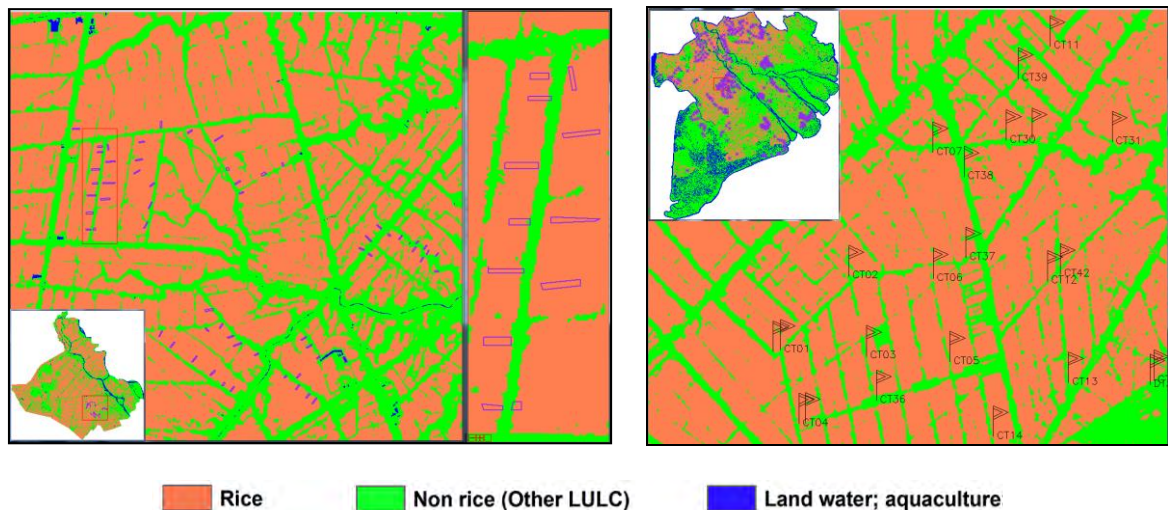
Figure 50. Example of rice map of the Summer-Autumn rice season in 2016 generated from Sentinel-1, overlayed by GIS file of the 60 surveyed rice fields in the An Giang province (left) and overlay of GPS independent check points at a different region in the Mekong Delta (right).

This result indicates the need i) to have a further check of the geometric quality of the products by using reliable references, ii) to investigate the effects of SAR data filtering and the values of the SAR indicator thresholds used in the methods on the mixed pixels (rice pixels of different calendars, rice and road, rice and other LULC).

At the present stage, the 10 m spatial resolution of the rice products allows to detect and localize most rice fields, except fields of dimensions of the order of 20 m (2 pixels) or less.

Table 12 lists the validation for rice growing area mapping in the Mekong River Delta. For 300 rice sample fields, the percentage of good rice detection is **98.6%**. Whereas for the independent GPS check point, the number of check points during the 3-8 July 2016 campaign in the Mekong Delta was 1500. The overall accuracy is **95%** with the omission error and commission error of rice class is 5.6% and 0.98%, respectively. More specifically, for 85 (over 1500) GPS check points of rice were detected as no-rice class and 14 (over 450) no-rice check points were detected as rice class, the error is mainly caused by error in GPS for small fields close to the road.

Table 12. Comparison in rice/non-rice check points from Ground Survey and the rice map derived from the Sentienl-1 data.

Validation data bases	Ground survey	Sentinel-1 product	Overall Accuracy
Rice sample fields	300	296	**98.6%**
Independent GPS points	1500	1415	**95%**
Other crops (pepper, mango, corn..)	450	436	

The rice map product of the Summer-Autumn rice season based on S1 data from April to August 2016 is used to calculate the number of rice pixels, and the area of rice planted area in each of the 13 provinces. Table 13 shows the comparison for each of the 13 provinces of the Mekong Delta between the estimated area and the Agency reported rice planted areas for the Summer-Autumn 2016 rice season.

Table 13. Rice planted area (in ha) provided by the 13 provinces and estimated by Sentinel-1 for the Summer-Autumn Rice season of 2016.

	Province	**Estimated areas (ha)**	**Agency data (ha)**	**%**
1	Long An	218490	219345	**99,6**
2	Đồng Tháp	156310	193392	**80,8**
3	An Giang	241450	239279	**100,9**
4	Tiền Giang	98361	107513	**91,5**
5	Vĩnh Long	51668	59339	**87,0**
6	Bến Tre	11788	14743	**80,0**
7	Kiên Giang	313380	296389	**105,7**
8	Cần Thơ	88968	77828	**114,3**
9	Hậu Giang	43217	68755	**62,8**
10	Trà Vinh	74307	77720	**95,6**
11	Sóc Trăng	169032	174467	**96,8**
12	Bạc Liêu	48727	57165	**85,2**
13	Cà Mau	35664	36362	**98,2**
Total	**Mekong Delta**	**1551362**	**1622297**	**95,6**

Although both estimates have multiple sources of error, they provide good agreement in the overall comparison (95,6% for the Mekong Delta). The most important under estimation was found in Dong Thap and Hau Giang, that was found to be due to the shift in crop calendar of those provinces specifically for Summer-Autumn rice season in 2016 (recommendation by province agency to avoid El Niño effect) compared to other provinces

(Table 11). The estimated areas using S1 product for these 11 provinces (with Dong Thap and Hau Giang excluded) account for **99.3%** of the Agency data.
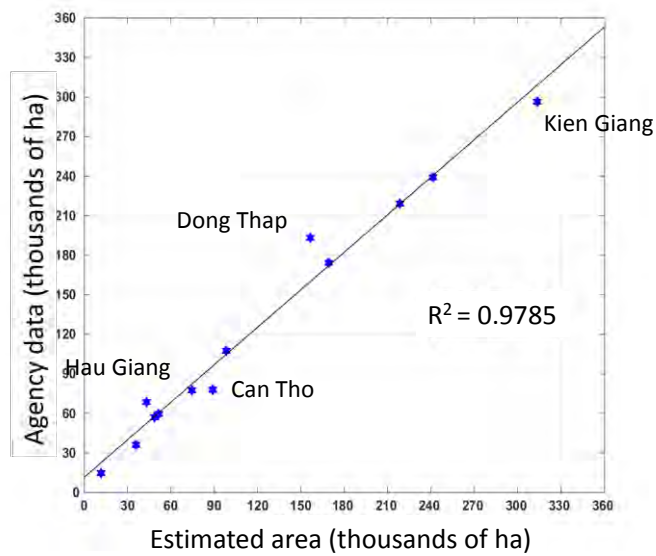
Figure 51. Comparison in rice planted areas from the Sentinel-1 product and the Agency data for the Summer-Autumn 2016 rice season.

The results show that the Sentinel-1 based estimate of rice planted area can contribute to the National Statistics of Rice planted areas. Furthermore, such remote sensing results can be obtained already before the end of the rice season.

6.1.3. Sowing date map

Figure 52 shows the sowing date map of in Winter-Spring 2017 in the MRD (left) and in the An Giang province (right).
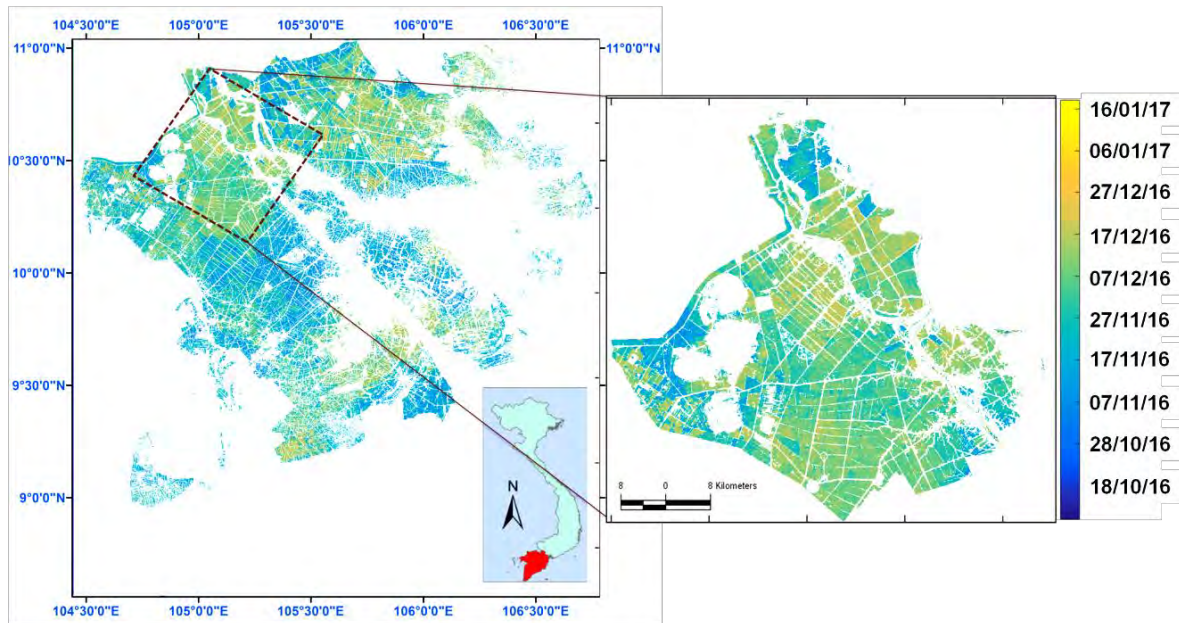
*Figure 52. Sowing date map derived from 20 images of Sentinel-1 (10m spatial resolution) in Winter-Spring 2017 in the Mekong Delta (left) and An Giang province (right).*

The sowing date maps derived from Sentinel-1 data are compared with the sowing dates of 60 sampled fields over 4 rice seasons showing a good agreement with a root mean square error of 3.7 – 4.8 days (Figure 53).

Determining the sowing date of rice fields in this region with an average error of ±4.3 days is an asset for water management, field treatment and harvest planning. However, for individual rice fields, an error of 4-5 days may not be sufficient for punctual management, and the contribution of the spatial distribution of sowing dates is more important at a regional scale, where water resources and available machinery need to be shared between communes and villages.
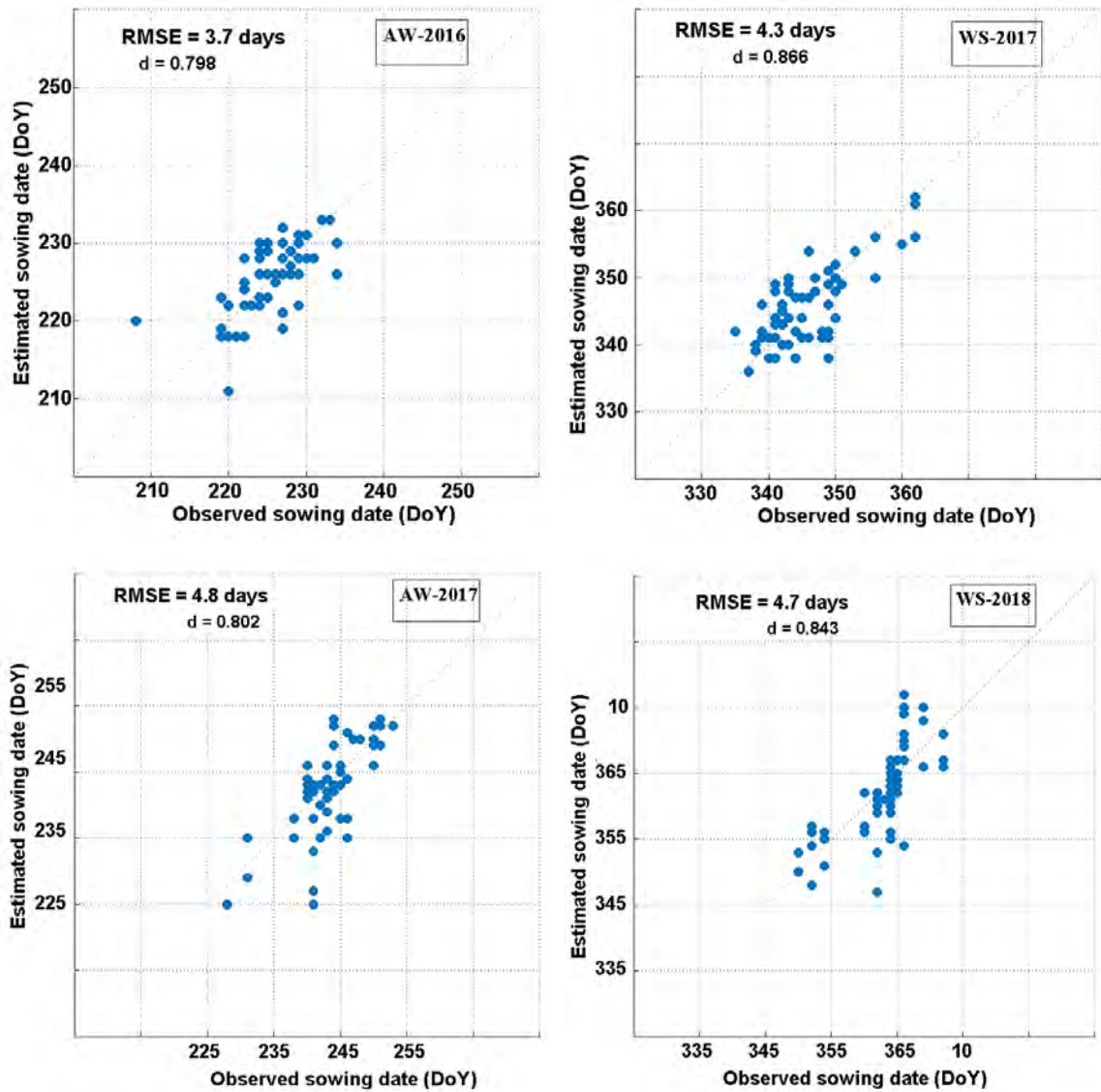
Figure 53. Retrieved sowing date in over 4 rice cropping seasons by Sentinel-1 vs. ground data collection of 60 rice fields in Chau Thanh and Thoai Son districts, An Giang province.

The sowing dates in Figure 53 have been estimated based on the time series of the ratio VH/VV in the range of d_{SoS} to d_{EoS} (as described in section 5.4). Then by reducing the number of images in the time series as well as calculating the sowing date estimation error, we address the question of how many images in the time series are needed to obtain reasonable sowing date estimates. Figure 54 shows an example of the sowing date estimation error versus the number of days after sowing (which defines the number of images). It is clearly seen that already 24 days after sowing (corresponds to 4 images of 6 days revisit and 2 images of 12 days revisit), the available time series can provide sowing date estimates with a standard error of about 4 days. After 24 days after sowing, the result for 6-day revisit is

slightly improved with an error of about 3-4 days. For the 12-day revisit, the error is variable, from 6 to 8 days, until about 40 days, where the error decreases to 4 days.
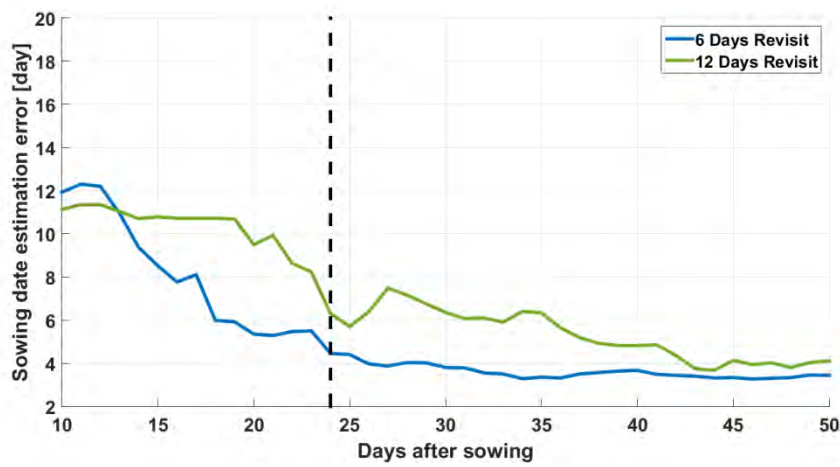
Figure 54. The sensitivity of the sowing date estimation using time series of Sentinel-1 with a 6-day revisit and 12-day revisit.
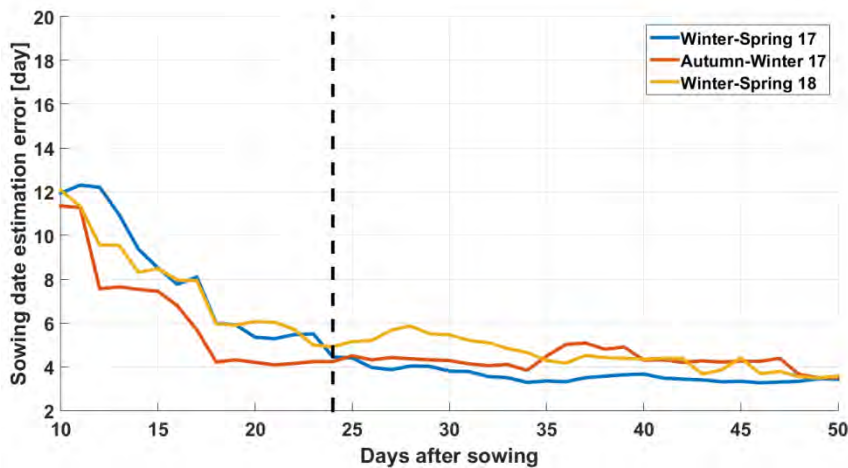
Figure 55. The sensitivity of the sowing date estimation using time series of Sentinel-1 with a 6-day revisit over 3 rice cropping seasons.

Figure 55 shows the results for 3 rice seasons, with 6-day revisit. The error is consistent between seasons.

6.1.4. Long/short rice cycle map

Figure 56 shows the long/short rice cycle map of Winter-Spring 2017 in the MRD (left) and in the An Giang province (right).
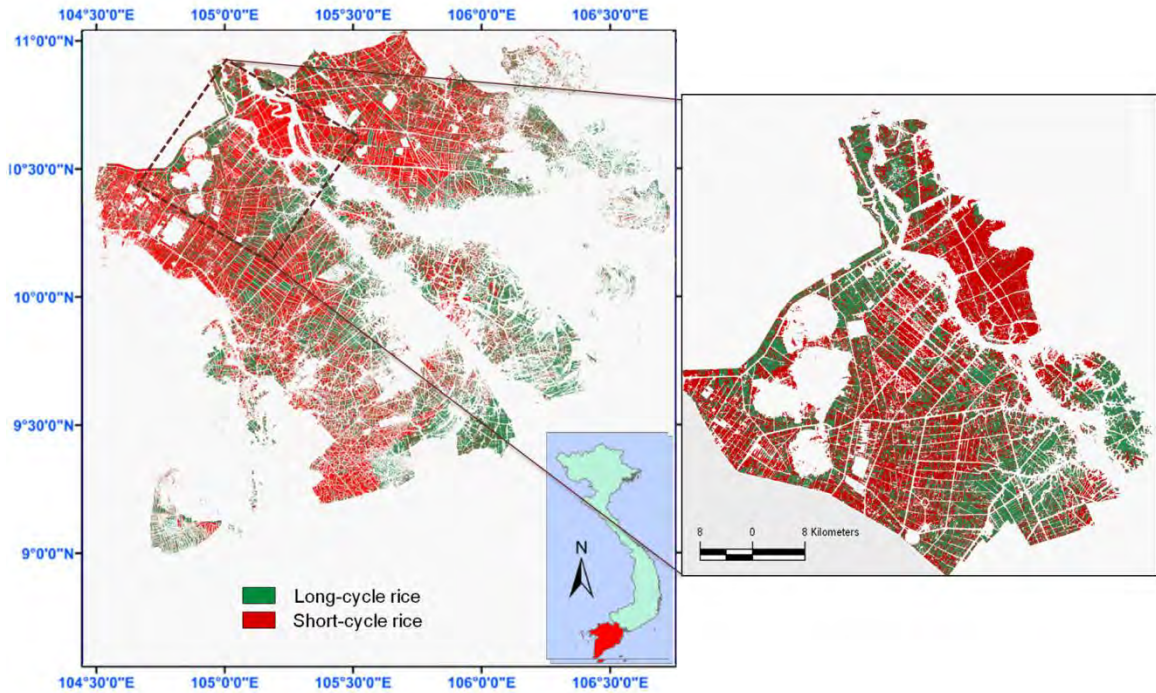
Figure 56. Long short cycle rice in Winter-Spring 2017 in the Mekong Delta (left) and An Giang province (right).

Short and long cycle rice fields are distributed in geographic clusters. Short-cycle rice is still dominant, despite the tendency to increase the production of long-cycle rice. The comparison between rice variety mapping in this study and 240 sampled fields (49 long and 191 short) is shown in Table 14.

Table 14. Comparison long/short cycle rice variety from Ground Survey and the Sentinel-1 product.

		Sentinel-1 products		
Ground survey		Long cycle rice	Short cycle rice	Total
	Long cycle rice	**49**	0	49
	Short cycle rice	20	**171**	191
	Total	69	171	**220/240**

The good identification score is therefore of 220/240 (**91.7%**). 20 sample fields of short-cycle rice variety that were detected as the long cycle variety. This error can come from the 11 samples not clearly identified as long or short cycle rice variety from the ground survey (Table 9, chapter 4).

More important is the derived area distribution and the proportion of long and short cycle rice within a region. In the study area (in Figure 56), 28.7% of the area is planted with

of long-cycle rice and 71.3% with short-cycle rice. Such proportion is expected to change annually.

The proportion of planted area with long-cycle high market value rice in a season against planted area with short-cycle lower market value rice is a major component of the economic income in this region. Having this information about two months after the sowing period will be beneficial for market planning.

6.1.5. Rice phenological stage map
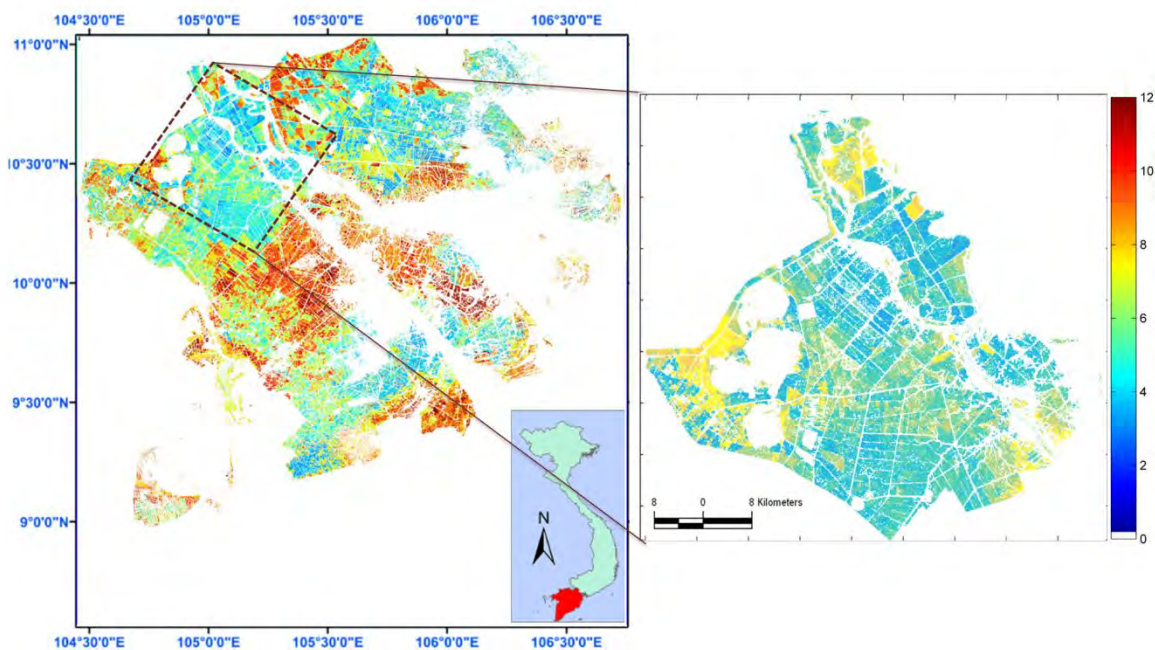
Figure 57. Phenological stage map (12 stages) on 12/01/2017 of Winter-Spring 2017 in the Mekong Delta (left) and An Giang province (right).

Figure 57 shows the phenological stage map on 12/01/2017 of in Winter-Spring 2017 in the MRD (left) and in the An Giang province (right).

The correct detection of phenological stages has been assessed using the data recorded for the 60 surveyed fields in An Giang. The 12 scale phenological stages used by Agricultural experts in Vietnam have been compared with the 12 phenological stages detectable by Sentinel-1. Figure 57 shows the map of phenological stages at the date of 12/01/2017 in the Mekong River Delta (left) and in the An Giang province (right).

The validation of the phenological stage map has been carried out for the rice season Winter-Spring 2017. Figure 58 shows the comparison of the phenological stages for 60

108

fields. For 59 fields, there are very good agreement between the two datasets. The accuracy for these 60 samples is therefore of **98.3%.**
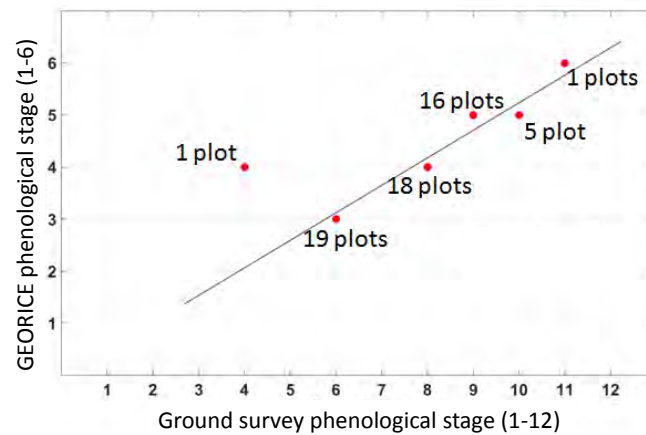
Figure 58. Comparison of the phenological stages detected by Sentinel-1 and recorded by ground survey.

During a field survey in Can Tho province on 25 October 2016 in the frame of the Georice project, a phenological map of 20 October 2016 has been provided to a group of identified users (agriculture managers at 13 provinces in the Mekong River Delta) for in situ visual assessment (Figure 59). Most users reported on correct detection of the phenological stages.

Figure 59. The fieldtrip for in situ visual assessment of phenological stages mapping using Sentinel-1 images in Can Tho province, Mekong Delta on 25 October 2016.

6.1.6. Plant height map

Figure 60 shows the plant height map on 12/01/2017 of the Winter-Spring 2017 rice crop in the MRD (left) and in the An Giang province (right).
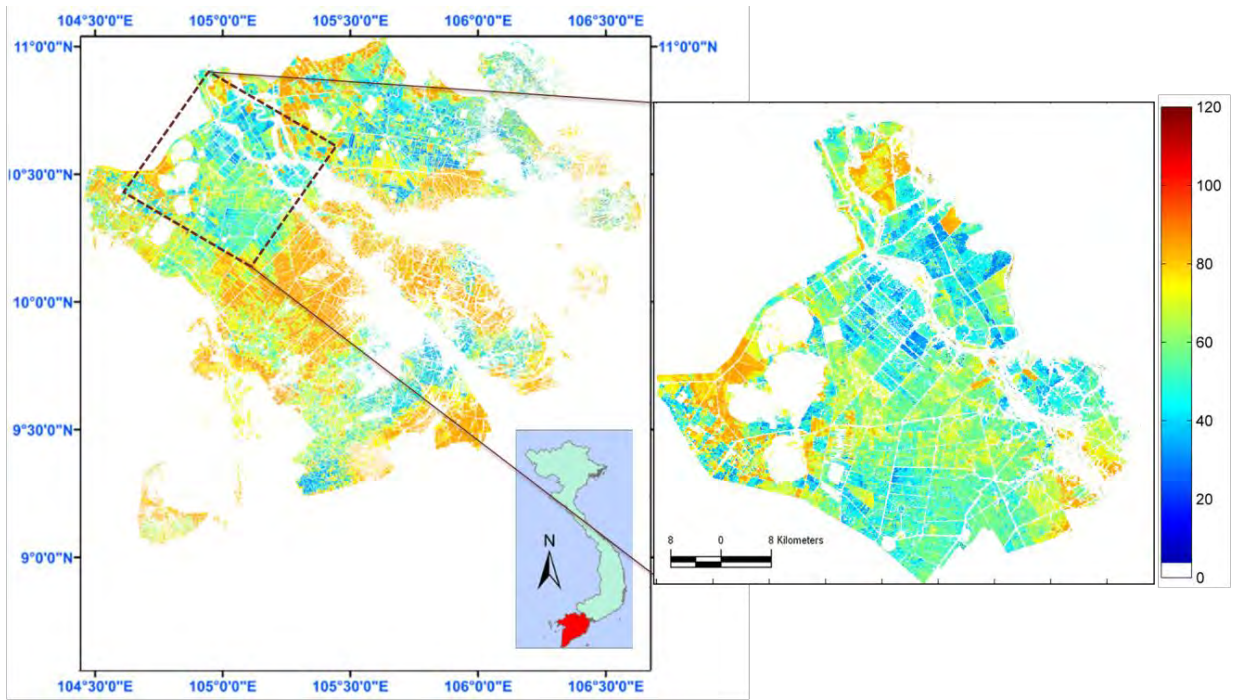
Figure 60. Plant height map in the Mekong River Delta on 12/01/2017 of Winter-Spring 2017 in the Mekong Delta (left) and An Giang province (right).

Figure 61 shows the comparison of the plant height retrieval from Sentinel-1 data respect to in-situ data during the Winter-Spring 2017 rice season (60 sampled rice fields by 5 times of ground measurement). A good correlation between retrieved plant height and measured plant height was obtained with a RMSE of 7.88 cm.
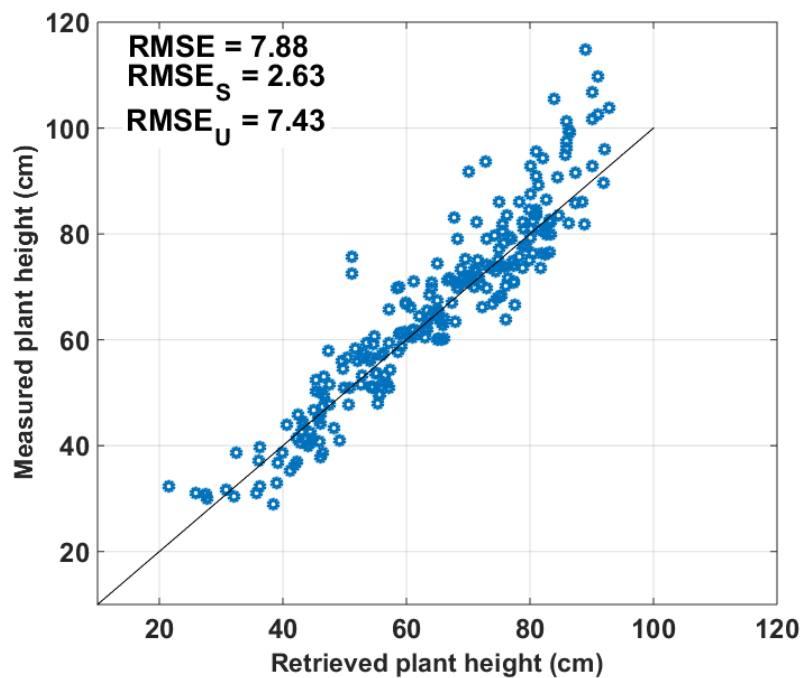
Figure 61. Plant height validation using the ground measurement of Winter-Spring 2017.

110

6.1.7. Rice cropping intensity map

Figure 62 shows the cropping intensity in the Mekong River Delta which is from single cropping rice to two or three irrigated rice crops per year in 2016. Single cropped rice is found at very limited area in the whole Mekong Delta compared to other patterns. In the coastal areas which are prone to salt intrusion in the dry season the major cropping patterns are therefore single rice with shrimp farming or double rice. Many other rice based cropping systems, such as rice-rice-corn, corn-rice-corn, rice-rice-peanut and rice-rice-vegetable exist in the region. This concerns part or all of the coastal provinces in the Mekong Delta (Kiên Giang, Cà Mau, Bạc Liêu, Sóc Trăng, Trà Vinh and Bến Tre).
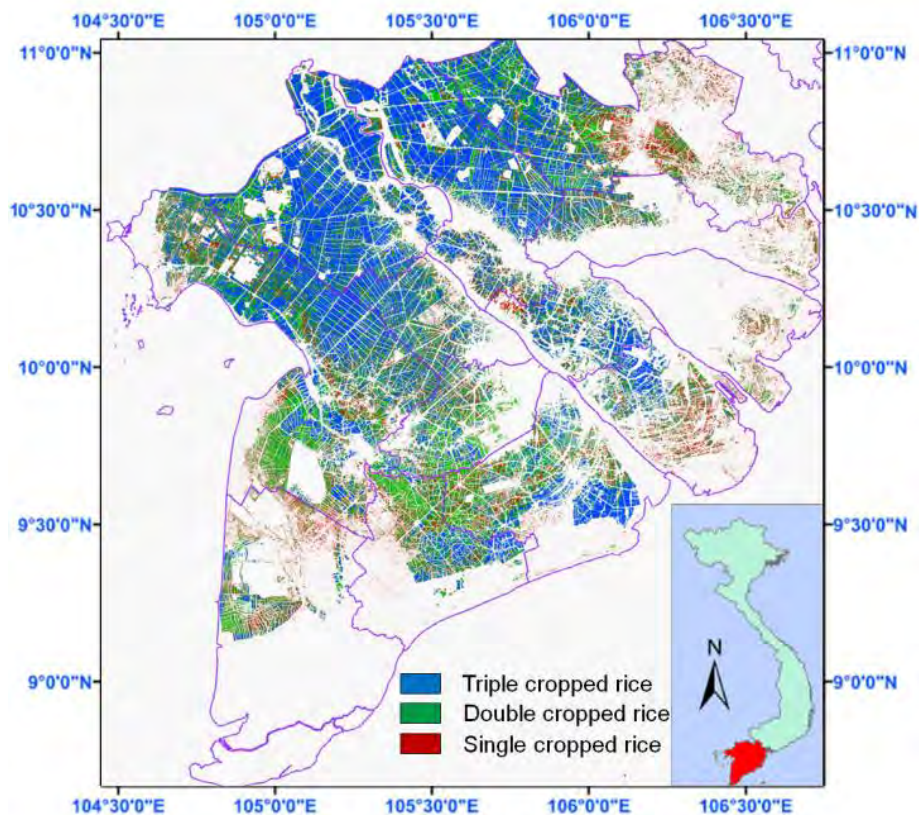
Figure 62. Rice crop intensity map in the Mekong River Delta in 2016.

Triple cropped rice was found in the north and center of the MRD where the rice fields are covered with a dense irrigation network and benefit from a fertile soil thanks to the sediments brought by the floods from the delta (mostly in An Giang, Đồng Tháp, Cần Thơ, Hậu Giang, Vĩnh Long, the western part of Tiền Giang, and Long An). However, the third rice crop is not encouraged by the government, because of the increase of pest damage deriving from year-round continuous cropping of rice.

111

6.1.8. Rice map product at national scale
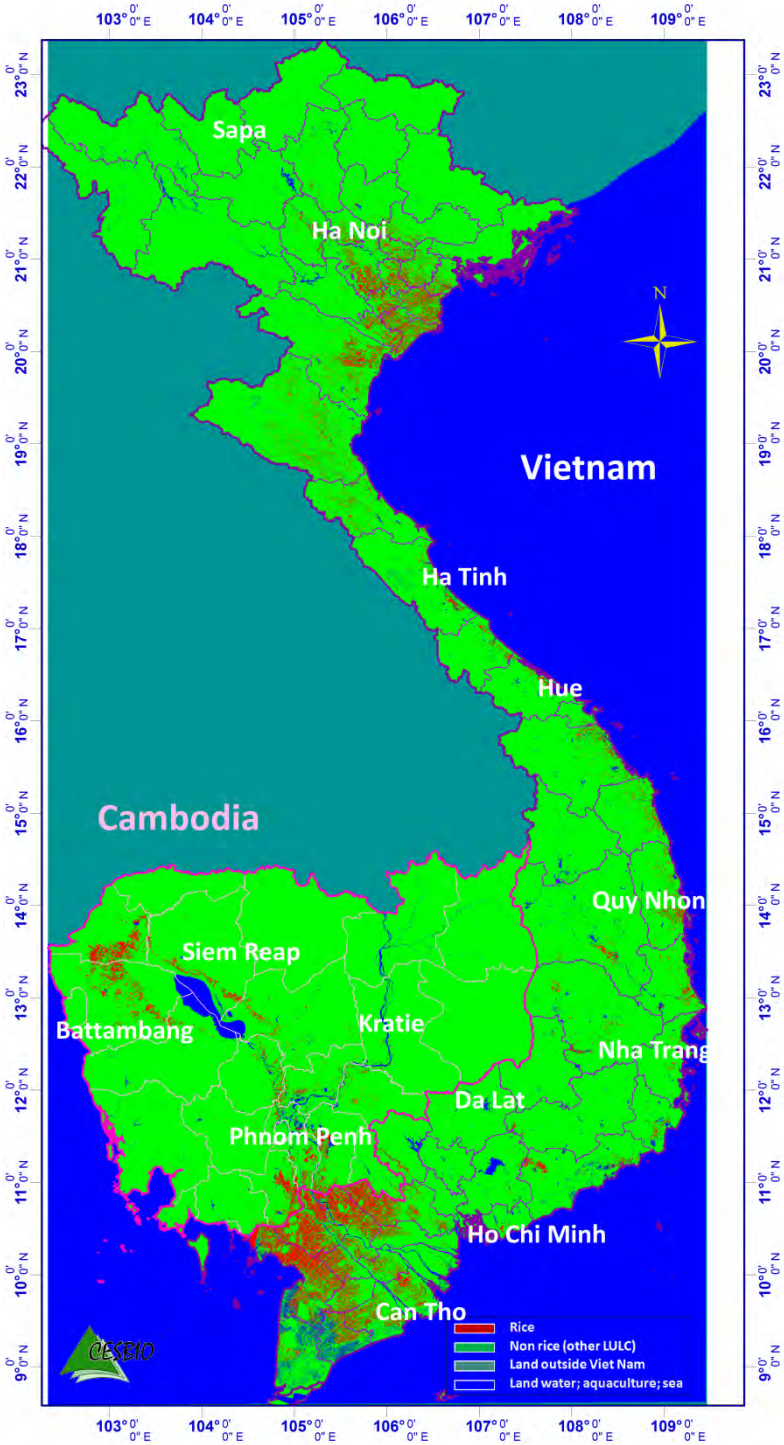
Figure 63. Mapping result in Vietnam and Cambodia using Sentinel-1 data from November 2015 to March 2016.

A test of rice mapping at national scale has been realized, over Vietnam and Cambodia, as shown in Figure 63. The difficulty to take into account is that for a national coverage, Sentinel-1 data to be used are acquired at different dates (as described in Figure 16), and the rice calendar differs between regions. For rice/non rice mapping, the data time series should cover the period corresponding to the maximum increase of the backscatter for the rice season, i.e. from the start of season to the peak season. The test was done on the data from November to March, covering the Spring rice for the Northern part and Winter-Spring in the South. However, in the Central part, the period may miss part of the rice fields, according to the general calendar of the country (Table 3). The results show consistency between different Sentinel-1 frame, but because of the lack of ground data for method refining and for products validation, the mapping results obtained could not be validated.

For Cambodia, the period from November to March covers the entire dry season rice (Table 4), and misses the Medium wet season and the Long Wet Season

The results show consistency with the National Statistics, as shown in Figure 64 where the dry season rice area estimate in Cambodia is in line with the increasing trend in the rice area of the National Statistics.
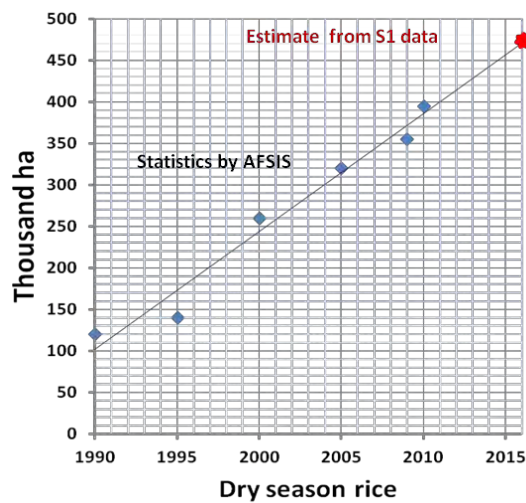
Figure 64. Dry season (12/2015-03/2016) 474.270k ha, compared to past AFSIS statistics in Cambodia.
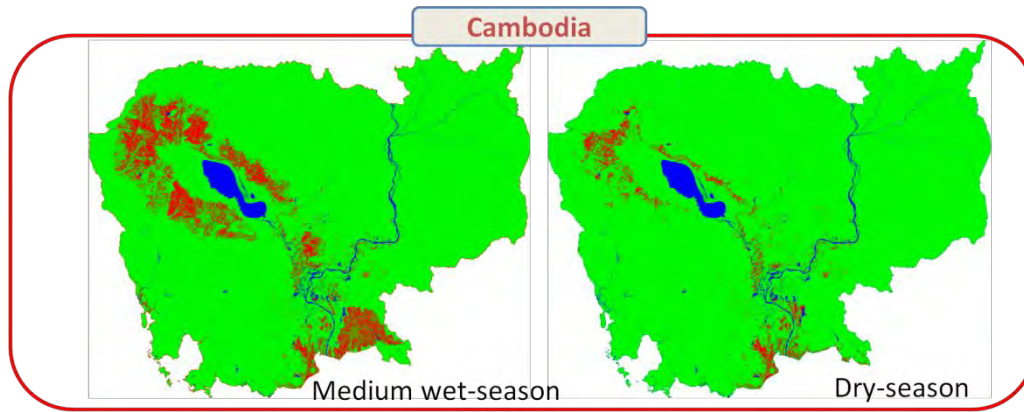
Figure 65. Rice mapping in Medium wet season 2015 is compared to Rice in Dry season 2016 in Cambodia. Red: Rice, Blue: Water, Green: non-rice (forest, urban, etc.)

Figure 65 shows an additional comparison between Medium Wet Season in 2015 and Dry season rice in 2016 using Sentinel-1 with the majority of the cultivated rice was found in the wet season (with more than 80% of total rice area).

6.2. Discussion and conclusion

Rice mapping products have been illustrated and validated in this chapter. The use of the Sentinel-1 SAR data for a large-scale near-real-time monitoring system and high accuracy has been evaluated. Especially the very short revisit time (6 days at present), high resolution (10m) and large coverage demonstrate the advantages of Sentinel-1 data for operational mapping of rice fields at regional and national level. The performance of each mapping product is successfully assessed using reference dataset.

The achieved maps in this study include general LULC, seasonal rice growing areas, sowing date map, long/short cycle rice map, phenological stage map, plant height map and rice crop intensity map for the whole Mekong River Delta. The rice map is extended to the national scale for two countries Vietnam and Cambodia in a preliminary test.

Products validation showed a good agreement with the reference data (sample fields and independent check points) with the accuracy higher than 98% for rice-non rice maps. In addition, the rice planted area estimates for a given rice season could be useful for Statistics Office, for their timeliness, since they can be obtained before, or at the end of the rice season.

The sowing date map derived from Sentinel-1 data is compared with the sowing dates of 240 sampled fields showing a good agreement with a root mean square error of about 4 days. This is a key information in several applications

including crop yield estimation and prediction, water demand for irrigated rice, or methane emission from rice fields. The comparison between long/short cycle rice variety mapping in this study and sampled fields has shown good identification with **91.7 %.** Because of the difference in market values of these two types of rice, the information is essential for market estimation. The phenology mapping has been assessed using the 60 surveyed fields, and also during the field trip during the User Assessment workshop. The detection was found in good agreement with the ground survey for 59/60 fields in the test, and for fields visited by the users during the user workshop. This product was found useful for a synoptic view of the rice growth status in a region, which is difficult to have in a timely manner by ground survey. The plant height estimated with the Sentinel-1 was overall in agreement with the ground measurements, presenting very good correlations (RMSE of 7.8 cm) when compared with the measurements.

Finally, the rice crop intensity has been estimated together with other rice parameters showing a potential of integration of EO products in crop production models. The technical challenges are important in the development of the methodology at national coverage at different dates with different time interval data in each region; different radar physical responses of rice canopy caused by the diversity in rice cultural practices; the very diverse landscape in each country, etc.

Further works need to be carried out to bring the methodology towards operational rice monitoring. More details will be discussed in perspectives (Chapter 8).

The maps can be used at local scale for planning of farm activities, for organizing labor at the right time. It also provides accurate information for the local government, planners and decision makers, to assess the rice grown area for each rice season, and to have early estimation of long and short cycle rice with different market values. The resulting information on rice cultivation is essential for planning, monitoring and food security applications.

Chapter 7

Use of Sentinel-1 retrieved information in models estimating rice yield and methane emission

Contents

7.1. Introduction

As stated in a previous chapter, more than 90% of the world's rice is produced and consumed in Asia (IRRI, 2013). At the economic level, world rice trade is volatile due to the uncertainty in the Asian demand, particularly in countries like Indonesia, the Philippines or Japan, where national production can vary as much as 20% from year to year. Accordingly, prices can fluctuate considerably.

Also, to cope with the increasing rice demand due to population growth, and because of the limitation in the land available for agriculture, rice production will have to increase through cropping density and increasing yield. The latter can be achieved through cultivation practices and through breeding high-yield cultivars (Yu Jiang et al., 2017). Yet, increasing rice growth and increasing cropping density can stimulate methane (CH4) emissions, exacerbating global climate change, as rice cultivation is a major source of this powerful greenhouse gas. Furthermore, increasing irrigated rice will require more water during the dry season, which impacts on the water availability for people consumption.

The challenge of maintaining food security while reducing water used and greenhouse gas emissions is an important tradeoff issue for scientists and policy makers. An evaluation of tradeoffs requires understanding of the complex interactions between rice growth, water and GHG processes across spatial scales and over time. In recent research works, experimental data have been conducted to capture key processes in crop biomass formation and methane emission (Katayanagi *et al.*, 2017; Torbick, Salas, *et al.*, 2017; Arai et al., 2018). Subsequently, experimental data have been used to parameterize process models on crop growth and development models (Le Toan *et al.*, 1997; Bouman and Van Laar, 2006; Pazhanivelan *et al.*, 2015; Tan, Cui and Luo, 2016; Li *et al.*, 2017; Setiyono *et al.*, 2018), and on soil denitrification-decomposition (Cai *et al.*, 2003; Awa, 2008; Fumoto *et al.*, 2010; Salas, 2010; Hayano *et al.*, 2013; Katayanagi *et al.*, 2016, 2017, Tian et al., 2018).

These process-based models can simulate yield or methane emission, but also the water demand, by capturing biophysical growth drivers (microclimate, water, and nutrient). However, for regional upscaling to obtain the regional crop productivity, and the regional methane emission, most studies rely on the concept of 'homogeneous' cropping zones for which the same processes and the same estimates of yields, water, or methane emissions are assumed.

In this study, we assess the possibility to use remote sensing for regional upscaling of the models. Specifically, we evaluate the use of Sentinel-1 data to provide spatial and temporal information related to agro-practices (e.g., crop establishment dates) and seasonal crop development (i.e., phenology) and vegetation status (e.g., height, biomass, etc.), in order to apply the models on a pixel basis for regional application. For this purpose, we will use the two major process-based models for rice fields, ORYZA 2000, for yield prediction, and the DNDC model for methane emission and water use.

In the first step, the models are tested against experimental data sets. Because our data sets for crop monitoring method development do not comprise all the relevant input parameters to run both models, we make use of data acquired by the University of Tokyo in a study on methane emission from rice fields (Arai et al., 2016).

In a second step, the input parameters describing the cultural practices and crop development in the models are replaced by the information retrieved from Sentinel-1.

The model outputs obtained by the two models will be used to discuss about the trade-off between crop productivity, methane emission and water use.

7.2. Description of the models

The two model versions under study are process models which were developed specifically for rice. Both contain the vegetation growth model and require information on climate and soil. ORYZA2000 focuses on crop yield estimates, whereas DNDC primary target was to estimate the GHG emission and water use.

7.2.1. The ORYZA2000 model

ORYZA2000 for modeling of lowland rice is the successor to a series of rice growth simulation models developed by IRRI and Wageningen University and Research Centre (WUR) in the early to mid-1990s. The first version was ORYZA-1 was for potential production, and updated versions ORYZA-W for water-limited situations, and ORYZA-N for nitrogen-limited production. The current version, ORYZA2000 allows a more explicit simulation of crop management options, such as irrigation and nitrogen fertilizer management. It can also be used in application-oriented research such as the analysis of the effects of climate change on crop growth.

The general structure of the model is shown in Figure 66 which represents the model in the situation of potential production in optimum conditions (Bouman and Van Laar, 2006). Under these conditions, light, temperature, and varietal characteristics for phenological, morphological, and physiological processes determine the growth of the crop. The model follows the daily calculation scheme for the rates of dry matter production of the plant organs and the rate of phenological development. By integrating these rates over time, dry matter production of the crop is simulated throughout the growing season.
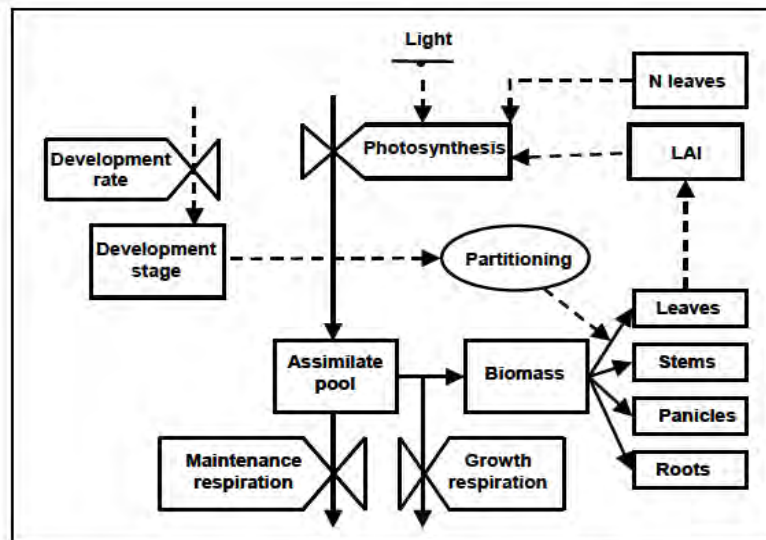
Figure 66. Schematic representation of ORYZA1 in the situation of potential production. Boxes are state variables, valves are rate variables, and circles are intermediate variables. Solid lines are flows of material and dotted lines are flows of information (Bouman and Van Laar, 2006).

Total daily rate of canopy CO_2 assimilation is calculated from daily incoming radiation, temperature, and leaf area index (LAI). Daily assimilation rate is obtained by integrating instantaneous rates of leaf CO_2 assimilation over the day and over all leaf layers in the canopy (Goudriaan, 1986). Photosynthesis of single leaves depends on leaf N content (on area basis), radiation intensity (separated into direct and diffuse radiation), stomatal CO_2 concentration, and temperature. Maintenance respiration requirements are subtracted from the gross assimilation rate to obtain net daily growth expressed in kg carbohydrate per ha per day. Carbohydrates produced are partitioned among roots, leaves, stems and panicles, using experimentally derived partitioning factors as a function of development stage, which is tracked as a function of daily average temperature and photoperiod. Conversion of carbohydrates into structural dry matter is based on equations derived by Penning de Vries et al., (1982). From flowering onward, leaf loss rate is simulated from an experimentally derived loss rate factor, which is a function of development stage, times the remaining green leaf biomass.

In the ORYZA model, all parameter values are listed in external data files and can be changed by the model user. About 10% of crop parameters are expected to be variety specific and need empirical derivation (Bouman and Van Laar, 2006). These parameters are development rates, assimilate partitioning factors, specific leaf area, relative leaf growth rate, leaf death rate, fraction of stem reserves, and maximum grain weight.

7.2.2. The process-based biogeochemistry DNDC model

DNDC is a biogeochemistry model that simulates crop growth and soil C and dynamics based on input data on soil properties, climate, and farming practices (e.g. Li et al., 1992, 1994). The model was expanded to simulate the emission of trace gases such as NO, N2O, NH4, and CH4 from agricultural ecosystems and natural wetlands (Zhang et al., 2002; Li et al., 2004).

Four major ecological drivers, namely climate, soil physical properties, vegetation, and anthropogenic activities, drive the entire model as shown in Figure 67.

DNDC consisted of 2 components: the first component consisting of the Soil climate, crop growth, and decomposition sub-models. The second component consisting of nitrification, denitrification, and fermentation sub-models. The soil climate sub-model calculates soil temperature, moisture, pH, redox potential (Eh) profiles by integrating air temperature, precipitation, soil thermal and hydraulic properties, and oxygen status. By integrating crop characters, climate, soil properties, and farming practices, the plant growth sub-model simulates plant growth and its effects on soil temperature, moisture, pH, Eh, dissolved organic carbon (DOC), and available N concentration. The decomposition submodel simulates concentrations of substrates (e.g., DOC, NH4 and NO3-) by integrating climate, soil properties, plant effect, and farming practices. The three sub-models interact with each other to finally determine soil temperature, moisture, pH, Eh, and substrate concentrations in the soil profiles at a daily time step and predict NH3, NO, N2O, CH4 fluxes.

Methane is an end product of the biological reduction of CO2 or organic carbon under anaerobic conditions. Methane fluxes were strongly controlled by soil available carbon (i.e., DOC) content, and soil temperature. The reduction of available carbon to methane is mediated by anaerobic microbes (e.g., methanogens) that are only active when the soil Eh is low enough. DNDC calculates methane production rate as a function of DOC content and temperature as soon as the predicted soil Eh reaches -150 mV or lower. Methane is oxidized by aerobic methanotrophs in the soil. A highly simplified scheme was employed in DNDC to model methane diffusion between soil layers based on methane concentration gradients, temperature, and porosity in the soil.
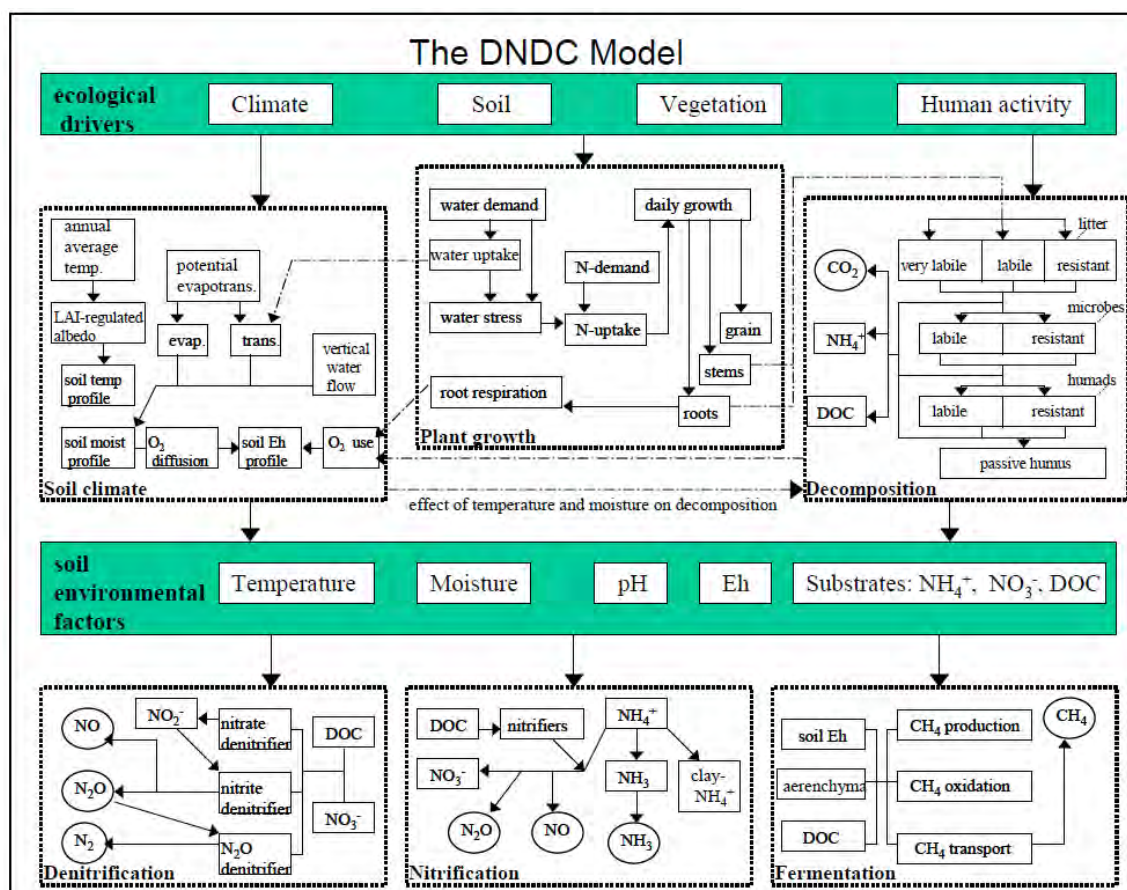
Figure 67. Structure of the DNDC model (New Hampshire, 2012).

For methane emission on agriculture land, DNDC needs site-specific input data of climate, soil, vegetation, and farming practices for the simulated agricultural land. Similarly to ORYZA2000, when the DNDC is used for regional estimates of trace gases emissions, the model needs the spatially and temporally differentiated input data stored in geographical information system type database in advance.

7.2.3. Model testing

In this study, the two models are tested with a selected experimental dataset having a complete set of input data for both ORYZA2000 and DNDC. Because of the lack of input data specific to each of the 60 sampled fields under study in the previous chapter, such as soil data and details in water and fertilizer management, we use instead an experimental data set available through a collaboration with the University of Tokyo. The objective of this experiment was to study the methane emission of rice fields with differences in field management: continuous flooding, alternate wetting and drying, post harvest management of straw (Arai et al., 2016). However, since the data set contains input parameters for both

DNDC and ORYZA 2000 models, they can be used for simulating both the rice yield and the methane emission.

<h4>🔸 Description of test site and dataset</h4>

The data sets that are used are data collected over two years, in 2015 and 2016 including 5 cropping seasons (Winter-Spring, Summer-Autumn and Autumn-Winter) in Tan Loi 2 Hamlet, Thot Not District in Can Tho City, Vietnam (10°18'N, 105°54'E), located in central Mekong Delta (Arai et al., 2016).

The experiment was performed on rice fields of triple-rice cropping. Available information includes a) rice variety: Jasmine 85 (an aromatic long-grain indica rice cultivar developed in Thailand) and OM4218 (a non-photoperiod-sensitive indica rice cultivar developed in Vietnam), b) methods of sowing (transplanting and direct wet seeding method, c) fertilization, d) hydro-meteorological and e) soil characteristics.

Three of the sampled rice blocks were used for an alternate wetting and drying (AWD) and the other three were for a continuously inundated/saturating treatment (CF). The amount of irrigation water use was estimated by using a PVC-made irrigation tube, into which irrigation water was pumped from a canal that ran parallel and close with one of the short sides (26-m long) of the whole experimental field across the community dike.

For rice yield, the weight of each rice plant sample (2×2 m) was estimated as having 14% moisture content.

For methane emission, a transparent acryl chamber (60×80 cm horizontal cross section $\times 100$ cm height with open bottoms) that was equipped with a 20 cm Teflon tube, an air-stirring electric fan and a thermometer in each plot. The collection of gas samples with the chamber was performed at least once a week and once every 3 days for 2 weeks after sowing, for 10 days after heading (flowering) and every day for five days after drainage, irrespective of water management. The gas fluxes were calculated using an equation that was described by Arai *et al*. (2015), and the cumulative gas emission (seasonally or annually) was calculated (Whittaker and Robinson, 1967).

These datasets from Arai et al., (2016) are used as inputs data for soil and crop management for the two process models under study.

<h4>🔸 Inputs in ORYZA2000 and DNDC models</h4>

Common to ORYZA2000 and DNDC models, the input data consist of climate data, soil data and data on crop management.

(1) **Climate data**

The climate data used in this study including maximum and minimum temperature, wind speed and solar radiation are data provided by global datasets, and precipitation data is from Arai et al., (2016). In particular, daily solar radiation (Mj/m²/day) and wind speed (m/s) data were obtained from the NASA POWER (Prediction Of Worldwide Energy Resource) website (http://power.larc.nasa.gov), minimum and maximum daily temperature (°C) data were obtained from the NCDC Global Summary of the Day (GSOD, http://www.ncdc.noaa.gov). These meteorological data were resampled to 15 arc minutes resolution.

(2) **Soil data**

The soil data are from Arai et al., 2016. The soil is silty-clay fluvisol (Clay 52%, Silt 48%, Sand 0.3%; Carbon (C) content of soils: $44.2 \pm 2.5 - 51.8 \pm 10.1$ g C kg-1, Nitrogen (N) content of soils: $3.5 \pm 0.7 - 4.5 \pm 0.3$ g C kg-1; pH (H2O2) of the soils at a 0-10-cm depth: 2.94-4.77, 10 – 20-cm depth: 3.84-5.22, 20 – 30-cm depth: 3.35-4.98 .

(3) Crop management

o Rice variety: Jasmine and OM4218. Transplanting method is used for long cycle rice variety. Twelve-day-old seedlings were transplanted and rice crop duration is about 110 to 120 days. Direct seeding method is used for short cycle rice with crop duration is about 90 days.

o Water management: as stated above, CF and AWD are used for 3 over 6 field blocks under study. Under CF, rice samples were kept flooded from 1 week after sowing till 2 weeks before expected rice harvest. Water was supplied to a depth of 5 cm (when the rice seedlings are still short, to a height not to submerge them) above the soil surface when the standing water level decreased to approximately 1 cm above the soil surface. Under AWD, though water management was the same as that of CF for 2 weeks after sowing, after that, until 2 weeks before expected rice harvest, rice plots were irrigated to a depth of 5 cm only when the field water level dropped to 15 cm below the soil surface, except for 10 days after heading.

o Fertilization was applied as following schedule:

  - 7-10 days after sowing: Phosphoric acid: 7kg/10a, urea 5kg/10a
  - 18-22 days after sowing: Phosphoric acid: 6kg/10a urea 7kg/10a
  - 40-55 days after sowing: potassium: 5kg/10a urea: 5kg/10a
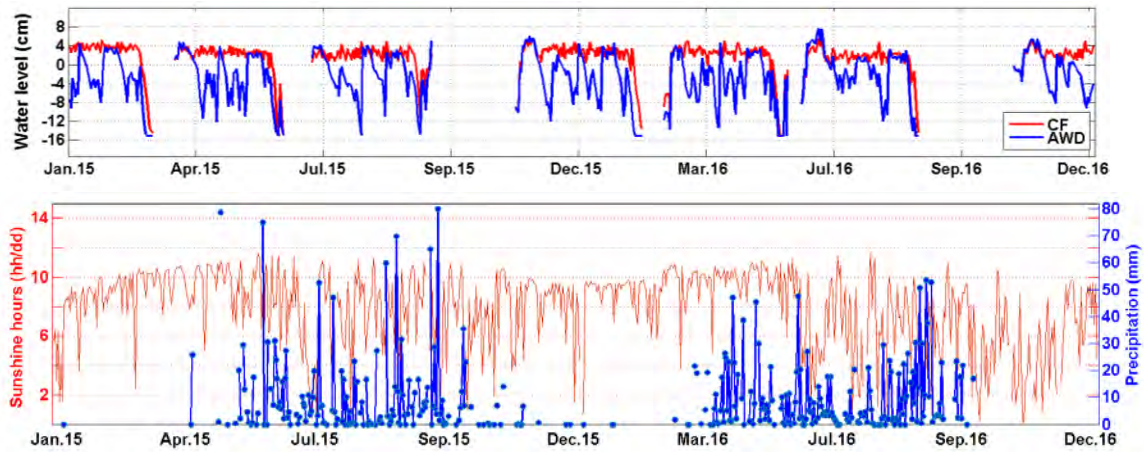
Figure 68. Variations of water level, sunshine hours and precipitation from January 2015 to December 2016 (adapted from data by Arai et al., 2016).

Figure 68 shows the water level (cm), the sunshine hours and precipitation obtained by Arai et al, 2016 during their experiment from January 2015 to December 2016 for CF and AWD rice fields. For AWD fields, the fields were inundated (up to 4 cm), about 3 times during the season (with the exception of the rainy season in 2016-AW16), and the minimum level can go down to -12 to -15 cm. The second panel shows the sunshine hours and precipitation during the 2 years. It can be observed that the number of sunshine hours is smaller during the rainy season in 2016 (starting June-July) than in 2017.

7.3. Rice production estimation using ORYZA2000 model

ORYZA-V3, the latest version since ORYZA Version 2.13 released in 2009 (https://sites.google.com/a/irri.org/oryza2000/home), was used for rice production estimation. The work was conducted in collaboration with the team from IRRI (Tri Setoyono). For most parameters, the base values are obtained from default values (adapted to the Mekong delta). In particular, the partitioning factors, leaf death rates and the development rates are set as an average of those values calculated with data (unpublished) from experiments conducted in 2014/2015 in An Giang province, provided by IRRI (Setiyono *et al.*, 2018).

7.3.1. ORYZA2000 modelling

ORYZA2000 was used to simulate rice fields over 5 rice seasons in 2015-2016: Summer-Autumn 2015, Autumn-Winter 2015, Winter-Spring 2016, Summer-Autumn 2016,

Autumn-Winter 2016. In general, 6 inputs files were created to run the model including (1) Climate data; (2) Soil data file; and (3) Experimental data file (crop management); (4) Crop data file; (5) Reruns file; and (6) Control file. Information of climate data, soil data and crop management (rice variety duration and its calendar, sowing method, water management, and fertilization was inferred for the study area) of each rice field is defined in the input files (1) to (3) as described previously. Crop data file contains all the parameter values that characterize the rice crop such as photosynthesis parameters, growth rates of each rice variety. In particular, the characteristics of two different rice varieties are used in this study for long cycle rice and short cycle rice. Most parameter values are used in a general sense for rice, but some are variety-specific. The parameters in those crop data files are provided by IRRI (unpublished experiments).

Finally, rerun file is created to group all individual simulation in one and there is no limit to the number of reruns that can be made. Reruns can be done on all parameter values of all input files specified in the control file to control the number of reruns made for simulation.

7.3.2. Results and Discussions

(1) **Simulation using Ground-based data:**
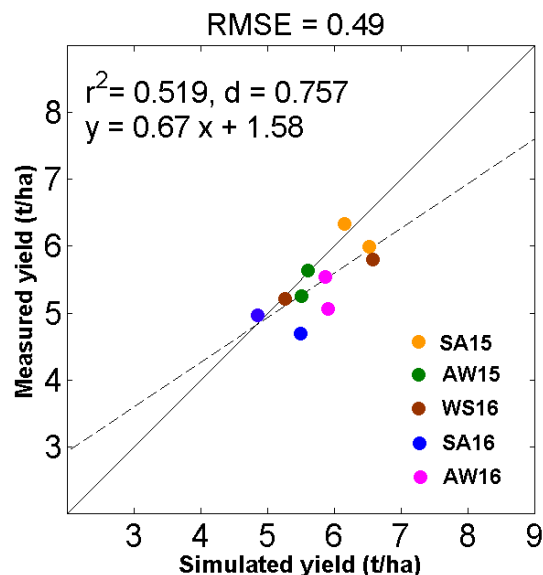
Figure 69. Comparison of rice yield simulated by ORYZA 2000 with in situ rice yields for 2 rice plots (CF and AWD) in Can Tho province over 5 rice seasons (SA-15, AW-15, WS-16, SA-16 and AW-16).

Figure 69 shows the simulated result comparison with the measured yields in the Can Tho province. For each season, the two fields of CF and AWD which show only slight difference in measured yields (as shown in Figure 70) are not singled out. Despite the small range of yields, the simulated values are in good agreement with the measured yields (R^2=0.519), and represent well the inter-annual variation of yields, for example on the lower rice yield in Summer-Autumn 2016 (SA-16) compared to Summer-Autumn 2015 (SA-15), because of the El Niño effect in 2016.
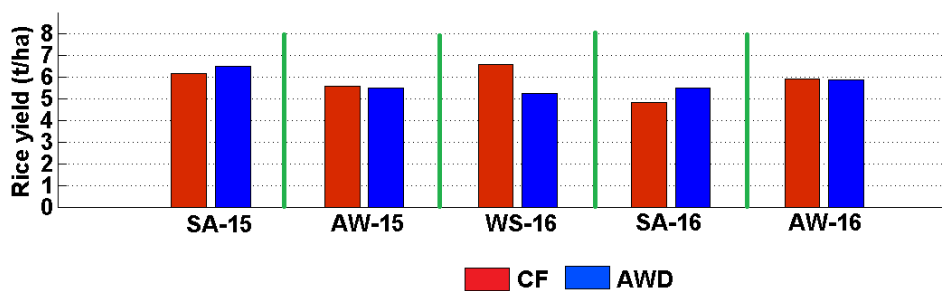
Figure 70. Rice yield simulation of rice sample at continuously-flooding (CF) and of the alternate-wetting-and-drying field-water treatment (AWD) over 5 rice cropping seasons Summer-Autumn 2015 (SA-15), Autumn-Winter 2015 (AW-15), Winter-Spring 2016 (WS-16), Summer-Autumn 2016 (SA-16) and Autumn-Winter 2016 (AW-16).

Figure 70 shows that simulated yields for AWD are equivalent or slightly higher than CF fields, except for Winter-Spring 2016. There is a noticeable inter-annual variation of yields: AW16 yield is higher than AW 15, whereas SA 16 has lower yield than SA-15. Since the soil parameters and rice varieties are the same from the 2 years, this result may indicate that the yield is highly dependent on climate.

(2) EO based simulation:

The Sentinel-1 products developed in this research are used as inputs for the model including information of rice areas extent, long/short rice cycle varieties, sowing date and harvest date, phenological stage, plant height and rice crop intensity extracted for the fields under study from the Sentinel-1 products, using geographic coordinates of the monitored fields.

Figure 71 shows the simulated yields as compared to the measured yields for the two fields in the 5 rice seasons.
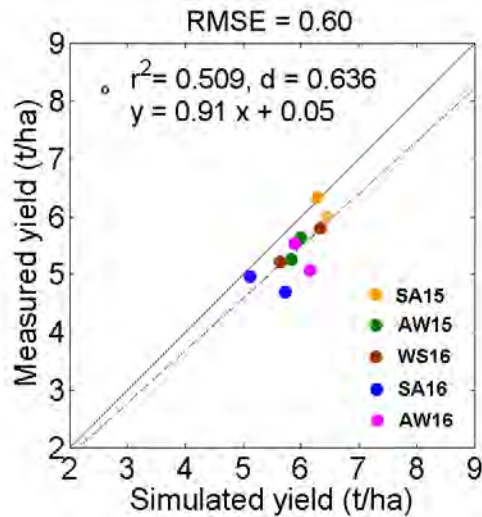
Figure 71. Comparison of rice yield simulated by ORYZA 2000, using inputs from Sentinel-1 products with in situ rice yields for 2 rice plots in Can Tho province over 5 rice seasons (SA-15, AW-15, WS-16, SA-16 and AW-16).

The result in Figure 71 indicates that replacing the major parameters characterizing the spatial variation of rice fields using Sentinel-1 will provides similar comparison with the measured yields (R^2= 0.509), in spite of the additional errors caused by the remote sensing retrieval.
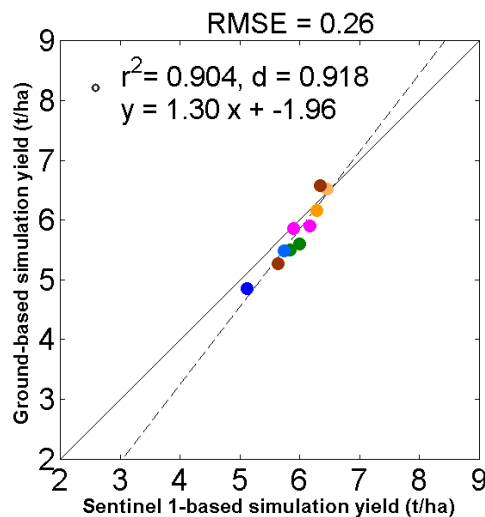
Figure 72. Comparison of rice yield simulated by ORYZA 2000, using inputs from Sentinel-1 products and using inputs from in situ data for 2 rice plots in Can Tho province over 5 rice seasons (SA-15, AW-15, WS-16, SA-16 and AW-16).

Figure 72 shows the good agreement (R^2= 0.904) between the yields simulated by ORYZA2000, when using the complete set of experimental data and when information on

128

long/short rice cycle varieties, sowing date and harvest date, and phenological stage have been retrieved from Sentinel-1.

The results in Figure 71 and Figure 72 indicate that the spatial and temporal variable parameters inputs to the rice production models can be retrieved from Sentinel-1 products.

7.4. Methane emissions estimation using DNDC model

DNDC model version 9.5 (www.dndc.sr.unh.edu/) is used to simulate the methane emission for the rice fields in the Can Tho province. This part of the DNDC work was carried out in collaboration with the team from AGS (Advanced Geophysical System in USA) (William Salas and Nathan Torbick). The Sentinel-1 products developed in this research are used as inputs for the model including information of rice areas extent, sowing date and harvest date, phenological stage and rice crop intensity extracted for the fields under study.

7.4.1. DNDC modelling

As described previously, DNDC also needs site-specific input data of climate, soil, and crop management of the rice fields for the methane emission simulation. To allow for stabilization of DNDC soil organic carbon pools (e.g. residues, microbial, humads and passive organic carbon) for the local land use and climate, a 5-year initialization timeframe preceded the 2016 calendar year for a 6-year total simulation duration (Torbick, Salas, *et al.*, 2017). Soil characteristics (pH, soil carbon, bulk density and soil texture) before 2016 were extracted from the Harmonized World Soils Data- base (http://www.fao.org/soils-portal/soil-survey/soil-maps-and-databases/harmonized-world-soil-database-v12/en/). Daily weather data (maximum and minimum temperature in °C and precipitation in cm) were used as climate datasets for ORYZA2000 simulation.

For water management, DNDC has been set up for 2 scenari simulations AWD and CF (as described in previous section). Seasonal rice maps, crop calendar and cropping intensity, phenological stage map from Sentinel-1 were used to extract the information for crop management of the rice field under study.

7.4.2. Results and Discussions

Figure 73 shows the simulated result comparison with the measured methane emission in the Can Tho province.
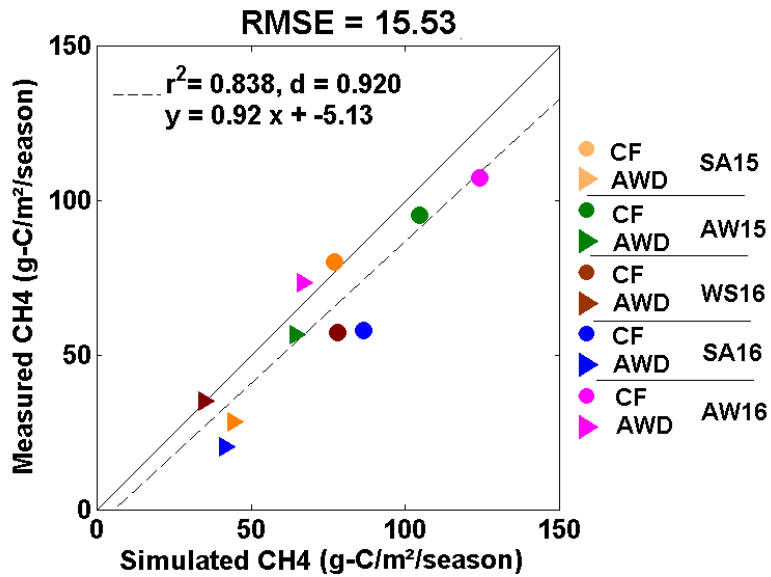
Figure 73. Comparison of simulated methane emission based on Sentinel-1 data using DNDC and measured methane emission for 2 rice plots per season (CF and AWD) in Can Tho province over 5 rice seasons (SA-15, AW-15, WS-16, SA-16 and AW-16).

Figure 73 shows that the simulated CH4 emissions are in agreement with the measured CH4 (R^2= 0.838). As expected, for the same season, continuous flooding fields have higher CH4 emission than AWD.
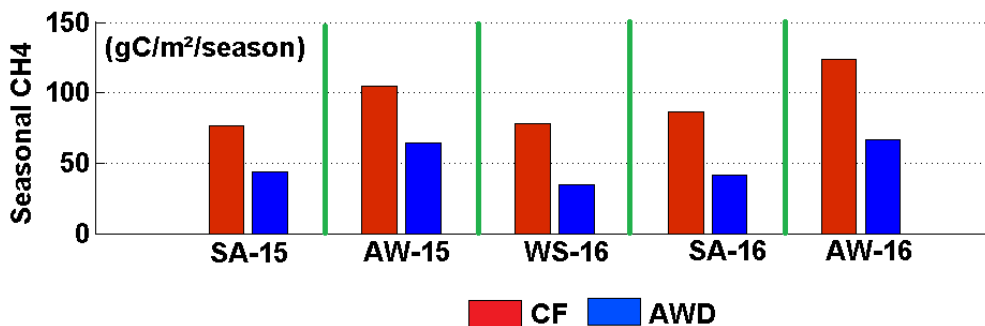
Figure 74. Methane emission simulation of rice sample at continuously-flooding (CF) and of the alternate-wetting-and-drying field-water treatment (AWD) over 5 rice cropping seasons Summer-Autumn 2015 (SA-15), Autumn-Winter 2015 (AW-15), Winter-Spring 2016 (WS-16), Summer-Autumn 2016 (SA-16) and Autumn-Winter 2016 (AW-16).

The methane emission varies among seasons. Figure 74 shows methane emission simulation of rice sample at continuously-flooding (CF) and of the alternate-wetting-and-drying field-water treatment (AWD) over 5 rice cropping seasons Summer-Autumn 2015 (SA-15), Autumn-Winter 2015 (AW-15), Winter-Spring 2016 (WS-16), Summer-Autumn 2016 (SA-16) and Autumn-Winter 2016 (AW-16).

AW-16 has the highest emissions and much higher than the emissions of the same season in the previous year AW-15. During the dry season SA-15 and WS-16, the emission is lower than during the other seasons.

Figure 75 shows an example of model outputs for 1 simulation of rice fields for crop yield, and heat, water, nitrogen stresses including:

- grain, leaf and stem, root weight (potential maximum, and actual)

- water demand and water uptake

- Nitrogen demand and N uptake

- temperature demand and actual temperature
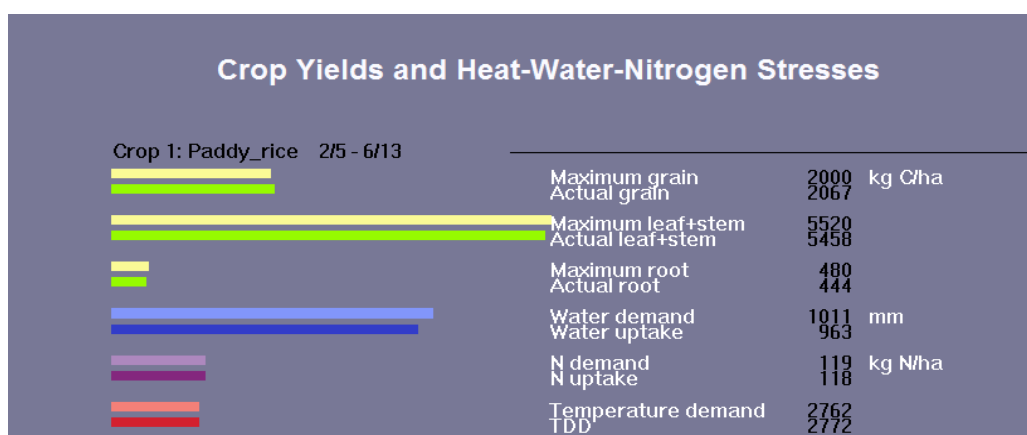
Figure 75. Model outputs of DNDC simulation

The model can be used to estimate crop yield from the grain weight ouputs. However, the model is optimized for methane emission, and crop yield module needs to be adapted to the rice variety and the specific conditions of the region of interest.

7.4.3. Simulation of water demand

The water requirement and uptake by rice crop under different management practices are also simulated.

Figure 76 shows an example of the water balance components, including precipitation, irrigation, ground water supply, transpiration, soil evaporation, surface evaporation, leaching, run off.
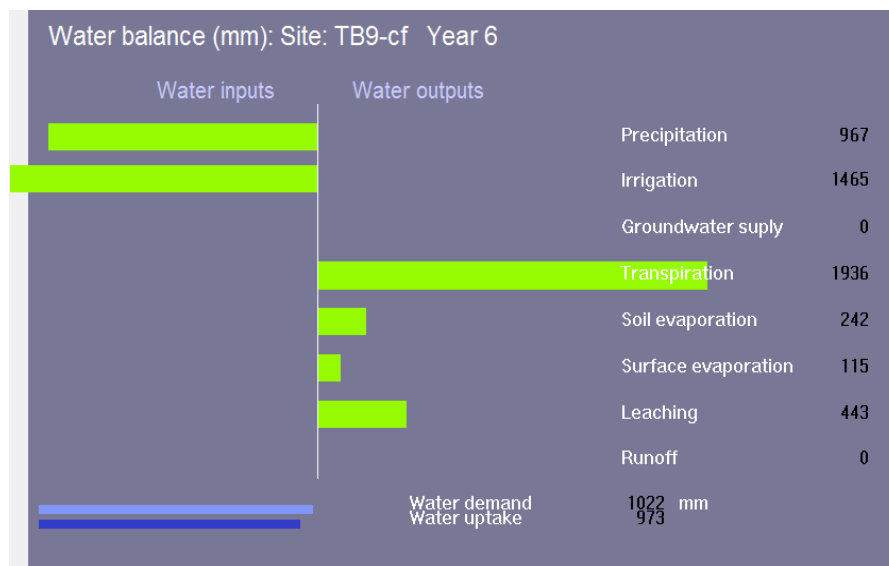
Figure 76. Model result of water balance.

The water received by the system includes the input fluxes from precipitation, irrigation and groundwater supply. The water lost from the system includes the output fluxes due to transpiration, soil evaporation, surface water evaporation (for flooded soil), leaching and runoff.

The model was run for 2 scenari, CF and AWD, for 3 rice cropping seasons. Table 15 shows the water demand for the 2 water management scenari: it is clear that water demand is higher for Continuous flooding, and in particular the high value of SA 2016 (1936 mm) indicates that much water is needed during the drought period of that year.

Table 15. Water demand under two water management scenari for 2016 rice seasons (triple crop).

Rice season	Water demand (mm)	
	CF	**AWD**
WS-16	1022	953
SA-16	1936	1210
AW-16	1407	1100

This was confirmed by the high values of irrigation water for SA-16 at Can Tho test fields measured experimentally, as shown in Figure 77.
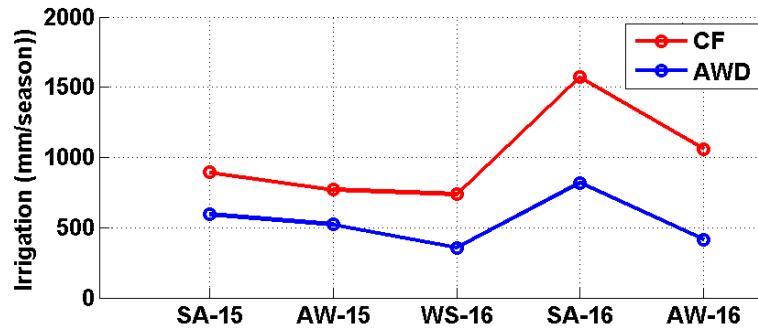
Figure 77. In situ data of irrigation water for each season in Can Tho experiment site for CF and AWD water managements (adapted from Arai et al. 2016).

In order to have a basis for the trade off discussion, the results from ORYZA 2000 and DNDC are put together.

Table 16 shows the simulated results of rice yield, CH4 emission and water demand for the fields under CF and AWD for the 3 rice seasons in 2016. For each rice season (WS, SA, AW), simulated yield, CH4 and water demand are listed. The question to be addressed in this case is to define in which cases to have reduced water demand and CH4 emission, without reducing rice productivity. Table 16 indicates that AWD reduces in most cases water and CH4, without decreasing the yield significantly. It was also shown that SA-16 (dry season) have the highest water demand and the lowest yield. However, to draw conclusions, the number of simulations needs to be increased. Nevertheless, this preliminary work shows a concept that could be extended regionally, to estimate the regional production, the water demand and the CH4 emission.

Table 16. The simulated results of rice yield, CH4 emission and water demand for the fields under CF and AWD for the 3 rice seasons in 2016

	Yield (ton/ha)		CH4 (gC/m²)		Water demand (mm)	
	CF	*AWD*	*CF*	*AWD*	*CF*	*AWD*
WS-16	6.58	5.26	68.12	41.46	1022	953
SA-16	4.85	5.49	83.38	54.65	1936	1210
AW-16	5.91	5.86	123.97	76.68	1407	1100

7.5. Discussion and conclusion-way forward

The approach described in this chapter shows a potential of driving process-based models such as DNDC and ORYZA2000 using information derived from Sentinel-1 data comprising rice map area (seasonal maps and crop intensity map), sowing date and harvest

date, and phenological stage and plant height to estimate rice production and methane emission from rice fields, at the regional scale.

However, further works still need to be done on a larger number of experimental fields, accounting for a large variability in rice ecosystems and cultural practices. Sensitivity analysis will be further done to identify for a region such as the Mekong Delta, the most sensitive input parameters, in order to replace the less sensitive parameters by default values (e.g. from literature).

For regional application the approach still has several limitations, such as:

(1) Limitation from meteorological data: spatial distribution of meteorological stations, incomplete and unavailable in a timely manner, and do not adequately represent the diversity over large areas;

(ii) Soil characteristics which were often available at a large scale, so that the spatial heterogeneity of soil properties (e.g., texture, SOC content, pH) cannot be taken into account.

(iii) More generally, those process-based models require too many input parameters. Although many the spatial and temporal varying parameters can be retrieved from remote sensing, knowledge of detailed water management, fertilization and culture practices still need to be provided.

(iv) There is a need to exploit the potential of Sentinel-1 to provide rice biomass and/or Leaf Area Index (LAI) that can be used to further reset the models. Alternatively, Sentinel-2 data need to be assessed for the provision of LAI (in terms of number of Sentinel-2 images available per rice season, and the accuracy of the retrieved LAI).

However, the models can be used at present for trade-off study for optimizing the cultural practices, determining the best periods for rice season, investigating the impact of climate on rice productivity, water demand, and methane emission.

134

Chapter 8

Conclusion

Contents

8.1. Conclusions

The overall objective of this thesis was to develop methods for rice monitoring using radar remote sensing. With Copernicus Sentinel-1 Synthetic-Aperture Radar data available systematically and worldwide, the methods developed have the potential to be used effectively in applications.

In this study, the specific objective is to provide tools for observation of the rice cultivation systems, by generating products such as map of rice planted area, map of rice start-of-season and phenological stages, and map of the number of rice crops per year, together with rice crop parameters such as category of rice varieties (long or short cycle), and plant height. The information to be provided is necessary to the estimation of crop production, and to the management of rice ecosystems at the regional scale. We also investigate on how the products derived from EO Sentinel-1 data can be integrated in process-based models for rice production estimation and methane emission estimation.

The first part of this thesis introduces the importance of rice production and its role in global economy, food security, and how the rice production is linked to environment and climate changes. This leads to the understanding of the information requirements to be

fulfilled by an observing system. In general, information of rice growing areas and rice parameters (rice variety, sowing date, phenological stage, plant height, crop intensity, etc) are strongly needed as a valuable data base for spatial decision support in farm management, cropping optimization, farming system intensification and policy definition in food provision management. On the other hand, remote sensing has the potential to provide spatial and temporal information related to agro-practices that can be used as direct input parameters to the process-based models for rice production estimation, water use and methane emission estimation, providing a significant contribution to global environment studies.

The test region used to develop methods based on Sentinel-1 data for rice monitoring is one of the major world rice regions which is the Mekong River Delta, in Vietnam. This region presents a diversity in rice cultivation practices, in cropping density, from single to triple crop a year, and in crop calendar. The methods to be developed should account for such diversity, and at the same time, without relying heavily on the in situ data for methods calibration. This requires knowledge-based methods rather than traditional statistical methods.

The first step was to understand the Sentinel-1 backscatter of rice fields, and specifically, the temporal variation of the backscatter, at VH and VV polarizations. For this purpose, experiment has been set up to collect in-situ data. During 2 years, data collected for the 5 rice seasons over 60 sampled fields have been used to interpret the Sentinel-1 backscatter temporal variation. It was found that backscatter time series of rice fields show very specific temporal behavior, as compared to other land use land cover types. In particular a simple indicator which is the backscatter maximum temporal increase could already be used to detect rice from other LULC classes. The temporal and polarization variations of the rice backscatter are interpreted with respect to physical interaction mechanisms to relate the backscatter dynamics (increasing, decreasing trends, and maximum and minimum values) to the key phenological stages, when the plants change its morphology and biomass. For example, the analysis pointed out that the beginning of tillering and the booting-heading stages correspond to remarkable characteristics of the backscatter temporal curves (respectively minimum and maximum). Because the same trend of temporal curves was observed for all the rice seasons in 2, 3 different years, it is possible to derive a mean curve to be used in the methodology developed for detecting rice phenology, for deriving information such as the date of sowing, the rice varieties of long and short duration cycle, or plant height at each SAR acquisition date.

The methods of rice mapping and mapping of rice phenology have been developed and applied to the Mekong delta. Products validation exercise based on in situ data dedicated to validation (1950 independent data points for rice-non rice, and for other parameters, the in situ data over 60 fields for one rice season are used for training, the data of 4 other rice seasons are used for validation. The accuracy of the rice/non rice map was found reaching 98%, the sowing dates have a RMSE of about 4 days, the RMSE in plant height is 7.8 cm, the long/short variety map has 91.7% accuracy and for phenology, only one season has been processed with good detection rate of 59/60. The methodology for rice mapping has also been applied at national scale for Vietnam and Cambodia to test the application of the methods on the mosaic of Sentinel-1 data acquired at different dates. Despite the lack of validation, the results demonstrate that it is possible to use Sentinel-1 data for mapping of rice fields at national level, especially with it capability to have short revisit time (6 days at present), high resolution (10m) and large coverage (250 km).

Finally, the uses of the rice monitoring products as inputs in two process-based models were assessed. The models are ORYZA2000 for rice production estimation and DNDC for methane emission and water demand estimation. Sentinel-1 data retrieved information (sowing date, phenology, long/short variety, plant height) are used as model inputs, giving good agreement with the results making use of ground survey only. It was possible to have an integrated result on rice yield, water use, and methane emissions based on the two process models with inputs from Sentinel-1 data. The preliminary results show good potential to determine the water management in rice field to reduce water use and GHG emission, without reducing much the yield.

8.2. Perspectives

To achieve the objective which is the effective use of Sentinel-1 data for rice monitoring for food security and global environment, more works need to be done concerning a) the consolidation of the rice monitoring method development, b) the integration of Sentinel-1 derived information in models aiming at estimating and predicting rice production, methane emission and water use, and also further conducting the trade-off studies.

❖ *To consolidate the remote sensing method development*

Central to the development of the rice monitoring methods based on the Sentinel-1 time series is the understanding of the temporal variation of the backscatter at C-band as a function of crop development, cultural practices, and SAR polarizations and incidence angle. For this purpose, experimental data have been collected in this study (60 fields over 5 rice cropping seasons in 2 years). However, to interpret the rice backscatter 'temporal signature', there is a need to conduct electromagnetic modelling of the SAR signal. This will require a detailed description of the rice canopy by measuring geometric and dielectric properties of the rice plants and the rice canopy frequently, at least at each Sentinel-1 observation. Alternatively, a 3D rice crop growth model, if validated locally, could be used for the simulations, through collaboration with specialist team.

Such models can be useful to simulate the effect of a diversity of crop characteristics and conditions, an essential step to the application of the methods worldwide.

Concerning the retrieval of crop parameters, because of the scarcity of biomass and LAI measurements in the data sets under study, only the retrieval of plant height has been performed. However, since LAI and biomass are two key parameters for yield estimation and methane emission, there is a need to conduct an additional campaign dedicated to the retrieval of these parameters.

In addition to Sentinel-1, Sentinel-2 data could be used for LAI and biomass retrieval, in particular during the dry season, when more cloud free Sentinel-2 data are expected to be available.

❖ *Integration of Sentinel-1 derived information in processed based models*

The study on integration of Sentinel-1 retrieved information in the process-based models for rice production estimation, methane emission and water use estimation needs to be pursued. The preliminary work conducted in this study has shown the potential use of remote sensing for trade-off analysis of the impacts of cultural practices, rice varieties, water management on the rice yield, GHG emission (CH_4 but also N_2O, CO_2..), and water balance. Also the model upscaling to regional scale will have to be investigated, taking into account the difficulty to have input data characterizing soil properties and cultural practices on a field basis. Alternatively, ORYZA2000 and DNDC models will be used for sensitivity and trade-off study, and their regional versions need to be adapted to contain only the most sensitive input parameters.

The methods developed need to be assessed and applied to a larger region, for example for countries in South East Asia, in order to provide timely information on crop planted area, or on anomaly in crop growth, following disasters such as drought or floods that occur more often in the recent year.

In this case, the challenges to be faced are the very large volume of data, the use of data platforms and cloud computing needs to be initiated.

<div align="right">

Chapitre 8

Conclusion

</div>

Sommaire

8.1. Conclusions

L'objectif général de cette thèse était de développer des méthodes pour le suivi du riz utilisant la télédétection radar. Avec les données du radar à synthèse d'ouverture Sentinel-1 de Copernicus disponibles de manière systématique et avec une couverture globale, les méthodes développées ont le potentiel pour être utilisées de manière effective dans des applications opérationnelles.

Dans cette étude, l'objectif spécifique est de fournir des outils pour l'observation des systèmes de culture du riz, en générant des produits tels que des cartes de surfaces plantées en riz, des cartes de la date du début de saison du riz et des stades phénologiques, et des cartes du nombre de cultures de riz par an, ainsi que des paramètres culturaux tels que les variétés de riz (à cycle long ou court) et la hauteur des plantes. Ces informations sont nécessaires pour l'estimation de la production et pour la gestion des écosystèmes rizicoles à l'échelle régionale. Nous explorons également de quelle manière les produits dérivés de Sentinel-1 peuvent être intégrés dans les modèles basés sur les processus pour l'estimation de la production du riz et des émissions de méthane dans les rizières.

La première partie de cette thèse introduit l'importance de la production du riz et son rôle dans l'économie mondiale et la sécurité alimentaire, et décrit comment la production de riz est liée à l'environnement et aux changements climatiques. Ceci a conduit à identifier les besoins en informations qui devront être couverts dans le cadre d'un système d'observation.

D'une manière générale, des informations sur les surfaces cultivées en riz et sur les paramètres du riz (variété, date de semis, stade phénologique, hauteur de la plante, nombre de cultures par an, etc) ont un rôle capital à jouer comme outils d'aide à la décision pour la gestion des fermes, l'optimisation des cultures, l'intensification des systèmes agricoles et la définition de politiques de gestion de fourniture de nourriture. La télédétection a le potentiel pour fournir des informations spatiales et temporelles liées aux pratiques agricoles qui peuvent être utilisées comme paramètres d'entrée directs dans les modèles d'estimation de production du riz basés sur des processus, et dans les modèles d'estimation d'utilisation de l'eau et d'émissions de méthane, fournissant ainsi une contribution importante aux études environnementales mondiales.

La région test utilisée pour développer les méthodes basées sur les données Sentinel-1 pour le suivi du riz est une des principales régions rizicoles dans le monde, à savoir le Delta du Mékong au Vietnam. Cette région présente une diversité de pratiques culturales, de nombre de cultures par an (de une à trois), et de calendrier cultural. Les méthodes à développer doivent tenir compte de cette diversité, sans pour autant se reposer trop lourdement sur les données *in situ* pour l'étalonnage des méthodes. Ceci nécessite des méthodes basées sur l'expertise plutôt que des méthodes statistiques traditionnelles.

La première étape a consisté à comprendre la rétrodiffusion des rizières telle que mesurée par Sentinel-1, et plus spécifiquement, la variation temporelle de cette rétrodiffusion, aux polarisations VH et VV. Pour cela, des campagnes de collectes de données in situ ont été mises en place. Pendant 2 ans, les données collectés pour 5 saisons de riz sur 60 champs ont été utilisées pour interpréter la variation temporelle de la rétrodiffusion de Sentinel-1. L'analyse de ces données a révélé que les séries temporelles de rétrodiffusion des champs de riz ont un comportement temporel très spécifique comparé aux autres classes de couverture et d'occupation du sol. En particulier, un simple indicateur tel que le maximum d'augmentation temporelle suffit à distinguer le riz des autres classes. Les variations temporelles et de polarisation de la rétrodiffusion des rizières sont interprétées en termes de mécanismes d'interaction physiques afin de relier la dynamique de la rétrodiffusion (augmentation, tendances décroissantes, et valeurs maximales et minimales) aux stades phénologiques clés, correspondant à des changements dans la morphologie et la biomasse des plantes. Par exemple, les analyses ont mis en avant le fait que le début du tallage et le stade de montaison/épiaison correspondent à des caractéristiques remarquables des courbes temporelles de rétrodiffusion (le minimum et le maximum, respectivement). Grâce au fait que la même tendance temporelle est observée à toutes les saisons de riz

observées sur 2 années différentes, il est possible d'extraire une courbe moyenne qui sera utilisée dans la méthodologie développée pour la détection de la phénologie du riz, afin d'estimer par exemple la date de semis, et pour déterminer la variété de riz (cycle de culture long ou court), ou la hauteur des plantes à chaque acquisition RSO.

La méthode de cartographie du riz et de cartographie de la phénologie a été développée et appliquée au Delta du Mékong. Un exercice de validation des produits à partir de données *in situ* dédiées à la validation (1950 points de données indépendants pour le riz/non-riz, et pour les autres paramètres, les données *in situ* de 60 champs sur une saison sont dédiés à l'apprentissage et les 4 autres saisons sont utilisées pour la validation). La précision de la carte riz/non-riz atteint 98%, la date de semis présente une erreur quadratique (RMSE) d'environ 4 jours, et la hauteur de plante une RMSE de 7,8cm, la classification de variété (cycle long/cours) a une précision de 91,7% et pour la phénologie, une seule saison a été traitée, avec un taux de bonne estimation de 59/60. La méthodologie de cartographie du riz a également été appliquée à l'échelle nationale au Vietnam et au Cambodge pour tester l'application des méthodes sur des mosaïques de données Sentinel-1 acquises à des dates différentes. En dépit du manque de validation, les résultats démontrent qu'il est possible d'utiliser Sentinel-1 pour la cartographie des rizières à l'échelle nationale, particulièrement grâce à sa capacité à avoir une courte période de revisite (6 jours actuellement), une résolution fine (10m), et une large fauchée (250km).

Enfin, l'utilisation des produits de suivi du riz comme entrées dans deux modèles basés sur des processus a été évaluée. Les modèles sont ORYZA2000 pour l'estimation de la production du riz et DNDC pour l'estimation des émissions de méthane et de la demande en eau. Les informations extraites des données Sentinel-1 (date de semis, phénologie, variété de cycle long/court, hauteur de la plante) sont utilisées comme entrées dans les modèles et fournissent des résultats qui concordent avec ceux issus de la seule utilisation de données de terrain. Des résultats intégrés ont pu être obtenus sur le rendement du riz, l'utilisation de l'eau et les émissions de méthane à partir de ces deux modèles et des données d'entrée issues de Sentinel-1. Les résultats préliminaires montrent un bon potentiel pour déterminer la gestion de l'eau dans les rizières afin de réduire l'utilisation d'eau et les émissions de gaz à effet de serre tout en préservant le rendement.

8.2. Perspectives

Pour atteindre l'objectif d'utilisation effective des données Sentinel-1 dans le suivi du riz pour la sécurité alimentaire et l'environnement, des travaux supplémentaires doivent être menés, qui concernent a) la consolidation des méthodes de suivi du riz, b) l'intégration des informations issues de Sentinel-1 dans les modèles d'estimation et de prédiction de la production de riz, des émissions de méthane et de l'utilisation de l'eau.

❖ *Consolider les méthodes basées sur la télédétection*

La compréhension des variations temporelles de la rétrodiffusion en bande C en fonction du développement des plantes, des pratiques culturales, et des paramètres RSO (polarisation, angle d'incidence) est capitale pour développer des méthodes de suivi du riz basées sur les séries temporelles de Sentinel-1. Pour cela, des données expérimentales ont été collectées lors de cette étude (60 champs sur 5 saisons réparties sur 2 ans). Cependant, l'interprétation de la "signature temporelle" de la rétrodiffusion du riz nécessite des travaux de modélisation électromagnétique du signal RSO. Cela implique une description détaillée du couvert de riz basée sur des mesures des propriétés géométriques et diélectriques des plantes de riz et du couvert de riz, et ce de manière fréquente (au moins à chaque acquisition Sentinel-1). Sinon, un modèle tridimensionnel de croissance du riz, à condition d'être validé localement, pourrait être utilisé pour les simulations, via une collaboration avec une équipe spécialisée.

De tels modèles sont utiles pour simuler l'effet d'un grand nombre de caractéristiques et de conditions culturales, une étape essentielle à la généralisation des méthodes à l'échelle mondiale.

En ce qui concerne l'estimation des paramètres culturaux, le faible nombre de mesures de biomasse et de surface foliaire (LAI) dans les jeux de données disponibles n'ont permis d'obtenir des résultats que sur l'estimation de la hauteur des plantes. Cependant, le LAI et la biomasse étant deux paramètres clés pour l'estimation du rendement et des émissions de méthane, il est nécessaire de mener de nouvelles campagnes dédiées à l'estimation de ces paramètres.

En plus de Sentinel-1, les données Sentinel-2 pourraient être utilisées pour l'estimation du LAI et de la biomasse, en particulier pendant la saison sèche, lorsque les données Sentinel-2 sans nuage sont plus susceptibles d'être disponibles.

❖ *Intégration des information issues de Sentinel-1 dans les modèles basés sur des processus*

L'étude de l'intégration des informations issues de Sentinel-1 dans les modèles basés sur des processus pour l'estimation de la production de riz, des émissions de méthane et de l'utilisation en eau doit être poursuivie. Le travail préliminaire mené dans cette étude a montré l'utilisation potentielle de la télédétection pour l'analyse des compromis liés aux impacts des pratiques culturales, des variétés de riz et de la gestion de l'eau sur le rendement du riz et les émissions de gaz à effet de serre (CH_4 mais aussi N_2O, CO_2...). Le passage à l'échelle régionale devra être exploré, en prenant en compte la difficulté d'obtenir des données d'entrée caractérisant les propriétés du sol et les pratiques culturales à l'échelle du champ. Sinon, ORYZA2000 et DNDC pourront être utilisés pour des études de sensibilité et de compromis, et leurs versions régionales devront être adaptées pour contenir seulement les paramètres d'entrée les plus sensibles.

Les méthodes développées doivent être évaluées et appliquées à des régions plus larges, par exemple sur des pays entiers d'Asie du Sud-Est, afin de fournir des informations sur les surfaces plantées, ou sur les anomalies de croissance des cultures suite à des catastrophes naturelles comme les sécheresses ou les inondations, qui deviennent de plus en plus fréquentes.

Les défis à affronter seront alors le très grand volume de données et l'utilisation de plateformes de données et de cloud-computing.

Bibliography

Aggarwal, P. K., Kalra, N., Chander, S., and Pathak, H. (**2004**): 'A generic simulation model for annual crops in tropical environments', *InfoCrop*, Indian Agricultural Research Institute, New Delhi.

Anastasi, C., Dowding, M., and Simpson, V. J. (**1992**). 'Future CH4 emission from rice production', *J. Geophys*. Res., 97, 7521–7125.

Arai, H., Takeuchi, W., Oyoshi, K., Nguyen, L. D., Tachibana, T., & Inubushi, K. (**2018**). Regional Evaluation Techniques on Greenhouse Gas-mitigation & Yield-increase Performance of a Water-saving Irrigation Practice's Dissemination in Rice Paddies in The Mekong Delta. *Monitoring of Global Environment and Disaster Risk Assessment from Space: the IIS Forum proceedings* (Vol. 26, pp. 43-50).

Arai, H., Takeuchi, W., Oyoshi, K., Nguyen, L., & Inubushi, K. (**2018**). Estimation of Methane Emissions from Rice Paddies in the Mekong Delta Based on Land Surface Dynamics Characterization with Remote Sensing. *Remote Sensing*, *10*(9), 1438. doi: 10.3390/rs10091438.

Arii, M., Yamada, H., Kobayashi, T., Kojima, S., Umehara, T., Komatsu, T., & Nishimura, T. (**2017**). Theoretical characterization of X-band multiincidence angle and multipolarimetric SAR data from rice paddies at late vegetative stage. *IEEE Transactions on Geoscience and Remote Sensing*, *55*(5), 2706-2715.

Baghdadi, N., Choker, M., Zribi, M., Hajj, M. E., Paloscia, S., Verhoest, N. E., ... & Mattia, F. (**2016**). A new empirical model for radar scattering from bare soil surfaces. *Remote Sensing, 8(11), 920.*

Baghdadi, N., N. Holah & M. Zribi (**2006**), 'Calibration of the Integral Equation Model for SAR data in C-band and HH and VV polarizations', *International Journal of Remote Sensing*, 27:4, 805-816, DOI: 10.1080/01431160500212278.

Bégué, A., Arvor, D., Bellon, B., Betbeder, J., De Abelleyra, D., PD Ferraz, R., ... & R Verón, S. (**2018**). Remote sensing and cropping practices: A review. *Remote Sensing*, *10*(1), 99.

Belder, P., Bouman, B. A. M., Cabangon, R., Guoan, L., Quilang, E. J. P., Yuanhua, L., ... & Tuong, T. P. (**2004**). Effect of water-saving irrigation on rice yield and water use in typical lowland conditions in Asia. *Agricultural water management*, *65*(3), 193-210.

Bellón, B., Bégué, A., Lo Seen, D., de Almeida, C., & Simões, M. (**2017**). A remote sensing approach for regional-scale mapping of agricultural land-use systems based on NDVI time series. *Remote Sensing*, *9*(6), 600.

Bolton, D.K.; Friedl, M.A. (**2013**). 'Forecasting crop yield using remotely sensed vegetation indices and crop phenology metrics'. *Agric. For. Meteorol*., 173, 74–84.

Boschetti, M., Stroppiana, D., Brivio, P. A., & Bocchi, S. (**2009**). Multi-year monitoring of rice crop phenology through time series analysis of MODIS images. *International journal of remote sensing*, *30*(18), 4643-4662.

Bouman, B. A. M. (**2001**). '*ORYZA2000: Modeling lowland rice'*.

Bouman, B. A. M. and Van Laar, H. H. (**2006**) 'Description and evaluation of the rice growth model ORYZA2000 under nitrogen-limited conditions', *Agricultural Systems*, 87(3), pp. 249–273. doi: 10.1016/j.agsy.2004.09.011.

Bouman, B. A. M., Peng, S., Castaneda, A. R., & Visperas, R. M. (**2005**). Yield and water use of irrigated tropical aerobic rice systems. *Agricultural Water Management*, 74(2), 87-105. doi: 10.1016/j.agwat.2004.11.007.

Bouman, B. A. M. and Tuong, T. P. (**2001**) 'Field water mangement to save water and increase its productivity in irrigated lowland rice', *Agricultural Water Management*, 1615, pp. 1–20. doi: 10.1016/S0378-3774(00)00128-1.

Bouvet, A., Le Toan, T. and Lam-dao, N. (**2009**) 'Delta Using ENVISAT / ASAR Dual Polarization Data Monitoring of the Rice Cropping System in the Mekong Delta Using ENVISAT / ASAR Dual Polarization Data', 47(2), pp. 517–526.

Bouvet, A., Le Toan, T., Floury, N., & Macklin, T. (**2010**). An end-to-end error model for classification methods based on temporal change or polarization ratio of SAR intensities. *IEEE Transactions on Geoscience and Remote Sensing*, 48(9), 3521-3538. doi: 10.1109/TGRS.2010.2047399.

Bouvet, A. and Le Toan, T. (**2011**) 'Use of ENVISAT/ASAR wide-swath data for timely rice fields mapping in the Mekong River Delta', *Remote Sensing of Environment*. Elsevier Inc., 115(4), pp. 1090–1101. doi: 10.1016/j.rse.2010.12.014.

Bouvet A., Le Toan T., Hoa P. (**2015**) 'Sentinel-1 and Radarsat 2 data for rice monitoring in the Mekong delta, Vietnam', *IGARSS, IEEE*.

Bruniquel, J. and Lopes, A. (**1997**) 'Multi-variate optimal speckle reduction in SAR imagery', *International Journal of Remote Sensing*, 18(3), pp. 603–627. doi: 10.1080/014311697218962.

C. Oliver; And S. Quegan (**2004**) 'Understanding Synthetic Aperture Radar Images', *SciTech Publishing*.

Cao, M., Dent, J. B., and Heal, O. W.: Modelling of methane emission from rice paddies, Global Biogeochem. Cy., 9, 183–195,**1995**a.

Cai, Z. C. (**2000**) 'Methane emission from rice fields in China: measurements and influencing factors', 105, pp. 231–242.

Cai, Z., Sawamoto, T., Li, C., Kang, G., Boonjawat, J., Mosier, A., ... & Tsuruta, H. (**2003**). Field validation of the DNDC model for greenhouse gas emissions in East Asian cropping systems. *Global Biogeochemical Cycles*, 17(4). doi: 10.1029/2003GB002046.

Chakraborty, M., Panigrahy, E. S., & Sharma, S. A. (**1997**). Discrimination of rice crop grown under different cultural practices using temporal ERS-1 synthetic aperture radar data. *ISPRS Journal of Photogrammetry and Remote Sensing*, 52(4), 183-191. doi: 10.1016/S0924-2716(97)00009-9.

Chakraborty, M., Manjunath, K. R., Panigrahy, S., Kundu, N., & Parihar, J. S. (**2005**). Rice crop parameter retrieval using multi-temporal, multi-incidence angle Radarsat SAR data. *ISPRS Journal of Photogrammetry and Remote Sensing*, 59(5), 310-322. doi: 10.1016/j.isprsjprs.2005.05.001.

Chen, J., Lin, H. and Pei, Z. (**2007**) 'Application of ENVISAT ASAR Data in Mapping Rice Crop Growth in Southern China', *Geoscience and Remote Sensing Letters, IEEE*, 4(3), pp. 431–435. doi: 10.1109/LGRS.2007.896996.

Chen, J., Lin, H., Huang, C., & Fang, C. (**2009**). The relationship between the leaf area index (LAI) of rice and the C-band SAR vertical/horizontal (VV/HH) polarization ratio. *International Journal of remote sensing*, *30*(8), 2149-2154. doi: 10.1080/01431160802609700.

Chen, C. and Mcnairn, H., (**2006**). A neural network integrated approach for rice crop monitoring. International Journal of Remote Sensing, 27, pp. 1367-1393.

Clauss, K., Ottinger, M., Leinenkugel, P., & Kuenzer, C. (**2018**). Estimating rice production in the Mekong Delta, Vietnam, utilizing time series of Sentinel-1 SAR data. *International journal of applied earth observation and geoinformation*, *73*, 574-585. doi: 10.1016/j.jag.2018.07.022.

De Bernardis, C. G., Vicente-Guijalba, F., Martinez-Marin, T., & Lopez-Sanchez, J. M. (**2015**). Estimation of key dates and stages in rice crops using dual-polarization SAR time series and a particle filtering approach. *IEEE Journal of Selected Topics in Applied Earth Observations and Remote Sensing*, *8*(3), 1008-1018. doi: 10.1109/JSTARS.2014.2372898.

Dong, J., Xiao, X., Menarguez, M. A., Zhang, G., Qin, Y., Thau, D., ... & Moore III, B. (**2016**). Mapping paddy rice planting area in northeastern Asia with Landsat 8 images, phenology-based algorithm and Google Earth Engine. *Remote sensing of environment*, *185*, 142-154. doi: 10.1016/j.rse.2016.02.016.

Doraiswamy, P.C.; Sinclair, T.R.; Hollinger, S.; Akhmedov, B.; Stern, A.; Prueger, J. (**2005**) Application of MODIS derived parameters for regional crop yield assessment. Remote Sens. Environ., 97, 192–202.

Erten, E., Lopez-Sanchez, J. M., Yuzugullu, O., & Hajnsek, I. (**2016**). Retrieval of agricultural crop height from space: A comparison of SAR techniques. *Remote Sensing of Environment*, *187*, 130-144. doi: 10.1016/j.rse.2016.10.007.

ESA (**2017**) 'The Sentinel Application Platform (SNAP), a Common Architecture for all Sen- tinel Toolboxes Being Jointly Developed by Brockmann Consult, Array Systems Com- puting and C-S'. Available at: http://step.esa.int/main/download/.

Fan, W., W. Chao, Z. Hong, Z. Bo and T. Yixian (**2011**). Rice Crop Monitoring in South China With RADARSAT-2 Quad-Polarization SAR Data. *Geoscience and Remote Sensing Letters*, IEEE 8(2): 196-200.

FAO (**2006**) *Calendrario de cultivos*.

FAO (**2017**) *Rice market monitor*.

FAO (**2012**) 'Feeding the world', *FAO Statistical Yearbook 2013*, pp. 123–158. Available at: papers2://publication/uuid/dfbc4388-5a7a-4c52-930a-28ef39f92320.

Ferencz, C.; Bognár, P.; Lichtenberger, J.; Hamar, D.; Tarcsai, G.; Timár, G.; Ferencz Árkos, I. (**2004**) Crop yield estimation by satellite remote sensing. Int. J. Remote Sens., 25, 4113–4149.

Forestry, F. B. R. C. for A. and (**2001**) *Growth stages of mono-and dicotyledonous plants BBCH Monograph*, *BBCH Monograph*. doi: 10.5073/bbch0515.

Freeman, A. (**1992**) 'SAR calibration: An overview', *IEEE Trans. Geosci. Remote Sensing*, 30(No 6.), pp. 1107 –1121.

From, B. and Canopy, R. (**2016**) 'Modeling and Characteristics of Microwave Backscattering From Rice Canopy Over Growth Stages', *IEEE Transactions on Geoscience and Remote Sensing*, 54(11), pp. 6757–6770. doi: 10.1109/TGRS.2016.2590439.

Fumoto, T., Kobayashi, K., Li, C., Yagi, K., & Hasegawa, T. (**2008**). Revising a process-based biogeochemistry model (DNDC) to simulate methane emission from rice paddy fields under various residue management and fertilizer regimes. *Global Change Biology*, *14*(2), 382-402. doi: 10.1111/j.1365-2486.2007.01475.x.

Fumoto, T., Yanagihara, T., Saito, T., & Yagi, K. (**2010**). Assessment of the methane mitigation potentials of alternative water regimes in rice fields using a process-based biogeochemistry model. *Global change biology*, *16*(6), 1847-1859. doi: 10.1111/j.1365-2486.2009.02050.x.

General Statistics Office of Vietnam (**2017**) *General Statistics Office of Vietnam*. Available at: http://www.gso.gov.vn/.

Gilhespy, S. L., Anthony, S., Cardenas, L., Chadwick, D., del Prado, A., Li, C., ... & Smith, P. (**2014**). First 20 years of DNDC (DeNitrification DeComposition): model evolution. *Ecological Modelling*, *292*, 51-62. doi: 10.1016/j.ecolmodel.2014.09.004.

University of Hampshire, (**2007**) 'User's Guide for the DNDC Model', *Oceans*, p. 61.

Hayano, M., Fumoto, T., Yagi, K., & Shirato, Y. (**2013**). National-scale estimation of methane emission from paddy fields in Japan: Database construction and upscaling using a process-based biogeochemistry model. *Soil science and plant nutrition*, *59*(5), 812-823. doi: 10.1080/00380768.2013.836943.

Holecz, F., Barbieri, M., Collivignarelli, F., Gatti, L., Nelson, A., Setiyono, T. D., ... & Obico, M. R. (**2013**). An operational remote sensing based service for rice production estimation at national scale. In *Proceedings of the living planet symposium*. doi: 10.13140/2.1.1492.8643.

Hong Van, N. P.*,* Nga, T. T., Arai, H., Hosen, Y., Chiem, N. H., & Inubushi, K. (**2014**) 'Rice Straw Management by Farmers in a Triple Rice Production System in the Mekong Delta, Viet Nam', *Tropical Agriculture Development*, 58(4), pp. 155–162. doi: 10.11248/JSTA.58.155.

Inoue, Y., Kurosu, T., Maeno, H., Uratsuka, S., Kozu, T., Dabrowska-Zielinska, K., & Qi, J. (**2002**). Season-long daily measurements of multifrequency (Ka, Ku, X, C, and L) and full-polarization backscatter signatures over paddy rice field and their relationship with biological variables. *Remote Sensing of Environment*, *81*(2-3), 194-204. doi: 10.1016/S0034-4257(01)00343-1.

Inoue, Y., Sakaiya, E. and Wang, C. (**2014a**) 'Capability of C-band backscattering coefficients from high-resolution satellite SAR sensors to assess biophysical variables in paddy rice', *Remote Sensing of Environment*. Elsevier Inc., 140, pp. 257–266. doi: 10.1016/j.rse.2013.09.001.

Inoue, Y., Sakaiya, E. and Wang, C. (**2014**b) 'Potential of X-band images from high-resolution satellite SAR sensors to assess growth and yield in paddy rice', *Remote Sensing*, 6(7), pp. 5995–6019. doi: 10.3390/rs6075995.

Ipcc (**1996**) 'Methane Emissions from Rice Cultivation : Flooded Rice Fields', *Revised 1996 IPCC Guidelines for National Greenhouse Gas Inventories: Reference Manual*, 3(June 1992), pp. 53–75.

Available at: http://www.ipcc-nggip.iges.or.jp/public/gl/invs1.html.

IRRI (**2010**) *Rice in the Global Economy*.

John C. Curlander, R. N. M. (**1991**) *Synthetic Aperture Radar: Systems and Signal Processing*.

Kai, F. M., Tyler, S. C. and Randerson, J. T. (**2010**) 'Modeling methane emissions from rice agriculture in China during 1961-2007', *Journal of Integrative Environmental Sciences*, 7(SUPPL. 1), pp. 49–60. doi: 10.1080/1943815X.2010.492227.

Karila, K., Nevalainen, O., Krooks, A., Karjalainen, M., & Kaasalainen, S. (**2014**) 'Monitoring changes in rice cultivated area from SAR and optical satellite images in ben tre and tra vinh provinces in mekong delta, vietnam', *Remote Sensing*, 6(5), pp. 4090–4108. doi: 10.3390/rs6054090.

Katayanagi, N., Furukawa, Y., Fumoto, T., & Hosen, Y. (**2012**) 'Validation of the DNDC-rice model by using CH4 and N2O flux data from rice cultivated in pots under alternate wetting and drying irrigation management', *Soil Science and Plant Nutrition*, 58(3), pp. 360–372. doi: 10.1080/00380768.2012.682955.

Katayanagi, N., Fumoto, T., Hayano, M., Takata, Y., Kuwagata, T., Shirato, Y., ... & Yagi, K. (**2016**) 'Development of a method for estimating total CH4 emission from rice paddies in Japan using the DNDC-Rice model', *Science of the Total Environment*. Elsevier B.V., 547, pp. 429–440. doi: 10.1016/j.scitotenv.2015.12.149.

Katayanagi, N., Fumoto, T., Hayano, M., Shirato, Y., Takata, Y., Leon, A., & Yagi, K. (**2017**) 'Estimation of total CH4emission from Japanese rice paddies using a new estimation method based on the DNDC-Rice simulation model', *Science of the Total Environment*. Elsevier B.V., 601–602, pp. 346–355. doi: 10.1016/j.scitotenv.2017.05.090.

Kern, J. S., Gong, Z., Zhang, G., Zhuo, H., and Luo, G.: Spatial analysis of methane emissions from paddy soils in China and the potential for emissions reduction, Nutr. Cycl. Agroecosys., 49, 181–195, 1997.

Koay, J. Y., Tan, C. P., Lim, K. S., bin Abu Bakar, S. B., Ewe, H. T., Chuah, H. T., & Kong, J. A. (**2007**). Paddy fields as electrically dense media: Theoretical modeling and measurement comparisons. *IEEE Transactions on Geoscience and Remote Sensing*, *45*(9), 2837-2849.

Koide, N.; Robertson, A.; Ines, A.; Qian, J.H.; DeWitt, D.; Lucero, A. (**2013**). Prediction of rice production in the Philippines using seasonal climate forecasts. J. Appl. Meteorol. Clim., 552–569.

Kucuk, C., Taskin, G. and Erten, E. (**2016**) 'Paddy-Rice Phenology Classification Based on Machine-Learning Methods Using Multitemporal Co-Polar X-Band SAR Images', *IEEE Journal of Selected Topics in Applied Earth Observations and Remote Sensing*, 9(6), pp. 2509–2519. doi: 10.1109/JSTARS.2016.2547843.

Kuenzer, C. and Knauer, K. (**2013**) 'Remote sensing of rice crop areas-A Review', *International Journal of Remote Sensing*, 34(6), pp. 2101–2139. doi: 10.1080/01431161.2012.738946.

Laborte, A. G., Gutierrez, M. A., Balanza, J. G., Saito, K., Zwart, S. J., Boschetti, M., ... & Koo, J. (**2017**). RiceAtlas, a spatial database of global rice calendars and production. *Scientific data*, *4*, 170074. doi: 10.1038/sdata.2017.74.

Lam-Dao, N., Le-Toan, T., Apan, A. A., Bouvet, A., Young, F., & Le-Van, T. (**2009**). Effects of changing rice cultural practices on C-band synthetic aperture radar backscatter using Envisat advanced synthetic aperture radar data in the Mekong River Delta. *Journal of Applied Remote Sensing*, *3*(1), 033563. doi: 10.1117/1.3271046.

Lam-Dao, N., Hoang-Phi, P., Huth, J., & Cao-Van, P. (**2011**) 'Estimation of the Rice Yield in the Mekong Delta Using SAR Dual Polarisation Data', *Asian Conference on Remote Sensing*.

Lasko, K., Vadrevu, K. P., Tran, V. T., & Justice, C. (**2018**). Mapping double and single crop paddy rice with Sentinel-1A at varying spatial scales and polarizations in Hanoi, Vietnam. *IEEE journal of selected topics in applied earth observations and remote sensing*, *11*(2), 498-512. doi: 10.1109/JSTARS.2017.2784784.

Le Toan, T., Henri L., Eric M., and A. L. (**1989**) 'Multitemporal and Dual-Polarization Observations of Agricultural Vegetation Covers by X-Band SAR Images', *IEEE Transactions on Geoscience and Remote Sensing*, 27(November).

Le Toan, T., Ribbes, F., Wang, L. F., Floury, N., Ding, K. H., Kong, J. A., ... & Kurosu, T. (**1997**). Rice crop mapping and monitoring using ERS-1 data based on experiment and modeling results. *IEEE Transactions on Geoscience and Remote Sensing*, *35*(1), 41-56. doi: 10.1109/36.551933.

Le Toan, T., M. Davidson, F. Mattia, P. Borderies, I. Chenerie, T. Manninnen, M. Borgeaud, (**1999**), 'Improved Observation and Modelling of Bare Soil Surfaces for Soil Moisture Retrieval", *ESA Newsletters, Earth Observation Quarterly*, n. 62.

Leon, A., Kohyama, K., Yagi, K., Takata, Y., & Obara, H. (**2017**). The effects of current water management practices on methane emissions in Japanese rice cultivation. *Mitigation and adaptation strategies for global change*, *22*(1), 85-98. doi: 10.1007/s11027-015-9665-9.

Li, T., Hasegawa, T., Yin, X., Zhu, Y., Boote, K., Adam, M., ... & Gaydon, D. (**2015**). Uncertainties in predicting rice yield by current crop models under a wide range of climatic conditions. *Global change biology*, *21*(3), 1328-1341. doi: 10.1111/gcb.12758.

Li, C., Mosier, A., Wassmann, R., Cai, Z., Zheng, X., Huang, Y., ... & Lantin, R. (**2004**). Modeling greenhouse gas emissions from rice-based production systems: Sensitivity and upscaling. *Global Biogeochemical Cycles*, *18*(1). doi: 10.1029/2003GB002045.

Li, T., Angeles, O., Marcaida III, M., Manalo, E., Manalili, M. P., Radanielson, A., & Mohanty, S. (**2017**). From ORYZA2000 to ORYZA (v3): An improved simulation model for rice in drought and nitrogen-deficient environments. *Agricultural and forest meteorology*, *237*, 246-256. doi: 10.1016/j.agrformet.2017.02.025.

Liew, S. C., Kam, S. P., Tuong, T. P., Chen, P., Minh, V. Q., & Lim, H. (**1998**). Application of multitemporal ERS-2 synthetic aperture radar in delineating rice cropping systems in the Mekong River Delta, Vietnam. *IEEE Transactions on Geoscience and Remote Sensing*, *36*(5), 1412-1420.

Lim, K.-S., Koo, V. C. and Ewe, H.-T. (**2008**) 'Multi-Angular Scatterometer Measurements for Various Stages of Rice Growth', *Progress In Electromagnetics Research*, 83, pp. 385–396. doi: 10.2528/PIER08070205.

Lopez-Sanchez, J. M., Ballester-Berman, J. D. and Hajnsek, I. (**2009**) 'Rice monitoring in Spain by means of time series of terraSAR-X dual-pol images', *European Space Agency, (Special Publication) ESA SP*, 668 SP(2), pp. 412–422.

Lopez-Sanchez, J. M. and David Ballester-Berman, J. (**2009**) 'Potentials of polarimetric SAR interferometry for agriculture monitoring', *Radio Science*, 44(2), pp. 1–20. doi: 10.1029/2008RS004078.

Lopez-Sanchez, J. M., Cloude, S. R. and Ballester-Berman, J. D. (**2012**) 'Rice phenology monitoring by means of SAR polarimetry at X-band', *IEEE Transactions on Geoscience and Remote Sensing*, 50(7 PART 2), pp. 2695–2709. doi: 10.1109/TGRS.2011.2176740.

Lopez-sanchez, J. M., Ballester-berman, J. D. and Cloude, S. R. (**2013**) 'Polarimetric Response of Rice Fields at C-band: Analysis and phenological retrieval', 52(5), pp. 1–24.

Maki, M.; Sekiguchi, K.; Homma, K.; Hirooka, Y.; Oki, K. (**2017**), Estimation of rice yield by SIMRIW-RS, a model that integrates remote sensing data into a crop growth model. J. Agric. Met., 73, 2–8.

Mary, J. K. *et al.* (**2014**) 'Simulation of rice water demand under conventional and modified water management practices using DNDC model in Bhavanisagar basin', *Ecology, Environment and Conservation*, 20(3), pp. 1247–1251.

Matthews, R. B., Wassmann, R., and Arah, J.: Using a crop/soil simulation model and GIS techniques to assess methane emmisions from rice fields in Asia, I. Model development, Nutr. Cycl. Agroecosys., 58, 141–159, **2000.**

Mattia, F., T. Le Toan, J.C. Souyris, G. De Carolis, N. Floury, F. Posa, G. Pasquariello (**1997**)," The effect of Surface Roughness on Multifrequency Polarimetric SAR data", *IEEE Trans. on Geosc. and Rem. Sensing,* vol. 35, n. 4.

Mattia, F., T. Le Toan (**1999**)," Backscattering Properties of Multi Scale Rough Surfaces", *Journal of Electromagnetic Waves and Applications*, vol.13, 491-526.

Mattia, F., T. Le Toan, M. Davidson (**2001**), 'An analytical, numerical and experimental study of backscattering from multi-scale soil surfaces', *Radio Science*, Vol. 36, No. 1 , p. 119.

Minamikawa, K., Fumoto, T., Iizumi, T., Cha-un, N., Pimple, U., Nishimori, M., ... & Kuwagata, T. (**2016**). Prediction of future methane emission from irrigated rice paddies in central Thailand under different water management practices. *Science of the Total Environment*, *566*, 641-651. doi: 10.1016/j.scitotenv.2016.05.145.

Mosleh, M. K., Hassan, Q. K. and Chowdhury, E. H. (**2015**) 'Application of remote sensors in mapping rice area and forecasting its production: A review', *Sensors (Switzerland)*, 15(1), pp. 769–791. doi: 10.3390/s150100769.

Ndikumana, E., Ho Tong Minh, D., Dang Nguyen, H., Baghdadi, N., Courault, D., Hossard, L., & El Moussawi, I. (**2018**). Estimation of rice height and biomass using multitemporal SAR Sentinel-1 for Camargue, Southern France. *Remote Sensing*, *10*(9), 1394. doi: 10.3390/rs10091394.

Nelson, A., Setiyono, T., Rala, A., Quicho, E., Raviz, J., Abonete, P., ... & Thongbai, P. (**2014**). Towards an operational SAR-based rice monitoring system in Asia: Examples from 13 demonstration sites across Asia in the RIICE project. *Remote Sensing*, *6*(11), 10773-10812. doi: 10.3390/rs61110773.

Nguyen, T. T. H., C. A. J. M. de Bie, A. Ali, E. M. A. Smaling and T. H. Chu (**2012**). Mapping the irrigated rice cropping patterns of the Mekong delta, Vietnam, through hyper-temporal spot NDVI image analysis. *International Journal of Remote Sensing* 33(2): 415-434.

Nguyen, D. B., Gruber, A. and Wagner, W. (**2016**) 'Mapping rice extent and cropping scheme in the Mekong Delta using Sentinel-1A data', *Remote Sensing Letters*. Taylor & Francis, 7(12), pp. 1209–1218. doi: 10.1080/2150704X.2016.1225172.

Nguyen, D., Clauss, K., Cao, S., Naeimi, V., Kuenzer, C., & Wagner, W. (**2015**). Mapping rice seasonality in the Mekong Delta with multi-year Envisat ASAR WSM data. *Remote Sensing*, *7*(12), 15868-15893. doi: 10.3390/rs71215808.

Olofsson, P., Foody, G. M., Stehman, S. V., & Woodcock, C. E. (**2013**). Making better use of accuracy data in land change studies: Estimating accuracy and area and quantifying uncertainty using stratified estimation. *Remote Sensing of Environment*, *129*, 122-131. doi: 10.1016/j.rse.2012.10.031.

Pandey, A., Vu, D. Q., Bui, T. P. L., Mai, T. L. A., Jensen, L. S., & de Neergaard, A. (**2014**). Organic matter and water management strategies to reduce methane and nitrous oxide emissions from rice paddies in Vietnam. *Agriculture, ecosystems & environment*, *196*, 137-146. doi: 10.1016/j.agee.2014.06.010.

Pazhanivelan, S., Kannan, P., Mary, N., Christy, P., Subramanian, E., Jeyaraman, S., ... & Yadav, M. (**2015**) 'Rice crop monitoring and yield estimation through COSMO Skymed and TerraSAR-X: A SAR-based experience in India', *International Archives of the Photogrammetry, Remote Sensing and Spatial Information Sciences - ISPRS Archives*, 40(7W3), pp. 85–92. doi: 10.5194/isprsarchives-XL-7-W3-85-2015.

Peña-Arancibia, J. L., Mainuddin, M., Kirby, J. M., Chiew, F. H., McVicar, T. R., & Vaze, J. (**2016**) 'Assessing irrigated agriculture's surface water and groundwater consumption by combining satellite remote sensing and hydrologic modelling', *Science of the Total Environment*. Elsevier B.V., 542, pp. 372–382. doi: 10.1016/j.scitotenv.2015.10.086.

Peyron, M., Bertora, C., Pelissetti, S., Said-Pullicino, D., Celi, L., Miniotti, E., ... & Sacco, D. (**2016**) 'Greenhouse gas emissions as affected by different water management practices in temperate rice paddies', *Agriculture, Ecosystems and Environment*. Elsevier B.V., 232, pp. 17–28. doi: 10.1016/j.agee.2016.07.021.

Phan, H., Le Toan, T., Bouvet, A., Nguyen, L., Pham Duy, T., & Zribi, M. (**2018**). Mapping of rice varieties and sowing date using x-band SAR data. *Sensors*, *18*(1), 316. doi: 10.3390/s18010316.

Portmann, F. T., Siebert, S. & Döll, P. (**2010**) 'MIRCA2000-global monthly irrigated and rainfed crop areas around the year 2000: a new high-resolution data set for agricultural and hydrological modelling', *Global Biogeochemical Cycles*, 24(1011).

Prasad, A.K.; Chai, L.; Singh, R.P.; Kafatos, M. Crop yield estimation model for Iowa using remote sensing and surface parameters. Int. J. Appl. Earth Obs. Geoinf. 2006, 8, 26–

33.

Prospects, C. and Situation, F. (**2018**) 'GIEWS Crop Prospects and Food Situation #4, December 2017', (december 2017).

Mishra, V. N., Prasad, R., Kumar, P., Srivastava, P. K., & Rai, P. K. (**2017**). Knowledge-based decision tree approach for mapping spatial distribution of rice crop using C-band synthetic aperture radar-derived information. *Journal of Applied Remote Sensing*, *11*(4), 046003. doi: 10.1117/1.JRS.11.

Quegan, S. and Le Toan, T. (**1998**) 'Analysing multitemporal SAR images', *European Space Agency- Publications*, 434(January), pp. 1183–1194. Available at: http://bibdigital.sid.inpe.br/rep-/dpi.inpe.br/lise/2005/01.13.18.00.

Redfern, S. K., Azzu, N. and Binamira, J. S. (**2015**) 'Rice in Southeast Asia: facing risks and vulnerabilities to respond to climate change', *Building Resilience for Adaptation to Climate Change in the Agriculture Sector*, (2002), pp. 295–314.

Ribbes, F. and Toan, T. L. E. (**1999**) 'Rice field mapping and monitoring with RADARSAT data', 20(4), pp. 745–765.

Rosenqvist, A. (**1999**) 'Temporal and spatial characteristics of irrigated rice in JERS-1 L-band SAR data', *Direct*, 20(8), pp. 1567–1587.

Sacks, W. J., Deryng, D., Foley, J. A. & Ramankutty, N. (**2010**) 'Crop planting dates: an analysis of global patterns', *Global Ecol. Biogeogr*, 19, pp. 607–620.

Salas, W., Boles, S., Li, C., Yeluripati, J. B., Xiao, X., Frolking, S., & Green, P. (**2007**). Mapping and modelling of greenhouse gas emissions from rice paddies with satellite radar observations and the DNDC biogeochemical model. *Aquatic conservation: Marine and freshwater ecosystems*, *17*(3), 319-329.

Saunois, M., Bousquet, P., Poulter, B., Peregon, A., Ciais, P., Canadell, J. G., ... & Janssens-Maenhout, G. (**2016**). The global methane budget 2000–2012. *Earth System Science Data*, *8*(2), 697-751. doi: 10.5194/essd-8-697-2016.

Seck, P. A., Diagne, A., Mohanty, S., & Wopereis, M. C. (**2012**) 'Crops that feed the world', *Food Security*, 4(1), pp. 7–24. doi: 10.1007/s12571-012-0168-1.

Setiyono, T., Quicho, E., Gatti, L., Campos-Taberner, M., Busetto, L., Collivignarelli, F., ... & Holecz, F. (**2018**) 'Spatial rice yield estimation based on MODIS and Sentinel-1 SAR data and ORYZA crop growth model', *Remote Sensing*, 10(2), pp. 1–20. doi: 10.3390/rs10020293.

Shao, Y., Fan, X., Liu, H., Xiao, J., Ross, S., Brisco, B., ... & Staples, G. (**2001**). Rice monitoring and production estimation using multitemporal RADARSAT. *Remote sensing of Environment*, *76*(3), 310-325. doi: 10.1016/S0034-4257(00)00212-1.

Sinha, S. K. (**1995**): Methane emission from rice paddies: excellent methodology but poor extrapolation, Curr. Sci., 68, 643–646.

Singha, M., B. Wu and M. Zhang (**2017**). Object-based paddy rice mapping using HJ-1A/B data and temporal features extracted from time series MODIS NDVI data. *Sensors* 17(1).

Son, N. T., Chen, C. F., Chen, C. R., Duc, H. N., & Chang, L. Y. (**2014**). A phenology-based classification of time-series MODIS data for rice crop monitoring in Mekong Delta, Vietnam. *Remote Sensing*, *6*(1), 135-156. doi: 10.3390/rs6010135.

Taminato, T., & Matsubara, E. (**2016**). Impacts of two types of water-saving irrigation system on greenhouse gas emission reduction and rice yield in paddy fields in the Mekong delta. *IDRE Journal*, (303), 84.

Tan, C. P., Ewe, H. T. and Chuah, H. T. (**2011**) 'Agricultural crop-type classification of multi-polarization sar images using a hybrid entropy decomposition and support vector machine technique', *International Journal of Remote Sensing*, 32(22), pp. 7057–7071. doi: 10.1080/01431161.2011.613414.

Tan, J., Cui, Y. and Luo, Y. (**2016**) 'Global sensitivity analysis of outputs over rice-growth process in ORYZA model', *Environmental Modelling and Software*. Elsevier Ltd, 83, pp. 36–46. doi: 10.1016/j.envsoft.2016.05.001.

Tan, L., Chen, Y., Jia, M., Tong, L., Li, X., & He, L. (**2015**). Rice biomass retrieval from advanced synthetic aperture radar image based on radar backscattering measurement. *Journal of Applied Remote Sensing*, 9(1), 097091. doi: 10.1117/1.JRS.9.097091.

Torbick, N., Chowdhury, D., Salas, W., & Qi, J. (**2017**). Monitoring rice agriculture across myanmar using time series Sentinel-1 assisted by Landsat-8 and PALSAR-2. *Remote Sensing*, 9(2), 119. doi: 10.3390/rs9020119.

Torbick, N., Salas, W., Chowdhury, D., Ingraham, P., & Trinh, M. (**2017**). Mapping rice greenhouse gas emissions in the Red River Delta, Vietnam. *Carbon Management*, 8(1), 99-108. doi: 10.1080/17583004.2016.1275816.

Tran, H., Tran, T. and Kervyn, M. (**2015**) 'Dynamics of land cover/land use changes in the Mekong Delta, 1973-2011: A Remote sensing analysis of the Tran Van Thoi District, Ca Mau Province, Vietnam', *Remote Sensing*, 7(3), pp. 2899–2925. doi: 10.3390/rs70302899.

USDA (**2018**) 'Office of Global Analysis', 4(July).

Veloso, A., Mermoz, S., Bouvet, A., Le Toan, T., Planells, M., Dejoux, J. F., & Ceschia, E. (**2017**) 'Understanding the temporal behavior of crops using Sentinel-1 and Sentinel-2-like data for agricultural applications', *Remote Sensing of Environment*, 199, pp. 415–426. doi: 10.1016/j.rse.2017.07.015.

Vicente-Guijalba, F., Martinez-Marin, T., & Lopez-Sanchez, J. M. (**2014**). Crop phenology estimation using a multitemporal model and a Kalman filtering strategy. *IEEE Geoscience and Remote Sensing Letters*, 11(6), 1081-1085.

Villard, L. (**2009**) Forward and Inverse Modelling for Synthetic Aperture Radar Observables in the Bistatic Configuration. Forest Remote Sensing Applications.

Wang, L., Ding, K. H. and Toan, T. Le (**2005**) 'Electromagnetic scattering model for rice canopy based on Monte Carlo simulation', pp. 153–171.

Xiao, X., S. Boles, J. Liu, D. Zhuang, S. Frolking, C. Li, W. Salas and B. Moore Iii (**2005**). Mapping paddy rice agriculture in southern China using multi-temporal MODIS images. *Remote Sensing of Environment* 95(4): 480-492.

Xiao, X., S. Boles, S. Frolking, C. Li, J. Y. Babu, W. Salas and B. Moore Iii (**2006**). Mapping paddy rice agriculture in South and Southeast Asia using multi-temporal MODIS images. *Remote Sensing of Environment* 100(1): 95-113.

Yan, X., Yagi, K., Akiyama, H., & Akimoto, H. (**2005**). Statistical analysis of the major variables controlling methane emission from rice fields. *Global Change*

Biology, *11*(7), 1131-1141. doi: 10.1111/j.1365-2486.2005.00976.x.

Jiang, Y., van Groenigen, K. J., Huang, S., Hungate, B. A., van Kessel, C., Hu, S., ... & Chen, J. (**2017**). Higher yields and lower methane emissions with new rice cultivars. *Global change biology*, *23*(11), 4728-4738. doi: 10.1111/ijlh.12426.

Yuzugullu, O., Erten, E. and Hajnsek, I. (**2015**) 'Rice Growth Monitoring by Means of X-Band Co-polar SAR: Feature Clustering and BBCH Scale', *IEEE Geoscience and Remote Sensing Letters*, 12(6), pp. 1218–1222. doi: 10.1109/LGRS.2015.2388953.

Zhang, X., Wu, B., Ponce-Campos, G., Zhang, M., Chang, S., & Tian, F. (**2018**). Mapping up-to-date paddy rice extent at 10 m resolution in China through the integration of optical and synthetic aperture radar images. *Remote Sensing*, *10*(8), 1200. doi: 10.3390/rs10081200.

Zhang, Y., Wang, Y. Y., Su, S. L., & Li, C. S. (**2011**). Quantifying methane emissions from rice paddies in Northeast China by integrating remote sensing mapping with a biogeochemical model. *Biogeosciences*, *8*(5), 1225-1235. doi: 10.5194/bg-8-1225-2011.

Zribi, M., Baghdadi, N., & Guérin, C. (**2006**). Analysis of surface roughness heterogeneity and scattering behavior for radar measurements. *IEEE transactions on geoscience and remote sensing*, *44*(9), 2438-2444.

Zribi, M., Baghdadi, N., Holah, N., Fafin, O., & Guérin, C. (**2005**). Evaluation of a rough soil surface description with ASAR-ENVISAT radar data. *Remote sensing of environment*, *95*(1), 67-76.

Rice Almanac (**2010**). Available at: http://ricepedia.org/rice-as-a-crop/rice-productivity.

USDA, available at: http://apps.fas.usda.gov/psdonline/.

*FAOSTAT, a*vailable at: http://www.fao.org/faostat/en/#home.